CHAOTIC DYNAMICS IN

FLOWS AND DISCRETE MAPS

ANTHONY CURRIE

Department of Physics
University of Warwick

This thesis is submitted to the
University of Warwick in partial fulfilment
of the requirements for admission to the
degree of Doctor of Philosophy

JANUARY 1987

FOR

SUZANNE

SUMMARY

This work attempts to utilise perturbation theory to derive discrete mappings which describe the dynamical behaviour of a continuous, and a discrete, chaotic system.

The first three chapters introduce some background to the theory of chaotic behaviour in discrete and continuous systems. Chapter 4 considers the dynamical behaviour of Duffings equation. Perturbation theory is applied to Hamiltonian solutions of the system, and a 1-D mapping is derived which models the bifurcation of the system to chaos. Chapter 5 introduces a 2-D chaotic difference map. The qualitative dynamics of the system are investigated and a form of perturbation theory is applied to a parameterised version of the map. The perturbative solutions are shown to exhibit dynamical behaviour very like the original system.

TABLE OF CONTENTS

TABLE OF CONTENTS (CONTINUED)

ILLUSTRATIONS

ILLUSTRATIONS
Contd...

ACKNOWLEDGEMENTS

I would like to thank all staff and students of the Physics Department at Warwick with whom I had many stimulating discussions and happy times. Special thanks are due to Dr. George Rowlands for his help and guidance, and for the many informal tutorials held at various bars around Warwickshire. I also thank my wife Suzanne for bearing with me during the writing of the thesis.

For financial support, I thank the Science and Engineering Research Council for a three year studentship, and the Marconi Research Centre for use of its word processing staff and facilities.

DECLARATION

Except where otherwise indicated, this thesis contains an account of my own independent research undertaken in the Department of Physics, University of Warwick, between October 1982 and September 1985 under the supervision of Dr. G. Rowlands.

Things fall apart; the centre cannot hold;

Mere anarchy is loosed upon the world,

W.B. Yeats
The Second Coming

CHAPTER 1

INTRODUCTION

1.0 Background

During the last century, attempts to formulate solutions to the three body problem of classical mechanics led to the development of the Hamiltonian formalism of mechanics. Up until this time it was naturally believed that the asymptotic behaviour of all mechanical systems was reducible to combinations of 'simple' forms such as oscillatory or stationary (equilibrium) behaviour. This situation ceased with the realisation, by Poincaré, of the extremely complicated motion present near the fixed points of a perturbed Hamiltonian system.

Concurrent with Poincarés observations regarding perturbed Hamiltonian systems, were the results due to Boltzman who considered the behaviour of gases to be explicable in terms of the random motion of very many molecules, each of which could explore the whole of state-space energetically available to it. This 'Ergodic hypothesis' formed the basis of classical statistical mechanics.

Given the possibility of stochastic behaviour in perturbed Hamiltonian systems and systems with many degrees of freedom, the problem remained as to how stochastic behaviour could be reconciled with physical observations. It was apparent, for example, that the solar system had remained relatively stable over hundreds of millions of years.

This remained an unsolved problem until the 1930's when Kolmogorov, and later Arnold and Moser postulated the so-called KAM

theorem. The theorem implies that, for systems perturbed away from integrable ones, the motion remains regular for most initial conditions. Whilst stochastic regions exist in the phase plane, they are bounded by invariant surfaces (KAM surfaces) which restrict the stochastic motion. The Ergodic hypothesis, therefore, was found not to hold in general.

The study of chaotic systems per se did not advance significantly beyond Poincaré's work until the 1960's, when E. Lorenz published his seminal paper on chaotic motion in a dissipative system [22].

Lorenz observed that the numerical solutions of a set of coupled non-linear ordinary differential equations appeared to be attracted to a subset of phase space in which the solution curves wandered in an erratic manner. Ruelle and Takens were later to coin the term 'strange attractor' to describe such attracting sets on which chaotic motion occurred.

Since Lorenz's work, many strange attractors have been found to appear in numerical solutions of differential equations. As the equations are usually derived from a physical system; in Lorenz's case the equations are abstracted from fluid equations, it would seem that the chaos found in numerical observations is related to physical notions of stochasticity such as turbulence in a fluid etc. However, the link between mathematical and physical chaos has still to be made precise.

A great simplifying procedure in the study of strange attractors is to consider the Poincaré map of the system. This reduction of the chaotic motion to one or two dimensions leads

naturally to consideration of chaos in discrete mappings of a line or plane. The nature of chaotic behaviour in one dimensional non-invertible discrete maps is now well understood, much pioneering work being due in this regard to Collett and Eckmann [10]. The development of high powered computers in the last two decades has enabled the highly complex, fractal, structure of strange attractors to be elucidated by iteration of the governing differential or difference equation many thousands of times.

Observation of the global behaviour of the system in this way can suggest a reduction of the full system to a form amenable to the methods of symbolic dynamics - the underlying mathematical basis of abstract chaotic systems.

An important mathematical development in the study of chaotic systems has been the introduction of bifurcation theory. This subject considers the changes in phase space topology resulting from variation of a parameter of the system, and provides an insight into the various routes a 'regular' system may take to a chaotic state.

1.1 Discussion

The preceeding section gave a very short account of developments in the subject of chaotic dynamics since Poincaré.

There are many inherent difficulties in this subject, not least of which is the problem of actually defining the chaotic state.

In the following two chapters, the chaotic state will be defined in terms of properties which a chaotic flow might possess.

A second difficulty is that it is impossible to rigorously prove the existence of chaos in a system, for all but a few (mostly abstract) systems. In considering systems such as Duffings' equation or the Hénon map, all that may be said is that the system appears to possess a strange attractor which persists for many iterations of the equations.

A final problem is that of obtaining an overall picture of the various routes to chaos. Bifurcation theory has provided a general picture of various instabilities in parameterised systems, but the subject is inherently messy and incomplete. In particular, an elucidation of the link between local, and global, bifurcations and their relationship to the appearance of strange attractors is needed to provide a coherent overview of chaos in flows and discrete maps.

1.2 Overview of Thesis

The thesis falls naturally into two parts. The first is concerned with chaos in Duffing's equation, and the second with a chaotic discrete two-dimensional map.

The aim of the work on Duffing's equation is to attempt to analytically derive a Poincaré map for the system using perturbation theory. A new perturbation method is developed in order to deal with the special symmetries of the Duffing system. The resulting equations are found to be too complicated to solve in two dimensions, however, a one-dimensional discrete map is derived from consideration of the amplitude equation and is indicated as a good candidate for describing the period doubling of the system to chaos.

The second part of the thesis considers the characteristics of a coupled logistic map which is referred to here as the symmetric map. The chaotic nature of the system can be understood qualitatively by consideration of the foldings near singularities of the map. The Lyapunov exponents of the system are numerically obtained and their relevance discussed.

Finally, a form of perturbation theory is applied to a parameterised form of the map. The results give the limit cycle solution observed in the system, which subsequently bifurcates to chaos. The correspondence between the chaos of the original map and that of the perturbation solution is discussed.

Before describing these results, a general introduction to chaotic behaviour in flows and discrete maps will be given in the following two chapters.

The thesis ends with a short resumé of results and conclusions.

CHAPTER 2

CHAOS IN FLOWS

1.0 Introduction

This chapter introduces some of the background material pertaining to chaotic dynamics in flows. In this section, the asymptotic behaviour to be expected of a one or two dimensional system is briefly described, followed by an overview of chaotic behaviour in three or more dimensional systems. Section 2 considers various routes by which a deterministic system may become chaotic upon variation of a parameter. This involves a brief description of local bifurcations in parameterised systems and also a consideration of global bifurcations including homoclinic tangencies and intersections.

The third section attempts to give a characterisation of the chaotic state. Some definitions are taken from the field of dynamical systems, in order to fix ideas, and the concept of a 'strange attractor' is introduced.

The final section gives three examples of systems which exhibit chaotic behaviour. One system in particular - the Duffing system - is considered in some detail as this system will be subsequently studied in Chapter 4.

1.1 Regular Flows

The flows in this chapter are determined by systems of ordinary differential equations of the form:

$$\frac{d\underline{x}}{dt} = \dot{\underline{x}} = f(\underline{x}) \quad , \qquad \ldots (1.1)$$

where $\underline{x} = \underline{x}(t) \in R^n$ is a vector function of time, and $f: U \to R^n$ is a smooth vector field defined on $U \subset R^n$. We then define the 'flow' generated by f to be a smooth function $\phi(t,x): U \times R \to R^n$, (defined $\forall x \in R^n$ and for t in some interval (a,b)) which satisfies Equation 1.1, i.e.

$$\frac{d}{dt}\,(\phi(t,x))_{t=t_0} = f(\phi(t_0,x)) \quad . \qquad \ldots (1.2)$$

Of particular interest is the 'asymptotic' behaviour of a given flow i.e. the behaviour of $\phi(t,x)$ $\forall$ x $\in$ U as $t \to \infty$.

In this respect, the points $\bar{x} \in U$ such that $f(\bar{x}) = 0$, assume particular importance as solutions initiated at these 'fixed points' remain there for all time. Remembering that $\phi(t,x)$ is a smooth function, the question is then 'what are the consequences for the flow of having fixed points in U?' this question is answered by way of 'stability analysis'.

The fixed point $\bar{x}$ is said to be 'stable' if for every neighbourhood V of $\bar{x}$ $\exists$ V_1 s.t. every solution $\phi(t,x_0)$ with $x_0 \in V_1$ lies in V $\forall t > 0$.

If, in addition to the above, V_1 can be chosen such that $x_0 \in V_1 \Rightarrow \phi(t,x_0) \to \bar{x}$ as $t \to \infty$, then x is said to be 'asymptotically stable.'

If none of the above apply, then $\bar{x}$ is said to be 'unstable'. For flows in two, or more, dimensions, solutions may be attracted to (or repelled from) a closed orbit, in this case we have a limit cycle in the flow. The stability of a given limit cycle is defined by obvious extension of the definition above except now the fixed points $\bar{x}$ are replaced by periodic solutions $\bar{x}(t)$. We may view

'area preserving' flows, such as Hamiltonian flows, as systems possessing stable (but not asymptotically stable) limit cycles.

It is apparent, then, that local behaviour of a flow may be obtained by studying the stability of fixed points of the system. The stability of a given fixed point is determined by the eigenvalues of the system linearised about the fixed point. Thus, given an equilibrium point $\bar{x}$ of Equation 1.1, the linearised system is given by:

$$\dot{\xi} = L\xi \quad , \quad \xi = (x-\bar{x}) \quad , \quad F(x) = L(x-\bar{x}) + O(x-\bar{x})^2 \qquad \ldots (1.3)$$

We now define three invariant subspaces of the 'state-space', (i.e. the space in which solutions to Equation 1.1 lie) as follows [15]:

$$E^s = \text{SPAN } \{V^1, \ldots, V^{ns}\}, \quad E^u = \text{SPAN } \{U^1, \ldots, U^{nu}\},$$
$$E^c = \text{SPAN } \{W^1, \ldots, W^{nc}\} \qquad \ldots (1.4)$$

where the V^i, are the n_s eigenvectors whose eigenvalues have negative real parts, the U^i are the n_u eigenvectors whose eigenvalues have positive real parts, and the W^i are the n_c eigenvectors whose eigenvalues have zero real part.

E^s, E^u, and E^c are called the 'stable', 'unstable' and 'centre' subspaces respectively, reflecting the fact that solutions in E^s are characterised by exponential decay, solutions in E^u by exponential growth, and solutions in E^c by neither.

The linear eigenspaces E^s, and E^u for system 1.3 have analogues for the (possibly) non-linear system 1.1. In this case we define the local stable and unstable manifolds of $\bar{x}$ to be

$$W^s_{loc} = \{x \in U \mid \phi(t,x) \to \bar{x} \text{ as } t \to \infty, \text{ and } \phi(t,x) \in U \ \forall t > 0\} \quad , \qquad \ldots (1.5)$$

$$W^u_{loc} = \{x \in U \mid \phi(t,x) \to \bar{x} \text{ as } t \to \infty, \text{ and } \phi(t,x) \in U \ \forall t < 0\} \quad ,$$

where U is a neighbourhood of $\bar{x}$.

The 'Stable Manifold Theorem' [15] then tells us that given a fixed point $\bar{x}$ with associated eigenspaces E^s, E^u, then there exist local stable and unstable manifolds for $\bar{x}$, which are tangent to E^s, E^u, at the equilibrium point.

Global stable and unstable manifolds are defined by iteration of the corresponding local ones, i.e.

$$W^s(\bar{x}) = \bigcup_{t \leq 0} \phi_t \left(W^s_{loc}(\bar{x})\right),$$

$$W^u(\bar{x}) = \bigcup_{t \geq 0} \phi_t \left(W^u_{loc}(\bar{x})\right). \qquad \ldots (1.6)$$

Stable and unstable manifolds of a limit cycle can be defined in an analogous manner.

We shall see in later sections that the behaviour of stable and unstable manifolds of a system can give global information on the flow.

The above discussion has introduced the concepts of fixed points and limit cycles for an n-dimensional flow. It turns out that in less than 3 dimensions, the asymptotic behaviour of a flow is completely determined by such structures.

The so-called Poincaré-Bendixon Theorem [2] states, in effect, that if an attracting (or repelling) set exists for a 2 dimensional flow, then it is either a fixed point or a limit cycle. Similarly, for a one dimensional flow, only fixed points may exist.

Thus, we may completely classify the types of behaviour to be expected from a linear system of dimension n, or a non-linear system of dimension one or two.

1.2 Chaotic Flows

For the case of a non-linear system of dimension greater than two, a qualitatively different type of asymptotic behaviour can occur. Typically, solution curves wander around some subset of state-space in a seemingly random manner, without collapsing into a fixed point or limit cycle. This type of behaviour has been labelled 'chaotic'. Although there is no agreed definition of a chaotic system, it is possible to state various attributes which may or may not be present in such a system, Section 3 of this chapter attempts such a characterisation.

The subspace around which trajectories wander is generally known as a 'strange attractor', although these objects are extremely complex it is possible to reduce the complexity of the system by taking a 'Poincaré map' of the flow. This mapping is generally defined on a two-dimensional surface which lies transverse to the flow. If the first point of intersection of the flow with the 2-D plane is labelled x_0, then the Poincaré map $P : R^2 \to R^2$ is formally defined by $x_1 = P(x_0)$, where x_1 is the second point of intersection, $x_2 = P(x_1)$, where x_2 is the third point etc. It is apparent that an analytical form for $P(x)$ may not exist, although in some cases an approximate expression may be derived [4], [32].

Before considering the characteristics of chaotic systems, a discussion of the various routes to chaos will be given in the next section.

2.0 Routes to Chaos

A situation which commonly occurs is that a system of differential equations whose solutions are 'well behaved' may be perturbed to a set of equations whose solutions appear random, or chaotic. Considering the system to be parameterised with some parameter, μ, i.e.

$$\dot{\underline{x}} = F_\mu(\underline{x}) \quad , \mu \in R \qquad \ldots (2.1)$$

then we may study the family of Equations 2.1 as μ is varied in some interval containing the parameter μ_c, where:

$\dot{\underline{x}} = F_{\mu c}(\underline{x})$ is our chaotic system. The nature (or topology) of the flows of Equation 2.1 will change in a certain manner as $\mu \to \mu_c$, thus giving a qualitative link between well-behaved and chaotic systems.

The above methodology is known as 'bifurcation theory'. In this section a brief discussion of the various codimension 1 bifurcations is given, followed by a consideration of global bifurcations.

2.1 Local Codimension 1 Bifurcations

We restrict ourselves to local codimension 1 bifurcations i.e. bifurcations which occur near fixed points of one-parameter systems. Given a parameterised system:

$$\dot{x} = F_\mu(x) \quad ,$$

which has an equilibrium at some point (p_0, μ_0), we may form the linearised system:

$$\dot{\xi} = L\xi \ , \ \xi = (x-p) \qquad \ldots (2.2)$$

If the matrix L has no eigenvalues which are zero or pure imaginary then p is called 'hyperbolic'. Such hyperbolic fixed points are 'structurally stable' in the sense that they remain hyperbolic when the system is perturbed in a suitable way [15].

For a fixed point without zero eigenvalues, the 'Implicit Function' theorem implies that there is a smooth function $g(\mu)$ of equilibria passing through (p_0, μ_0) i.e. there is no change in the number of equilibria at (p_0, μ_0). If, however, the point has a zero eigenvalue, then several branches of equilibria may come together and we have a 'bifurcation point'.

It can be shown that there are four generic codimension 1 bifurcations, epitomised by the following systems [18].

$$\dot{x} = \mu - x^2 \qquad \text{(saddle-node)}$$

$$\dot{x} = \mu x - x^2 \qquad \text{(transcritical)}$$

$$\dot{x} = \mu x - x^3 \qquad \text{(pitchfork)}$$

$$\left.\begin{aligned} \dot{x} &= -y + x\,(\mu - (x^2 + y^2)) \\ \dot{y} &= x + y\,(\mu - (x^2 + y^2)) \end{aligned}\right\} \qquad \text{(Hopf)}$$

The saddle-node bifurcation corresponds to the creation of a stable and an unstable equilibrium, in this case there is no 'unperturbed solution' from which the equilibria bifurcate, in a sense they are created from nothing.

The transcritical bifurcation occurs when a stable and an unstable equilibrium exchange their stability, and the pitchfork bifurcation corresponds to an equilibrium splitting into 2 equilibria, this 'period doubling' bifurcation will be encountered many times in the discussion of chaotic systems.

The two-dimensional Hopf bifurcation occurs when an equilibrium possesses two pure imaginary eigenvalues. In this case a fixed point bifurcates into a periodic orbit, again, the Hopf bifurcation will be encountered often in the following chapters.

This completes the discussion of local codimension 1 bifurcations. The theory of bifurcations in 2 or more codimension systems is difficult and far from complete, further details may be found in [18].

2.2 Global Bifurcations

In previous sections the concept of a hyperbolic fixed point was introduced. In this section, we will consider a common type of global bifurcation which occurs for systems possessing a particular kind of hyperbolic fixed point known as a 'saddle'. A fixed point $\bar{x} \in R^n$ for a system of the form (1.1) is called a 'saddle point' if the system linearised about $\bar{x}$ has at least one eigenvalue with negative real part, and at least one eigenvalue with positive real part. In this situation, $\bar{x}$ will have associated stable and unstable manifolds passing through it.

Although, by the theory of existence and uniqueness of solutions for a system like (1.1), a stable or unstable manifold may not intersect itself in state-space, it is quite possible for the stable manifold of one point to be identified with the unstable manifold of another point, in this case we have a 'saddle connection' between the two points. It is also possible for the stable manifold of a point to be identified with the unstable manifold of the same point, in which case we have a 'saddle-loop' or 'homoclinic orbit'. Such structures are very common in Hamiltonian systems such as the ordinary pendulum, or Duffing's equation with zero forcing and damping [p(44)].

The saddle-loop as described above is structurally unstable, i.e. if a system possessing a saddle-loop is perturbed, then the saddle-loop will disappear, or rather, deform into some new structure. This is an example of a 'global bifurcation'.

Three possibilities exist for the form of the new structure created after the perturbation: (i) the saddle-loop breaks, the unstable manifold lies outside the stable one, (ii) as (i) with the stable manifold lying outside the unstable one, (iii) the perturbation is time dependant and the stable and unstable manifolds intersect an infinite number of times when they are viewed on a surface of section (Poincaré map).

Although it is difficult to say precisely what has happened to the flow in case (iii), it can be proved that the appearance of 'homoclinic intersections' for the Poincaré map implies the existence of a 'Smale-horseshoe' [34]. The horseshoe is the product of 2 'Cantor sets' in $U \subset \mathbb{R}^2$, it possesses a countable set of

periodic orbits of all periods and an uncountable set of nonperiodic motions. Therefore, if we observe the intersection of stable and unstable manifolds in the Poincaré map of the system we know that very complex orbits exist in the flow. However, the horseshoe does not attract anything, therefore, we cannot say that the system is automatically chaotic i.e. that a strange attractor exists, rather, the above bifurcation is important as it often precedes global chaotic behaviour of a system (c.f. Duffing's system Section 4.3) The existence of a horseshoe in the Poincaré map of a flow can lead to a phenomenon known as 'preturbulence' [33] in which orbits wander erratically before being attracted to some stable solution.

Associated with the onset of homoclinic intersections in a system is an infinite sequence of saddle-node bifurcations of periodic orbits leading to the creation of the horseshoe [9]. Thus, a common scenario in a parameterised system is that an infinte number of local bifurcations occure leading to a global bifurcation (homoclinic intersections) followed by the onset of global chaotic motion. The link between the local bifurcations and the global one is not clear, however, the existence of periodic orbits for the horseshoe can be seen as a direct result of the preceeding local bifurcations.

A useful criterion for predicting the existence of homoclinic intersections in a given parameterised system is the 'Melnikov-Condition' [7]. The condition is derived from consideration of the distance between perturbed stable and unstable manifolds, where the distance is approximated by using a perturbation expansion about the unperturbed homoclinic orbit.

For a system of the form:

$$\dot{x} = f_0(x) + \epsilon f_1(x,t) \quad , \qquad \ldots (2.4)$$

where $x \in R^2$, f_1 is periodic in t with period T and the unperturbed system possesses a homoclinic orbit, we define the 'Melnikov distance', D, as:

$$D = -\int_{-\infty}^{\infty} f_0 \wedge f_1 \, dt \quad , \qquad \ldots (2.5)$$

where $f_0 \wedge f_1 = f_{01} f_{12} - f_{02} f_{11}$.

Then if D remains strictly positive (or strictly negative) for all t, the manifolds do not intersect, however, if D changes sign for some $t = t_0$, then we have a homoclinic intersection. In general, the condition imposes restrictions on the parameters of the system, from which a reasonably accurate prediction of homoclinic intersection can be made in terms of the parameter space of the system.

In this section, various bifurcations of one parameter systems have been described. A tacit assumption throughout has been that the systems are dissipative i.e. energy is not in general conserved along trajectories. In the case of a Hamiltonian system, the transition to chaos is somewhat different, a brief description of chaos in such a system will be given in Section 4 where three examples of chaotic systems are described.

3.0 Characterisation of the Chaotic State

There is no generally agreed, all encompassing definition of a chaotic system. Rather, such systems are best characterised by listing the various properties which a chaotic system may possess. In this section, some of these properties are described. Some mathematically (though not fully rigorous) definitions are given in order to fix ideas. In this respect it is found to be more convenient to introduce some definitions in terms of the Poincaré map of the system, there is no loss of generality in doing this, as all dynamical properties of a flow carry over to the Poincaré map. We thus frame such definitions as 'mixing' and 'ergodicity', in terms of a mapping $f:R^n \to R^n$, the definitions thus apply also to the discrete chaotic systems to be described in the next chapter. We begin with perhaps the simplest property to frame.

3.1 No Stable Periodic Orbits

A system which possesses stable periodic orbits is not chaotic. We are thus excluding from our definition of a chaotic system flows which possess horseshoes together with a stable attracting region (c.f. Duffing's system, p(27)).

It should be noted that chaotic systems can possess unstable periodic orbits, in fact many such systems contain an infinity of unstable periodic orbits created by bifurcation to chaos.

3.2 Sensitivity To Initial Conditions

A mapping $F:U \to U$, $U \subset R^n$, $U \neq \phi$, is said to have sensitivity to initial conditions if $\exists\ \varepsilon > 0$ such that $\forall\ x \in U$ and every neighbourhood N of x, $\exists y \in N$ and an $m > 0$ such that:

$$| f^m_{(x)} - f^m_{(y)} | > \varepsilon \quad ,$$

Intuitively, initial conditions started very close together will be noticeably separated after a finite number of iterates (returns of the flow).

In a practical situation, therefore, where there will be numerical errors in the initial conditions supplied to the computer simulation, say, the subsequent orbit of a given point will become totally unpredictable in a finite time interval. This is the essence of chaotic motion in deterministic systems.

3.3 Mixing Behaviour

A mapping $f:U \to U$ is 'mixing' if $\forall$ non-empty open subsets V, W, of $U \exists n$ such that:

$$f^p W \cap V \neq \emptyset \qquad \forall_p > n$$

That is, any given subset of U is progressively 'stretched out' to cover the whole of U.

A similar, and related, concept is afforded by the following:

3.4 Ergodicity

A mapping $f:U \to U$ is 'ergodic' if given $x \in U$, $y \in U$, $y \neq x$, and an $\varepsilon > 0$, then $\exists n > 0$ such that:

$$|f^n(x) - y| < \varepsilon$$

Thus, an ergodic mapping maps a given point arbitrarily close to every other point in U.

It can be shown that if a map is mixing, then it is ergodic.

3.5 Lyapunov Exponents

Beginning with a system of the form 1.1, we take two initial conditions, x_0 and $x_0 + \Delta x$. Considering their evolution in time we define:

$$d(x_0,t) = |\Delta x (x_0,t)| \quad , \qquad \ldots (3.1)$$

i.e. $d(..)$ measures the distance between the two trajectories as a function of time. We now define the mean divergence rate of the two trajectories to be:

$$\sigma(x_0) = \lim_{\substack{t\to\infty \\ d(0)\to 0}} \left(\frac{1}{t}\right) \ln \left(\frac{d(x_0,t)}{d(x_0,0)}\right) \qquad \ldots (3.2)$$

It can be shown that there exists an n-dimensional basis for Δx such that σ takes on one of n values (σ_i) which can be ordered:

$$\sigma_1 \geq \sigma_2 \geq \ldots \geq \sigma_n$$

The σ_i's measure the average expansion rate of trajectories in their corresponding subspaces.

For overall contraction of a flow, we must have

$$\sum_i \sigma_i < 0,$$

if the flow is chaotic, then one or more of the exponents must be greater than zero.

3.6 Hyperbolicity

An 'invariant set' $\Lambda \subset R^n$ for a mapping $f: R^n \to R^n$, is a subset of R^n such that $f(\Lambda) = \Lambda$ i.e. f maps Λ into itself.

If we can define a continuous invariant direct sum decomposition

$$T_\Lambda R^n = E^u_\Lambda \oplus E^s_\Lambda,$$

of R^n such that there exist constants $C > 0$, $0 < \lambda < 1$ with the property:

(i) $\quad V \in E^u_x \Rightarrow \| Df^{-m}_{(x)} V \| \leq C \lambda^m \| V \|$

(ii) $\quad V \in E^s_x \Rightarrow \| Df^{m}_{(x)} V \| \leq C \lambda^m \| V \|$

then we say that Λ is a 'uniformly hyperbolic set'.

Hyperbolicity of an invariant set usually implies the existence of chaotic orbits in the system (c.f. Smale-horseshoe [34]). However, many chaotic systems possess invariant sets which are not uniformly hyperbolic, the Duffing attractor is an example of such a set.

3.7 Strange Attractors

A chaotic flow is characterised by global contraction onto an invariant set which possesses some (not necessarily global) hyperbolic structure. The term 'strange attractor' has been coined to define these objects in a broad sense although no universal definition of a strange attractor exists.

The envelope of the orbits ' captured' by the strange attractor defines the shape, or topology, of the attractor. Recent efforts in the attempt to simplify the study of these very complicated objects have concentrated on attempting to classify strange attractors by their topology [33].

One fairly substantiated fact is that strange attractors are 'fractal' i.e. self-similar objects with non-integer dimension [23].

Their associated fractal or 'Hausdorff' dimension can be shown to be related to the Lyapunov exponents and so-called 'entropy' of the flows associated Poincaré map [37].

This section has concentrated on some general aspects of chaotic motion. In the next section, some examples of chaotic systems will be described.

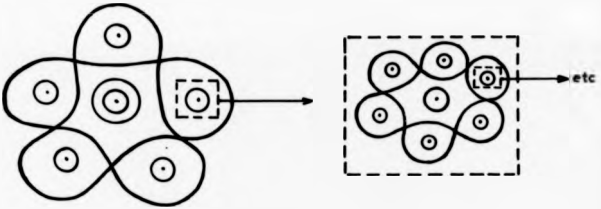

Figure 2a : Islands and Separatrices of a Perturbed Hamiltonian

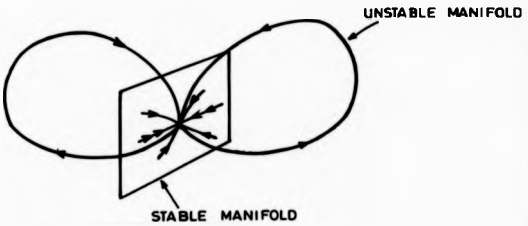

Figure 2b : Homoclinic Loop for Lorenz Equations

4.0 EXAMPLES OF CHAOTIC SYSTEMS

4.1 Hamiltonian Systems

In order to illustrate chaotic behaviour in Hamiltonian systems, we first consider autonomous, periodic systems, governed by the equations:

$$\dot{p}_i = -\frac{\delta H}{\delta q_i} \quad , \qquad i = 1, \ldots, N \qquad \ldots (4.1)$$

$$\dot{q}_i = \frac{\delta H}{\delta p_i} \quad ,$$

where the p_i, q_i are the generalised momentum and position coordinates respectively, and $H = H(p,q)$ is the Hamiltonian of the system. By a periodic system is meant one for which the p_i are periodic functions of the q_i for each degree of freedom.

Given that the system is periodic, we may make a canonical change of variable [12] : $p_i \rightarrow J_i$, $q_i \rightarrow \theta_i$, $H(p,q) \rightarrow \overline{H}(J)$, such that the new Hamiltonian $\overline{H}$ is independent of the θ_i. Such a procedure is equivalent to solving the original system as N integrals of the motion, namely the J_i, have been found.

The J_i, θ_i are known as action-angle variables [12]. The new equations of motion are given by:

$$\dot{J}_i = -\frac{\delta \overline{H}}{\delta \theta_i} = 0 \quad , \qquad \ldots (4.2)$$

$$\dot{\theta}_i = \frac{\delta \overline{H}}{\delta J_i} = w_i \quad ,$$

with solutions:

$$J_i = \text{constant}$$
$$i = 1, \ldots, N \qquad \ldots (4.3)$$
$$\theta_i = w_i t + \beta_i$$

The solutions thus lie on N-tori in the 2N dimensional phase-space. The dimensions of each torus are defined by the magnitude of the J_i, and solutions wind around the tori with frequencies w_i.

Considering the case N=2, we may reduce the dimension of the phase space by taking a 2N-1 = 3 dimensional constant energy cross section, the dynamics can then be further simplified by considering the motion on the $J_2 - \theta_2$ plane.

Viewing the motion on this plane, we must consider two distinct cases: (i) w_1, w_2 not rationally related.

(ii) w_1, w_2 rationally related.

In the former (generic) case, orbits wind around the torus ergodically, giving rise to concentric circles (KAM curves) in the $J_2 - \theta_2$ plane, whilst in the latter case solutions form closed orbits on the torus which are manifest as periodic point orbits on the $J_2 - \theta_2$ plane. The latter situation is known as primary resonance.

Having described the dynamics of the integrable Hamiltonian we now consider a near integrable system, i.e. a system which is a small perturbation of an integrable one. In 2 dimensions we may write the perturbed Hamiltonian as:

$$H(J_1,J_2,\theta_1,\theta_2) = H_0(J_1J_2) + \epsilon H_1(J_1,J_2,\theta 1,\theta_2) \qquad \ldots (4.4)$$

where H_0 is the unperturbed Hamiltonian, and H_1 is periodic in the θ_1.

The main result bearing on this case is the Kolmogorov-Arnold-Moser (KAM) theorem [21], which states that for ϵ small (in a special sense), a finite fraction of the regular KAM curves, referred to above, remain after perturbation. The remaining fraction of phase space is covered by chaotic trajectories bounded by the remaining KAM curves. As the perturbation is increased more KAM curves are destroyed and chaotic trajectories cover more of the phase space until, at some value of ϵ, the last KAM curve is destroyed leading to 'global stochasticity' [8].

We may understand the chaotic motion in this case by considering the motion near a general resonant curve. Such a curve corresponds to a set of periodic points in the $J_2 - \theta_2$ plane as described above. Each of the periodic points is encircled by so-called primary islands, and between each pair of points is a hyperbolic fixed point. The islands are therefore encompassed by separatrices between the hyperbolic points Figure 2a. Associated with the primary resonance is a secondary resonance in which orbits encircle each of the primary fixed points in order an integer number of times. Thus, for example, a period 5 primary periodic orbit may be associated with a period 15 secondary periodic orbit which returns to the vicinity of each primary fixed point 3 times. Associated with the secondary resonance are secondary islands which give rise to third order resonances and so on ad infinitum. The motion near these resonances is therefore extremely complicated, even though the governing system is completely deterministic. The chaotic motion in this case can also be viewed as resulting from

transversal intersection of the stable and unstable manifolds of the infinite number of hyperbolic fixed points present in the system.

4.2 The Lorenz System

In his classic paper of 1967 [22] E.N. Lorenz described the dynamical behaviour of a set of 3 coupled ordinary differential equations which represented a three mode truncation of the Oberbeck-Boussinesq equations for fluid convection. The equations so derived for a two dimensional fluid heated from below are:

$$\begin{aligned} \dot{x} &= \sigma(y - x) \ , \\ \dot{y} &= px - y - xz \ , \\ \dot{z} &= -\beta z + xy \ , \end{aligned} \qquad \ldots (4.5)$$

where σ is the Prandtl number, p the Rayleigh number, and β an aspect ratio [15]. The above equations are an accurate representation of the physical system for $p = 1$. Lorenz considered the above system for $p = 28$, fixing $\sigma = 10$, $\beta = 8/3$. For large p the numerically integrated solutions appeared to behave in a random manner, spiralling about 2 fixed points in the phase space, the orbits alternately spiralling about one fixed point, then crossing to the other with no apparent periodicity.

The above system with its associated strange attractor, later called the Lorenz attractor, has since received considerable attention in the literature, a comprehensive account of the system may be found in the book by Sparrow [35]. Although the details of the Lorenz bifurcations and chaotic attractors for $p \gg 1$ are complicated and incomplete, it is possible to give a general overview of the major bifurcations to chaos of the Lorenz system.

In the parameter range $0 < p < 1$, the system has a stable globally attracting fixed point at the origin. At $p = 1$ a pitchfork bifurcation occurs in which the origin becomes a saddle point with one dimensional unstable manifold, and two stable fixed points are created at $q \pm = (\pm \sqrt{\beta(p-1)}, \pm \sqrt{\beta(p-1)}, p-1)$.

As p is increased the two branches of the unstable manifold increase until at $p = 13.926$, they join to form a double homoclinic loop (Figure 2b). As p is increased a little beyond this value, the two branches cross over to the opposite side of the stable manifold, at this point two unstable periodic orbits have been created by the saddle-loop bifurcation and a (non-attracting) Smale horseshoe is created.

Finally, as p is increased further, a strange attractor is created at $p = 24.06$, this attractor coexists with the fixed points, $q\pm$, until at $p = 24.74$ the unstable periodic orbits collapse onto the fixed points in an inverse Hopf bifurcation, and the strange attractor becomes globally attracting.

Much of the analysis of the Lorenz bifurcations involves the study of Poincaré maps of the flow, the map being taken at $z = p-1$, the general behaviour of the flow can then be represented as a two dimensional map which is amenable to the methods of symbolic dynamics.

Lorenz, in his original paper, actually considered a one dimensional representation of his system, the Poincaré map being defined as the relation between z_{n+1} and z_n, where z_n is the maximum value of z which occurs for an orbit just before it crosses over to the other side of the stable manifold. Numerical results strongly

suggest that such a 1-D map exists for the system, and has the form of a 'tent map' [15]. Recently, Rowlands [32] has derived an approximation to this 1-D map using perturbation theory on the original equations.

4.3 The Duffing System

We consider Duffings equation with negative linear stiffness:

$$\ddot{x} + \delta\dot{x} - \beta x + \alpha x^3 = f \cos \omega t \qquad \ldots (4.6)$$

The above system has been studied in detail by Holmes [19], who performed a numerical analysis of the equations using the forcing, f, as a parameter. In this section, the bifurcations to chaos of the system will be described, and in Chapter 4 an attempt will be made to extract a 1-D map from the system.

A convenient starting point is to consider Equations 4.6 in the absence of forcing and damping i.e. $f = \delta = 0$. In this case, the system is Hamiltonian and possesses a double homoclinic loop (Figure 2c). If the forcing were increased from zero with $\delta = 0$, then we would expect the breakup of KAM surfaces with associated chaotic motion described earlier in this section. However, in the following we take δ to be a non-zero positive constant and consider the behaviour of the (dissipative) system as f is increased from zero.

Fixing α, β, $\delta > 0$, and taking $f = 0$, the system possesses a hyperbolic fixed point, 'p' at the origin , and two stable sinks at $x = \pm \sqrt{\beta/\alpha}$. It can be shown [19] that these sinks are globally attracting and therefore all initial conditions (except those initiated on the stable manifold of p) will converge to one or the

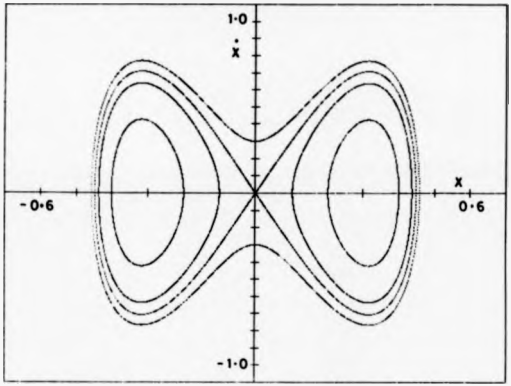

Figure 2c : Duffing Equation Phase Plane for $f = \delta = 0$

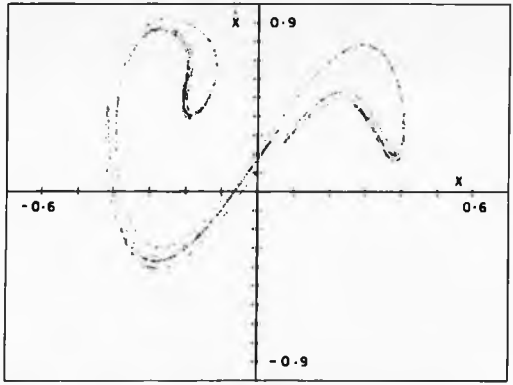

Figure 2d : Poincaré Map for Duffing Attractor

other. As f is increased, the sinks become attracting periodic orbits (limit-cycles) due to the fact that the system is now non-autonomous with a three dimensional state space.

It is now convenient to view the motion on a 2-D Poincaré map P defined by $P:R^2 \to R^2$, $R^2 = \{\dot{x}, x \mid t = 0, 2\pi/\omega, 4\pi/\omega, \ldots\}$. As f is increased further, the stable and unstable manifolds of p, viewed on P, eventually intersect for some $f = f_c$. Using Holmes choice of parameters: $\alpha = 100$, $\beta = 10$ $\delta = 1$, $\omega = 3.76$, this occurs for $f = f_c = 0.76$. For $f > f_c$ we would therefore expect the system to have a Smale horseshoe for the Poincaré map. Due to the symmetry of the equations (if x(t), $\dot{x}(t)$ is a solution of 4.6 then so is $-x(t + \pi/\omega)$, $-\dot{x}(t + \pi/\omega)$) intersection of stable and unstable manifolds occurs simultaneously on both sides of $x = 0$. As f is further increased, the pair of stable limit cycles undergo a period-doubling bifurcation to a pair of period 2 cycles, these subsequently period double to a pair of period 4 cycles, the successive period-doubling continuing until an accumulation point at $f = 1.08$ is reached at which point the orbits move in an irregular manner. At this point a strange attractor appears to be present. Figure (2d) shows the structure of the strange attractor when viewed as a Poincaré map. Holme's computational results indicate that the strange attractor persists for $f \in [1.08, 2.45]$, above these values the chaos is replaced by a periodic orbit which encompasses p and the two unstable fixed points at $\pm \sqrt{\beta/\alpha}$.

Although the strange attractor persists over most of the interval [1.08, 2.45], there is a small 'window' around $f = 1.2$ in which the strange attractor is replaced by a stable period 5 orbit. This phenomenon is strikingly similar to that encountered in 1

dimensional chaotic discrete maps (Chapter 3), and may lend credence to the existence of an underlying 1-D map for the system, similar to the 1-D representation of the Lorenz attractor.

The structure of the strange attractor shown in Figure 2d is actually the structure of the unstable manifold of the system. Trajectories are contracted onto the unstable manifold and then follow the complicated windings caused by the homoclinic intersections mentioned above. When different Poincaré sections are taken of the system, the attractor is found to rotate 2π radians every period $2\pi/\omega$. The full structure of the attractor defined on $R^2 \times S$ therefore resembles a Möbius strip. This type of topology is akin to that of the so-called Rössler attractor [33].

When a chaotic orbit is numerically iterated and viewed on the plane $(x,\dot{x})$, it is observed to orbit one fixed point a number of times then cross over to the other point in a similar manner to the Lorenz system. However, in this case the point of crossover does not seem to correspond to a maximum in the amplitude of the orbit, and hence no 1-D map can be obtained from consideration of the amplitude at crossover. A major difference between the dynamics of the Lorenz and Duffing systems is that in the former case all three degrees of freedom are coupled and can all go chaotic, whereas in the Duffing case only two of the three degrees of freedom can exhibit chaos. This is most clearly seen by considering Equation 4.6 as a 3 dimensional system:

$$\dot{x}_1 = x_2$$

$$\dot{x}_2 = \beta x_1 - \delta x_2 - \alpha x_1^3 + f \cos \theta \qquad \ldots (4.7)$$

$$\dot{\theta} = \omega \ ,$$

where the third degree of freedom 'θ' is uncoupled from x_1 and x_2.

Summarising the above bifurcations to chaos for the Duffing system, we see that the successive period doubling bifurcations of the two limit cycles accumulate at a point corresponding to the birth of the strange attractor. The link between these local bifurcations and the global appearance of chaos is not clear. The existence of homoclinic intersections in the system leads to Smale horseshoes which do not seem to affect the dynamics of the system. When the accumulation point has been reached, orbits are attracted to, and follow, the complex windings of the unstable manifold. The Smale horseshoe is created before the period doubling begins and it would therefore seem that the horseshoe and period doubling cascade occur quite independently of each other, and that therefore the horseshoe has no bearing on the subsequent transition to chaos. It is also clear, however, that the homoclinic intersections of the stable and unstable manifolds are necessary for the onset of chaotic motion and that the behaviour of the manifolds must be intimately related to the period doubling of the limit cycles. The demonstration of a connection between the above processes would be a significant advance in the understanding of chaotic behaviour in systems such as the Duffing equations.

CHAPTER 3

CHAOS IN DISCRETE MAPS

1.0 Introduction

In this chapter we consider parameterised families of discrete maps in one or two dimensions. In particular, the bifurcation sequence of so-called 'unimodal ' maps will be described, followed by two examples of 2 dimensional chaotic discrete systems.

The characterisation of the chaotic state for discrete maps in terms of ergodicity, mixing behaviour etc., carries over naturally from the continuous case described in the last chapter. The main difference between the discrete and continuous case is that there is no restriction on the dimensionality of a discrete system in order for chaotic motion to occur. This is in contrast to the continuous case in which the dimensionality of the system must be greater than or equal to three.

1.1 Maps on an Interval of R

The case of a mapping $f:I \to I$, $I \subset R$,

$$x_{n+1} = f(x_n, \lambda) \quad , \qquad \ldots (1.1)$$

where $\lambda \in R$ is some parameter, has been studied in some depth by various authors, and their general dynamical behaviour is now well understood [10].

In Equation (1.1), f is a non-invertible mapping of some subset R to itself. We restrict our study of such systems to maps which are 'unimodal' on the interval $[-1,1]$:

Definition. A mapping $f:[-1,1]\to[-1,1]$ is called 'unimodal' if:

i) f is continuous

ii) $f(0) = 1$

iii) f is strictly increasing on $[-1,0)$ and strictly decreasing on $(0,1]$.

The general form of such mappings is exemplified by a standard example, the so-called 'logistic map' defined by the relationships:

$$x_{n+1} = 1 - \lambda x_n^2 \quad , \quad x_n \in [-1,1] \quad , \quad \lambda \in [0,2] \quad , \quad \ldots (1.2)$$

or in its equivalent form:

$$x_{n+1} = \lambda x_n (1 - x_n) \quad , \quad x_n \in [0,2] \quad , \quad \lambda \in [0,4] \quad , \quad \ldots (1.3)$$

where the second form is not unimodal in the above sense, but nevertheless possesses identical dynamics to the first.

The logistic map has the property of 'Negative Schwartzian Derivative'.

Definition. A mapping $f:[-1,1]\to[-1,1]$ has a negative Schwartzian derivative if:

$$Sf(x) = \frac{f'''(x)}{f'(x)} - \frac{3}{2}\left(\frac{f''(x)}{f'(x)}\right)^2 < 0 \quad , \quad \forall x \in [-1,1] \quad ,$$

such a map is termed 'S-unimodal'.

An important theorem concerning the stable periodic orbits of S-unimodal maps is the following:

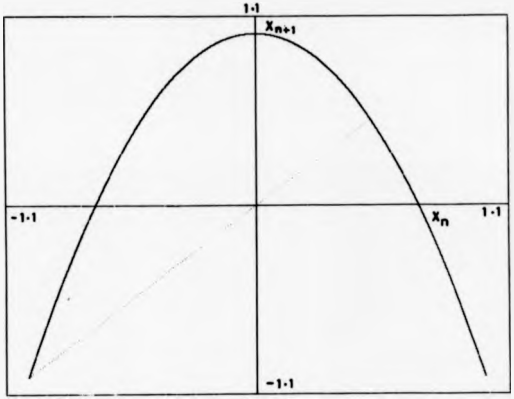

Figure 3a : Logistic Map for $\lambda = 2$

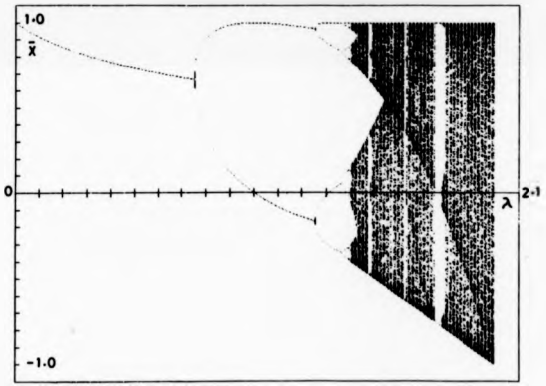

Figure 3b : Bifurcation Diagram for Logistic Map

Theorem. If f is S-unimodal then it has at most one stable periodic orbit in [f(1),1].

We now consider the bifurcations of stable periodic orbits occurring in the logistic map.

1.2 Bifurcations of Stable Periodic Orbits

A graph of Equation 1.2 is shown in Figure 3a for the case $\lambda = 2$, together with the diagonal map $x_{n+1} = x_n$. The point of intersection of the graph with the diagonal represents a fixed point of the mapping, the stability of this fixed point is determined by the gradient of the slope at the point of intersection i.e.:

$$\mu = | f'(x_0) |$$

if $\mu < 1$ then x_0 will be stable i.e. almost all points will be attracted to it. For $\mu > 1$ the point becomes unstable, the case $\mu = 1$ being denoted a point of criticality.

The question of what occurs after λ is increased beyond the critical value λ_c, at which point x_0 becomes unstable, is answered by reference to the graph of $f_2(x) = f \circ f(x)$. This 'second iterate' graph intersects the diagonal in two places at which the slope is less than unity for $\lambda > \lambda_c$ [24]. Thus exactly at the point at which x_0 becomes unstable two new stable fixed points are created, this is an example of a pitchfork bifurcation.

As λ is further increased, the period two fixed points bifurcate in an analogous way to give a stable period 4 orbit, the bifurcations continuing through period 8, 16, 32, ..., etc., until some critical value $\lambda = \lambda_\infty$ is reached at which the stable orbit has 'bifurcated to infinity'. At this point the system is chaotic, the

chaos persisting in the parameter range $[\lambda_\infty, 2]$ except for parameter 'windows' in which stable periodic motion exists. Figure 3b shows the bifurcation diagram of the logistic map, the first few pitchfork bifurcations are clearly visible together with the large stable period 3 window present in the chaotic regime.

The chaotic nature of the orbits lying to the right of the period 3 window is indicated by the following theorem due to Sarkovskii [10]:

Theorem. Order the integers as follows:

$$3 \succ 5 \succ 7 \succ 9 \succ \ldots$$
$$\ldots \succ 2.3 \succ 2.5 \succ 2.7 \succ \ldots$$
$$\ldots \succ 2^n.3 \succ 2^n.5 \succ \ldots$$
$$\ldots \succ \ldots \succ 2^m \succ \ldots \succ 8 \succ 4 \succ 2 \succ 1$$

Then if f is unimodal and has a point with period p, then it has a point with period q $\forall q \prec p$ in the sense of the above ordering.

Thus, after the point λ_3 at which the stable period 3 orbit appears, the map will have a countable infinity of unstable periodic orbits of every integer period. This result is related to a theorem due to Li-Yorke which indicates that 'period 3 implies chaos' [15].

1.3 Feigenbaum Sequences

For a given value of $\lambda = \lambda_n$ at which a 2^n stable periodic cycle has been created, the graph of:

$$f^{2^n}(x) = \overbrace{f \circ f \circ \ldots \circ f}^{2^n \text{ times}}(x) \quad ,$$

viewed locally near these fixed points is a rescaled copy of the original mapping. This observation led Feigenbaum to consider a renormalisation procedure for a general unimodal mapping which produced a universal scaling law for the parameters λ_n, characterised by a universal constant δ.

Denote by λ_n the parameter value at which there is a bifurcation from period 2^{n-1} to period 2^n, then the ratio:

$$\left(\frac{\lambda_n - \lambda_{n-1}}{\lambda_{n+1} - \lambda_n} \right) \to \delta \quad \text{as } n \to \infty,$$

where δ is a universal constant: $\delta = 4.66920$.

Stated another way:

$$\lambda_n = \lambda_\infty + A\,\delta^{-n} \quad ,$$

where λ_∞ is the parameter value for which the bifurcations accumulate and A is a constant.

The above scaling law is independent of the particular mapping used, exactly the same scaling applies to all unimodal maps.

1.4 Lyapunov Exponents

The general definition of Lyapunov exponents for a flow was given in the last chapter. Intuitively the exponents measure the mean expansion rate of trajectories of a system. For 1-D discrete maps there exists a single Lyapunov exponent which is defined as follows:

$$\sigma(x_0) = \lim_{N\to\infty} \frac{1}{N} \sum_{i=1}^{N} \ln \left| \frac{df}{dx_i} \right| \quad , \qquad \ldots (1.4)$$

where the x_i are the i-th iterates of the initial condition x_0. The exponent therefore measures the average slope of the map around an orbit. Except for a set of measure zero the exponent is independent of the initial condition, x_0.

A negative value of σ indicates an average slope less than unity and corresponds to stable periodic behaviour, whilst the case of σ positive implies an average slope greater than unity and corresponds to chaotic behaviour.

Numerically obtaining the graph of σ as a function of λ is difficult due to the fact that stable period orbits are dense in the parameter space, and hence the graph of σ is extremely complicated with an infinity of regions where σ is negative superimposed on the general upward trend of the curve with increasing λ [10]. Nevertheless, regions such as the stable period 3 window are clearly visible in numerical experiments of this type.

1.5 Probability Distributions

An invariant distribution for a mapping f is a function P(x) with the property:

$$P(x) = f\,P(x)\ , \qquad \ldots (1.5)$$

i.e. the function is mapped into itself by f.

We call P(x) a probability distribution if:

$$\int_{-\infty}^{\infty} P(x)\,dx = 1\ .$$

A unique probability distribution is singled out from the many invariant distributions for a given map by repeated iteration of the map. For the case of a stable periodic orbit of period n, P(x) will be a set of n delta functions (each weighted by 1/n) located at the values of the n fixed points of f^n. In the general case of a chaotic map we may find P(x) numerically by iterating the functional equation:

$$P(x)\,dx = P(x_1)\,dx_1 + P(x_2)\,dx_2$$

$$\text{or} \quad P(x) = \frac{P(x_1)}{(df/dx_1)} + \frac{P(x_2)}{(df/dx_2)} \quad , \qquad \ldots (1.6)$$

where x_1 and x_2 are the preimages of x.

Equation 1.6 can be solved exactly for one case of a chaotic logistic map. Considering the second form of the logistic map with $\lambda = 4$:

$$x_{n+1} = 4x_n\,(1-x_n) \quad , \qquad \ldots (1.7)$$

we make a change of variable:

$$\bar{x} = \left(\frac{2}{\pi}\right) \sin^{-1} \sqrt{x} \qquad \ldots (1.8)$$

Inserting Equation 1.8 into Equation 1.7 yields a so-called 'tent map':

$$\bar{x}_{n+1} = f(\bar{x}_n)$$

$$f(\bar{x}_n) = \begin{cases} 2\bar{x}_n & 0 \le \bar{x}_n < \frac{1}{2} \\ 2 - 2\bar{x}_n & \frac{1}{2} \le \bar{x}_n < 1 \end{cases} \qquad \ldots (1.9)$$

The probability distribution for the tent map is easily derived from Equation 1.6: $\bar{P}(\bar{x}) = 1$.

Now, using the property: $\overline{P(\bar{x})}\, d\bar{x} = P(x)\, dx$, we obtain the invariant distribution for Equation 1.7:

$$P(x) = \frac{1}{\pi} \left(x(1-x)\right)^{-\frac{1}{2}} . \qquad \ldots (1.10)$$

The existence of a continuous probability distribution for a map implies that the system is ergodic. In fact, the dynamics of the logistic map for $\lambda = 4$ are both mixing and ergodic.

Of particular interest is the existence of singularities in P(x). These occur for x = 0, and x = 1, for the above case and are due to the mapping of the maximum of the logistic curve (a point of infinite contraction) onto the points x = 1, and x = 0 (an unstable fixed point). The 'singularity points' x = 1, 0, form the boundaries of the chaotic motion in the interval. For the case $\lambda = 4$ (or $\lambda = 2$ for Equation 1.2) these points lie at the extremes of the interval, as the parameter is decreased, the singularity points move inwards and the chaotic motion is bounded in a smaller interval, this is clearly visible in Figure 3b. At a certain parameter value ($\lambda = 1.5436$), the maximum is mapped onto 3 points, the last of which is an unstable fixed point, producing 3 singularities in the probability distribution. As λ is decreased a little below this value, two disjoint regions are formed for P(x), the region of chaos has therefore bifurcated into two regions. This 'period-doubling' bifurcation continues and accumulates on λ_∞, in fact the parameter values at which the bifurcations occur form a Feigenbaum sequence and are characterised by the same 'Feigenbaum constant' δ.

1.6 Summary

This section has dealt with the dynamics of 'unimodal' maps with particular reference to the logistic map. Many qualitative features of the system are similar to those described for flows in the last chapter, in particular, the period doubling cascade to chaos is also a common occurrence in continuous dynamical systems.

The main difference between the 1-D systems described above and the dynamics of flows is that global attraction to a strange attractor is here replaced by singularities in the probability distribution of the map which form sharp boundaries for the chaotic regions. Such bounding of chaotic regions by singularities is also found for a 2-dimensional map to be described in Chapter 5. The unimodal maps are also unique in that a universal scaling is associated with their bifurcation properties, no such universality is apparent in continuous systems.

In the remainder of this chapter two examples of chaotic 2-D discrete systems will be described.

2.0 Examples of 2-D Discrete Systems

2.1 The Hénon Map

Hénons map [16] is defined by the equations:

$$x_{n+1} = y_n + 1 - a\,x_n^2 \qquad \ldots (2.1)$$
$$y_{n+1} = bx_n \ ,$$

where a and b are constants.

During one iteration of the above, the mapping contracts area by a factor $|J|$ where:

$$J = -b \quad , \qquad \ldots (2.2)$$

is the Jacobian of the mapping.

For x_n large, solutions of Equation 2.1 are unbounded, however, for x_n, y_n, within some finite region of the origin, solutions converge torwards an attractor.

Two fixed points of the mapping exist provided:

$$a > a_0 = \frac{-(1-b)^2}{4} \quad , \qquad \ldots (2.3)$$

one of these fixed points is always unstable whilst the other is stable for 'a' in the interval:

$$a_0 = \frac{-(1-b)^2}{4} < a < \frac{3(1-b)^2}{4} = a_1 \quad , \qquad \ldots (2.4)$$

For $a > a_1$ the fixed point is observed to undergo a cascade of period doubling bifurcations until some accumulation point a_∞ after which a strange attractor appears to exist for 'a' in some finite interval (a_∞, a_2). When 'a' is further increased from a_2 most orbits escape to infinity.

Although the presence of a strange attractor for $a \in (a_\infty, a_2)$ is strongly indicated by numerical iterations of the equations (typically, the chaotic motion is seen to persist for 5 million iterates) it has not proved possible so far to prove the chaotic nature of the Hénon map in this region. In fact, Newhouse [15] has suggested that the chaotic motion observed is really the motion near a very large period sink.

For the singular case b = 0, Equations 2.1 reduce to the logistic map for which chaotic motion is known to exist, it could

be argued that the logistic map provides a good approximation to the Hénon map along its unstable manifold, and hence that strange attractors would be expected to exist for some range of 'a's. However, the link between the theory of the one dimensional system and the Hénon map has not been made and the question of the existence of strange attractors for the Hénon system remains an open question.

The difficulty in proving chaotic motion for the Hénon map is related to the fact that the attracting region has a fold due to the unstable manifolds folding back on themselves. Therefore, a hyperbolic structure cannot be defined for the system as stable and unstable manifolds will not in general intersect transversely (a 'stable foliation' of the system does not exist).

This situation pertains also to the Duffing system considered in the last chapter, the unstable manifolds of which have this folding structure. Thus, the existence of a strange attractor for the Duffing equations also remains an open question.

The constant area contraction property of the system indicates that areas will be contracted down to one dimensional curves. When the attracting region is observed numerically, the attractor is seen to consist of an infinite number of concentric curves having an apparently 'fractal' structure. The structure of the strange attractor corresponds to the cross product of a line with a 'Cantor set'.

The fractal dimension of the Hénon map has been numerically determined to be: $d = 1.202$ for $a = 1.2$, $b = 0.3$, i.e. the attractor 'almost fills' an area. Orbits on the attractor move

between these 'Cantor Leaves' and exhibit exponential divergence of initially close orbits. Given the difficulties in proving chaos in the Hénon system therefore, there would appear to be strong numerical evidence that the dynamics on the attractor are truely chaotic.

2.2 The Chirikov Map

The Chirikov, or 'standard' map introduced by B. Chirikov [8] is an example of an area preserving 2-dimensional map i.e. a mapping with unit Jacobian. The map, which can be written:

$$I_{n+1} = I_n + K \sin \theta_n \ ,$$
$$\theta_{n+1} = \theta_n + I_{n+1} \ , \ \text{Mod } 2\pi \qquad \ldots (2.5)$$

K = constant.

is derived from a Hamiltonian system and can be viewed as the response of a pendulum to a sequence of short 'kicks'.

In the above equations, K plays the role of a perturbation parameter where the case K = 0 corresponds to an integrable Hamiltonian system with a phase plane consisting of concentric circles filled with dense irrational orbits.

As K is increased, resonant KAM surfaces are destroyed giving rise to rings of elliptic and hyperbolic fixed points as in the continuous Hamiltonian case. For the mapping to preserve area, the stable and unstable manifolds of the hyperbolic points must intersect, in general they intersect "transversely" giving rise to regions of stochasticity bounded by closed KAM curves.

Within these stochastic layers, orbits diverge exponentially, and the dynamics may be modelled as a diffusion process.

Finally, as K is further increased, more KAM curves are destroyed until global stochasticity ensues.

The study of perturbed Hamiltonian systems, therefore, is greatly simplified by the reduction to an area preserving mapping such as Equation 2.5.

Chirikov has labelled the above equations 'the standard map' because of its ubiquitous nature when considering perturbed continuous, and discrete, Hamiltonian systems. The Chirikov map appears in considerations of, among other things: perturbed pendulums, particles in a magnetic mirror trap, atomic-lattices, and balls bouncing on an oscillating table.

CHAPTER 4

DUFFINGS EQUATION

1.0 Background and Aim

In this chapter we consider the dynamical behaviour of Duffings Equation with negative linear stiffness:

$$\ddot{x} + \delta\dot{x} - \beta x + \alpha x^3 = f \cos \omega t \qquad \ldots (1.1)$$

where δ is the coefficient of damping, f, the strength of forcing, and ω, the forcing frequency.

The numerical results due to Holmes, described in the last chapter, strongly suggest that a region of chaotic motion exists in the 'window' $f\varepsilon(1.08, 2.5)$, preceded by a period doubling cascade, with global attraction to a limit cycle for $f > 2.5$.

In the following we shall assume that the system is indeed chaotic for the above values of f, and, where appropriate, set the other system parameters equal to the values given by Holmes, i.e. $\delta = 1$, $\alpha = 100$, $\beta = 10$, $\omega = 3.76$.

The aim of the work in this chapter will be to use approximate analytical solutions of the system in an attempt to reduce the complicated dynamics of the Duffing equation to a simple difference map. The motivation for this type of approach stems principally from work by Rowlands et al. on the analytic derivation of Poincaré maps ([4], [32]), and also from Holme's suggestion of a simple map for the Duffing system [19].

The underlying method will be to solve the equations of motion approximately, using perturbation theory, and hence derive a Poincaré map for the system by defining a discretised time: $t_n = n\tau$, where τ is a suitable time interval, and relating the expressions for the variables at $t_n = n\tau$ to those at $t_{n+1} = (n+1)\tau$. The resulting Poincaré map, being derived from a perturbation scheme, cannot be expected to exhibit chaotic behaviour. However, the assumption will be that the map does contain information about the chaotic system and that extra input in the form of a global consideration of the system will lead to the true chaotic map. This is tantamount to assuming that the Poincaré map of a system is in some sense structurally stable. Thus the approximate map, plus global information, will exhibit at least the main features of a map derived from the exact solutions of the equations.

The nature of the additional global information will, in general, depend on the details of the particular system. In the case of the Lorenz equations, for example, Rowlands [31] was able to derive one branch of the Lorenz map analytically and then used a symmetry argument to append the opposite branch. A similar scheme will be followed for the Duffing equations. The resulting map will be found to be quite different in form from a Lorenz-type map, although superficially the orbital details of both systems, involving trajectories spiralling between two fixed points, would appear to be quite similar.

2.0 Analytical Results

The phase plane for Duffing's equations in the absence of damping and forcing (Figure (2c)) indicates three types of qualitively different behaviour, and provides a basis for the perturbation analysis. The homoclinic orbit, or separatrix, separates two symmetrical regions of periodic motion about fixed points at $\pm \sqrt{\beta/\alpha}$ from self-symmetrical periodic orbits on the outside. It will be recalled from the previous chapter that the homoclinic orbit breaks under perturbation and that the subsequent chaotic motion is confined to a small region about the perturbed stable and unstable manifolds. There is also a symmetry breaking at the homoclinic orbit between the self-symmetric outside orbits and the inner orbits. It would therefore seem reasonable to base our analysis on orbits inside (but away from) the separatrix, and outside the separatrix and use a 'global' argument to fit the two resulting maps together. The symmetry breaking presents a difficult problem as any perturbation analysis would have to be around one or other of the fixed points, the problem could be overcome by considering the derived Poincaré map to be in variables common to both inner orbits and outer ones, this will be the strategy adopted later in the analysis. As a first step we apply ordinary perturbation theory to one of the inner orbits.

2.1 Multiple Scales Method

In order to obtain an approximate solution of Duffings equation, the method of multiple scales (Appendix C) is applied to the equations:

$$\ddot{x} - \beta x + \alpha x^3 = f \cos \omega t - \delta \frac{dx}{dt}$$

The origin of the system is first moved to the (unperturbed) fixed point at $(+ \sqrt{\beta/\alpha},\ 0)$, thus the substitution

$$x \to X + \sqrt{\frac{\beta}{\alpha}}, \quad \text{gives}$$

$$\ddot{X} + 2\beta X + \alpha X^3 + 3\sqrt{\alpha\beta}\, X^2 = f \cos \omega t - \delta \dot{X} \qquad \ldots (2.1)$$

The new variable, and derivatives thereof, are now expanded according to the method of multiple scales:

$$X \to \varepsilon x_1 + \varepsilon^2 x_2 + \ldots . , \quad t_n = \varepsilon^n t$$

$$\frac{d}{dt} \to D_0 + \varepsilon D_1 + \ldots . , \quad \frac{d^2}{dt^2} \to D_0^2 + 2\varepsilon D_0 D_1 + \ldots .$$

f is taken to be of order ε^3, and δ to be of the order ε^2, in order to bring both the forcing and damping in together at third order.

Substituting the expansions into (2.1) gives for first order (ε):

$$\frac{d^2 x_1}{dt_0^2} = - 2\beta x_1 := - \lambda^2 x_1 \quad (\lambda^2 = 2\beta),$$

with solution: $x_1 (t_0) = C\, e^{i\lambda t_0} + \overline{C}\, e^{-i\lambda t_0}$. $\qquad \ldots (2.2)$

The second order (ε^2) equation is:

$$\frac{d^2 x_2}{dt_0^2} + 2 \frac{d^2 x_1}{dt_0 dt_1} = - \lambda^2 x_2 - 3 \sqrt{\alpha\beta}\, x_1^2,$$

or $\quad \mathcal{L} x_2 = - 2 \frac{d}{dt_1} [\, i \lambda C\, e^{i\lambda t_0} - i \lambda \overline{C}\, e^{-i\lambda t_0} \,] -$

$$- 3 \sqrt{\alpha\beta} [\, C^2 e^{2i\lambda t_0} + \overline{C}^2 e^{-2i\lambda t_0} + 2 C\overline{C} \,],$$

where $\hat{L} = \left[\frac{d^2}{dt_0^2} + \lambda^2 \right]$,

this gives

$$\hat{L}x_2 = -2i\lambda e^{i\lambda t_0} \frac{dC}{dt_1} - 3\sqrt{\alpha\beta}\left[C^2 e^{2i\lambda t_0} + \bar{C}\bar{C} \right] + c.c.$$

(c.c. = complex conjugate)

... (2.3)

The criterion for the elimination of secular terms is then simply: $\frac{dC}{dt_1} = 0$, i.e. C does not depend on the timescale t_1.

Eliminating the above term leaves the following equation for x_2:

$$\hat{L}x_2 = -3\sqrt{\alpha\beta}\, e^{2i\lambda t_0} C^2 - 3\sqrt{\alpha\beta}\, \bar{C}\bar{C} + c.c.$$

with particular solution:

$$x_2(t_0) = \frac{\sqrt{\alpha\beta}}{\lambda^2} C^2 e^{2i\lambda t_0} - \frac{3\sqrt{\alpha\beta}}{\lambda^2} \bar{C}\bar{C} + c.c. \qquad \text{... (2.4)}$$

After eliminating derivatives in t_1, the third order (ε^3) equation gives:

$$\hat{L}x_3 = -2\frac{d^2 x_1}{dt_0 dt_2} - 6\sqrt{\alpha\beta}\, x_1 x_2 - \alpha x_1^3 + f\cos\omega t - \delta\frac{dx_1}{dt_0}.$$

Inserting the expressions for x_1 and x_2, and ordering ω to be: $\omega = \lambda + \varepsilon^2\bar{\omega}$ gives:

$$Lx_3 = -2\frac{d}{dt_2}\left[i\lambda C e^{i\lambda t_0} \right] - 6\sqrt{\alpha\beta}\left(\frac{\sqrt{\alpha\beta}}{\lambda^2}\left[C^3 e^{3i\lambda t_0} - 5 C^2 \bar{C} e^{i\lambda t_0} \right] \right) - \alpha\left[C^3 e^{3i\lambda t_0} + 3 C^2 \bar{C} e^{i\lambda t_0} \right] + \frac{f}{2}\left[e^{i\lambda t_0} e^{i\bar{\omega} t_2} \right] - \delta i\lambda C e^{i\lambda t_0} + c.c. \qquad \ldots (2.5)$$

where the product of the frequency shift with t_0 has been written as: $\bar{\omega}\, t_2$.

At this stage we are not interested in the solution of (2.5), but rather the consistency condition given by the criterion for the elimination of secular terms. Thus, considering only the terms in $e^{i\lambda t_0}$ and demanding that these vanish, gives the following equation for C:

$$2 i\lambda \frac{dC}{dt_2} = 12\alpha C^2 \bar{C} + \frac{f}{2} e^{i\bar{\omega} t_2} - \delta i\lambda C, \qquad \ldots (2.6)$$

with a similar expression for the conjugate $\bar{C}$.

We now express C as $C = \rho e^{i\phi}$, $(\bar{C} = \rho e^{-i\phi})$ where ρ is an amplitude and ϕ a phase. Substituting these expressions into (2.6) gives:

$$2 i\lambda \left[\frac{d\rho}{dt} + i\rho \frac{d\phi}{dt} \right] = 12\alpha\rho^3 - \delta i\lambda\rho + \frac{f}{2} e^{i(\bar{\omega} t - \phi)},$$

where 't_2' has been written as 't' for convenience.

Separating real and imaginary parts gives:

$$\frac{d\rho}{dt} = \frac{f}{4\lambda} \operatorname{Sin}(\bar{\omega} t - \phi) - \frac{\delta\rho}{2}$$

$$\rho \frac{d\phi}{dt} = -\frac{6\alpha\rho^3}{\lambda} - \frac{f}{4\lambda} \operatorname{Cos}(\bar{\omega} t - \phi)$$

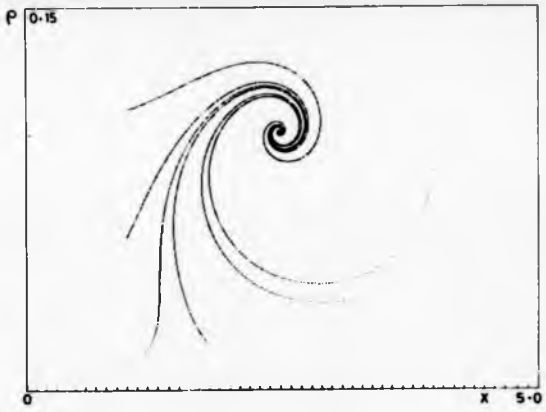

Figure 4a : Phase Portrait for Multiple-Scales Solution

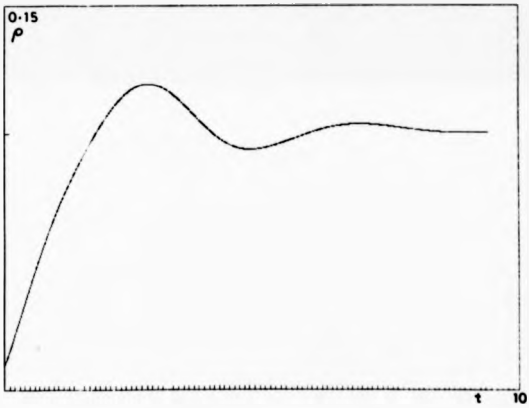

Figure 4b : Time Dependance of Multiple-Scales Solution

Defining a new variable $X = \bar{\omega}t - \phi$, $\dot{X} = \bar{\omega} - \dot{\phi}$ gives finally:

$$\frac{d\rho}{dt} = \frac{f}{4\lambda} \sin X - \frac{\delta\rho}{2}$$

$$\rho \frac{dX}{dt} = \frac{6\alpha\rho^3}{\lambda} + \frac{f}{4\lambda} \cos X + \rho\bar{\omega} \; . \qquad \ldots (2.7)$$

A typical phase portrait for Equation (2.7) obtained numerically, is shown in Figure (4a) and clearly indicates the fact that a stable fixed point exists for the system. The fixed point does not lose its stability as the forcing 'f' is increased. This result agrees with that obtained by Nayfeh [28].

Considering the expression for $x_1 = \rho \cos(\lambda t + \phi) = \rho \cos(\omega t - X)$, it is clear than an asymptotic fixed point in ρ and X implies that our perturbation solution asymptotically converges to a limit cycle given by:

$$x(t) = \rho_0 \cos(\omega t - X_0) + (\text{order } \varepsilon^2)$$

As the amplitude converges to ρ_0, the original frequency λ is entrained to the frequency of the driving term ω, this mutual convergence of amplitude, frequency, and phase, causes the amplitude to oscillate in time around its final value as shown in Figure (4b). The fact that the amplitude repeatedly overshoots the final equilibrium would seem to imply that it is the interaction between the 'inside' and 'outside' orbits which produces the final state. It is evident, therefore, that the perturbation method picks up the limit cycle which is known to exist for f up to $f_c = 0.95$, however, it fails to reproduce the period doubling cascade for $f > f_c$. It will be recalled that for $f = 0.79$, the stable and unstable

manifolds intersect and give rise to a 'Smale-horseshoe' Ω_s which persists for a large range of subsequent values of f. It is significant that the set Ω_s exists for values of f for which a globally attracting limit cycle exists but, being a non-attracting set of measure zero, does not influence the converging orbits from outside the separatrix. It is only when the limit cycle is close to Ω_s that period doubling to chaos occurs. It would appear, therefore, that Ω_s in some way causes this period doubling behaviour. A simple explanation of the perturbation result could therefore be that, in the physical system, a limit cycle is forced through Ω_s as f is increased (accompanied by symmetry breaking at the separatrix) and that the combination of Ω_s and the global attraction of the limit cycle produces the period doubling to chaos. As f is further increased the (now self-symmetric) limit cycle is expanded out of Ω_s and forms a globally attracting cycle again. Thus the perturbation method which is unable to 'pick up' Ω_s (or the symmetry breaking) gives the limit cycle solution and nothing else.

The scenario sketched above of a limit cycle passing through Ω_s is obviously a great simplification of the true situation, in particular the smooth period doubling of the limit cycle close to Ω_s is difficult to explain, however, it seems plausible that the overall idea may be correct, and that this provides an insight into the perturbation solution.

Returning to Equation (2.7) we now proceed to construct a Poincaré map for the amplitude ρ. The equations cannot be solved exactly, however, for a given forcing value, we may use a multiple scale analysis around the fixed point ρ_0 to give an approximate expression for the amplitude as a function of time. We begin by

reducing Equations (2.7) to a single second order equation in the variable ρ. We write the equations as:

$$\dot{\rho} = \frac{f}{4\lambda} \operatorname{Sin} X - \frac{\delta\rho}{2} . \qquad \ldots (2.8)$$

$$\rho\dot{X} = \rho \left[\frac{6\alpha\,\rho^2}{\lambda} + \bar{\omega} \right] + \frac{f}{4\lambda} \operatorname{Cos} X . \qquad \ldots (2.9)$$

Differentiating (2.8) gives:

$$\ddot{\rho} = \frac{f}{4\lambda} \dot{X} \operatorname{Cos} X - \frac{\delta\,\dot{\rho}}{2} \qquad \ldots (2.10)$$

Substituting (2.9) into (2.10) yields

$$\ddot{\rho} = \frac{f}{4\lambda} \left[\frac{6\alpha\,\rho^2}{\lambda} + \bar{\omega} \right] \operatorname{Cos} X + \frac{f^2}{16\lambda^2\,\rho} \operatorname{Cos}^2 X - \frac{\delta\,\dot{\rho}}{2} \qquad \ldots (2.11)$$

Using the fact that $\operatorname{Sin} X = \frac{4\lambda}{f} \left[\dot{\rho} + \delta\rho/2 \right]$ from (2.8),

$\operatorname{Cos} X = \left[1 - \frac{16\lambda^2}{f^2} \left(\dot{\rho} + \delta\rho/2 \right)^2 \right]^{\frac{1}{2}}$, gives:

$$\rho\ddot{\rho} = \rho \left(A\rho^2 + B \right) \left(C - \left(\dot{\rho} + D\rho \right)^2 \right)^{\frac{1}{2}} + \left(C - \left(\dot{\rho} + D\rho \right)^2 \right) - D\,\rho\dot{\rho} , \qquad \ldots (2.12)$$

where $A = \frac{6\alpha}{\lambda}$, $B = \bar{\omega}$, $C = \frac{f^2}{16\lambda^2}$, $D = \frac{\delta}{2}$

We eliminate the square root in (2.12) by rearranging terms and squaring both sides to give:

$$\left[\rho\ddot{\rho} + D\rho\dot{\rho} + (\dot{\rho})^2 + 2D\,\dot{\rho}\rho + D^2\rho^2 - C \right]^2 = \rho^2 \left(A\rho^2 + B \right)^2 \left(C - \left(\dot{\rho} + D\rho \right)^2 \right) .$$

Writing $\rho + \rho_0 + \bar{\rho}$, where ρ_0 is the fixed point of the equation yields, finally, the following equation for $\bar{\rho}$ (the bars are dropped for convenience):

$$[\,(\rho_0+\rho)\ddot{\rho}\,]^2 + A_1(\rho_0+\rho)^2\dot{\rho}^2 + \dot{\rho}^4 + A_2(\rho_0+\rho)^4 +$$
$$+ A_3(\rho_0+\rho)^2\ddot{\rho}\dddot{\rho} + 2(\rho_0+\rho)\dot{\rho}^2\ddot{\rho} + A_4(\rho_0+\rho)^3\ddot{\rho} +$$
$$+ C^2 + A_5(\rho_0+\rho)\ddot{\rho} + A_6(\rho_0+\rho)\dot{\rho}^3 + A_7(\rho_0+\rho)^3\dot{\rho} +$$
$$+ A_8(\rho_0+\rho)\dot{\rho} + A_9(\rho_0+\rho)^2\dot{\rho}^2 + B_1\dot{\rho}^2 +$$
$$+ B_2(\rho_0+\rho)^2 = B_3(\rho_0+\rho)^6 + B_4(\rho_0+\rho)^6\ddot{\rho}^2 +$$
$$+ B_5(\rho_0+\rho)^7\dot{\rho} + B_6(\rho_0+\rho)^8 + B_7(\rho_0+\rho)^4\dot{\rho}^2 +$$
$$+ B_8(\rho_0+\rho)^5\dot{\rho}\,. \qquad \ldots (2.13)$$

Where the A_1, B_1 are given in Appendix A.

We now solve this equation, up to second order, by the method of multiple scales, thus we write:

$$\rho + \varepsilon\rho_1 + \varepsilon^2\rho_2 + \ldots \qquad \frac{d}{dt} + D_0 + \varepsilon D_1 + \ldots \quad \text{etc.}$$

Ordering out the damping, at first order, we obtain by inspection of terms:

$$\ddot{\rho}_1 = -\theta^2\rho_1$$

where

$$\theta^2 = \left| \frac{(-6\rho_0^5 B_3 - 8\rho_0^7 B_6 + 4\rho_0^3 A_2 + 2B_2\rho_0)}{(A_4\rho_0^3 + A_5\rho_0)} \right|$$

with solution

$$\rho_1 = K\, e^{i\theta t} + \bar{K}\, e^{-i\theta t}$$

The second order equation gives:

$$\begin{aligned} L\rho_2 = \frac{1}{\left(A_4 \rho_0^3 + A_5 \rho_0 \right)} \Big[& - \rho_0^2 \left(\theta^4 K^2 e^{2i\theta t} + \theta^4 K\bar{K} \right) + \\ & + \bar{A}_1 \left(- \theta^2 K^2 e^{2i\theta t} + \theta^2 K\bar{K} \right) + \bar{A}_2 \left(K^2 e^{2i\theta t} + K\bar{K} \right) + \\ & + \bar{A}_3 \left(- i\, \theta^3 K^2 e^{2i\theta t} \right) + \bar{A}_4 \left(- \theta^2 K^2 e^{2i\theta t} - \theta^2 K\bar{K} \right) + \\ & + \bar{A}_5 \frac{d}{dt_1} \left(i\, \theta K e^{i\theta t} \right) + \bar{A}_6 \left(i\, \theta K e^{i\theta t} \right) + \\ & + \bar{A}_7 \left(i\, \theta K^2 e^{2i\theta t} \right) + \text{c.c.} \Big] \end{aligned} \qquad \ldots (2.14)$$

where $\hat{L} = \left[\frac{d^2}{dt_0^2} + \theta^2 \right]$,

and the $\bar{A}_i$ are given in Appendix A.

The criterion for the elimination of secular terms gives:

$$\bar{A}_5 \frac{dK}{dt_1} + \bar{A}_6 K = 0,$$

with solution

$$K(t_1) = \rho e^{-\eta t_1} \ , \ \eta = \frac{\bar{A}_6}{\bar{A}_5} .$$

The solution of Equation (2.14) is then:

$$\rho_2(t_0) = \left(\alpha + i\beta \right) K^2 e^{2i\theta t_0} + K\bar{K} + \text{c.c.}$$

where

$$\alpha = \frac{1}{\left(A_4 \rho_0^2 + A_5 \rho_0 \right)} \left\{ \frac{\rho_0^2 \theta^2}{3} + \frac{\bar{A}_1}{3} - \frac{\bar{A}_2}{3\theta^2} + \frac{\bar{A}_4}{3} \right\} ,$$

$$\beta = \frac{1}{\left(A_4 \rho_0^2 + A_5 \rho_0 \right)} \left\{ \frac{\bar{A}_3 \theta}{3} - \frac{\bar{A}_7}{3\theta} \right\} ,$$

$$\gamma = \frac{1}{\left(A_4 \rho_0^2 + A_5 \rho_0 \right)} \left\{ - \rho_0^2 \theta^2 + \bar{A}_1 + \frac{\bar{A}_2}{\theta^2} - \bar{A}_4 \right\} .$$

Thus, finally, we have the following second order expression for $\rho(t)$:

$$\rho(t) = \rho_0 + 2Pe^{-\eta t} \cos \theta t + 2P^2 e^{-2\eta t} \left[\alpha \cos 2\theta t - \beta \sin 2\theta t \right] + 2\gamma P^2 e^{-2\eta t} . \qquad \ldots (2.15)$$

We now proceed to construct a Poincaré map from Equation (2.15). The determination of the Poincaré map is not unique, however, in this case we shall follow the Lorenz-map construction by considering the maximum amplitude $\rho_n = \rho(n\tau)$ where τ is defined such that $\dot{\rho}(n\tau) = 0$ to first order. The result will be a first order one-dimensional map relating ρ_n to ρ_{n+1}.

To first order we have that:

$$\dot{\rho}(t) = - 2Pe^{-\eta t} \theta \sin \theta t ,$$

thus $\dot{\rho}(t_n) = 0 \Rightarrow t_n = \frac{2n\pi}{\theta}$, where we take the factor 2π to give successive maxima (or minima) of $\rho(t)$.

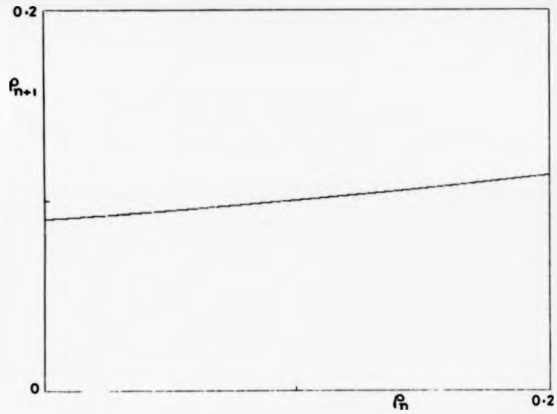

Figure 4c : Multiple-Scales Poincaré Map

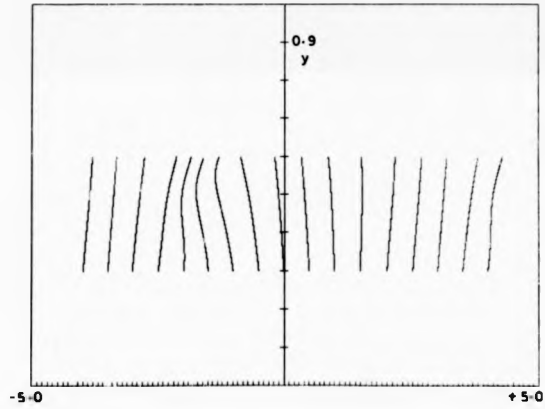

Figure 4d : Phase Portrait for Integral Method Solutions

Inserting t_n into (2.15) gives:

$$\rho_n = \rho_0 + 2P\, e^{\frac{-2n\pi\eta}{\theta}} + \alpha 2\, P^2\, e^{\frac{-4n\pi\eta}{\theta}} + 2P^2\gamma\, e^{\frac{-4n\pi\eta}{\theta}}$$

$$= \rho_0 + 2P\, e^{\frac{-2n\pi\eta}{\theta}} + 2P^2\, e^{\frac{-4n\pi\eta}{\theta}} (\alpha + \gamma) ,$$

and

$$\rho_{n+1} = \rho_0 + 2P\, e^{\frac{-2n\pi\eta}{\theta}} e^{\frac{-2\pi\eta}{\theta}} + 2P^2 (\alpha + \gamma) e^{\frac{-4n\pi\eta}{\theta}} e^{\frac{-4\pi\eta}{\theta}} .$$

Expressing ρ_{n+1} in terms of ρ_n to first order gives:

$$(\rho_{n+1} - \rho_0) = e^{\frac{-2\pi\eta}{\theta}} (\rho_n - \rho_0) .$$

Using the fact that, to first order, $(\rho_n - \rho_0) = 2Pe^{\frac{-2n\pi\eta}{\theta}}$, we write $(\rho_n - \rho_0)^2 = 4P^2 e^{\frac{-4n\pi\eta}{\theta}}$, and obtain, finally:

$$\rho_{n+1} = \rho_0 + e^{\frac{-2\pi\eta}{\theta}} (\rho_n - \rho_0) + \frac{(\alpha + \gamma)}{2} e^{\frac{-4\pi\eta}{\theta}} (\rho_n - \rho_0)^2 .$$

... (2.16)

Inserting the value f = 1.5, for which the real system is chaotic, giving $\theta = 1.534$, $\eta = 0.529$, $\alpha = 5.998$, $\beta = 5.641$, we obtain a typical graph of ρ_n against ρ_{n+1} shown in Figure (4c). Apart from the fact that the map has a fixed point at ρ_0, which we would of course expect, it is evident that the strong contraction towards ρ_0 has 'flattened' the curve, and that information from outside the homoclinic orbit is needed to give a globally defined map. For this particular value of 'f' the limit cycle is very close to the homoclinic orbit and we would thus expect that our perturbation analysis has broken down, thus the flatness of the curve is in this case spurious. However, the underlying philosophy

of what follows will be that a global 1-D map can be defined for the system, perturbation methods will always give a limit cycle, i.e. a stable fixed point for the Poincaré map, however, we shall use global considerations to 'break' the fixed point assuming that the 1-D map is analytic and varies smoothly with the parameter f.

Although the preceding analysis has produced a 1-D amplitude map, the method is limited in that it cannot account for symmetry breaking, being a local analysis around one of the fixed points, and also, the behaviour of 'outside' orbits cannot be defined. It is also clear that a 'fundamental' global map cannot be based on the frequency of oscillation to the fixed point, i.e. the timestep: $\frac{2\pi}{\theta}$. To attempt to overcome these difficulties, a new perturbation method, the 'integral method' (Appendix C) will now be applied to the unperturbed orbits of the system.

2.2 The Integral Method

The integral method, as used here, is based on perturbation about solutions to a Hamiltonian system.

We thus begin by considering Duffing's equation in the absence of damping and forcing. The system is then Hamiltonian with:

$$H = \frac{V^2}{2} - \frac{\beta x^2}{2} + \frac{\alpha x^4}{4}, \quad \left(V = \frac{dx}{dt} \right).$$

Solving this system for orbits inside the separatrix yields the solutions:

$$x(t) = \sqrt{\frac{2\beta}{\alpha}} \frac{1}{(2-k^2)^{\frac{1}{2}}} \, dn \left[\frac{\sqrt{\beta}}{(2-k^2)^{\frac{1}{2}}} (t + \phi) \right], \; k^2 \in [0,1],$$

where dn( ) is a Jackobian elliptic function, k^2 is the modulus, and the product: $\frac{\sqrt{\beta}}{(2-k^2)^{\frac{1}{2}}}\,\phi$ is a phase (ϕ has the dimensions of time) [1].

Similarly, solving the system for 'outside' orbits yields the elliptic solution:

$$x(t) = \sqrt{\frac{2\beta}{\alpha}}\,\frac{k}{(2k^2-1)^{\frac{1}{2}}}\,\mathrm{cn}\left[\frac{\sqrt{\beta}}{(2k^2-1)^{\frac{1}{2}}}\,(t+\phi)\right],\quad k^2 \in \left[\tfrac{1}{2}, 1\right],$$

here, ϕ again has the dimensions of time.

2.2.1 The Outside Orbits

We concentrate first on the outside solutions, writing $x(t) = A\,\mathrm{cn}\,(\lambda(t+\phi))$, where

$$A = \sqrt{\frac{2\beta}{\alpha}}\,\frac{k}{\sqrt{2k^2-1}},\quad \lambda = \frac{\sqrt{\beta}}{\sqrt{2k^2-1}}.$$

This exact solution could, in principle, be derived from a perturbation analysis around the origin of the system, thus the expression for the amplitude A is in some sense equivalent to the expression obtained from an infinite order expansion in some quantity ρ, similar to the expansion obtain in the last section.

The advantage of the integral method, then, is that we may use the relatively complicated form of A to define our Poincaré map by assuming k to be a slowly varying quantity which is a 'simple' function of t_1. The disadvantage of the method, as will be seen below, is that assumptions have to be made about the slowly varying frequency λ, and phase $\lambda\phi$, to avoid excessively complicated consistency equations. Applying the integral method to the outside solution yields:

$$\int_0^\tau \frac{d\psi^2}{dt_1}\, dt_0 = f \int_0^\tau \cos \omega t_0\ \psi\, dt_0 - \delta \int_0^\tau \psi^2\, dt_0 \ . \qquad \ldots (2.17)$$

where τ, the period of the unperturbed orbit, is given by $\tau = \frac{4K(k^2)}{\lambda}$ where $K(k^2)$ is the complete elliptic integral of the first kind, and $\psi = \frac{dx}{dt_0} = -\lambda A\ sn\{\lambda(t+\phi)\}\ dn\{\lambda(t+\phi)\}$.

We now assume a slow time variation in the amplitude A, the frequency λ, and the phase $\lambda\phi$. The integral on the left hand side of (2.17) then becomes:

$$\frac{d\psi^2}{dt_1} = \frac{dk}{dt_1}\left[\frac{d(\lambda^2A^2)}{dk}\, sn^2\theta\, dn^2\theta + \lambda^2 A^2 \frac{d\theta}{dk}\frac{d\, sn^2\theta\, dn^2\theta}{d\theta}\right] +$$

$$+ \lambda \frac{d\phi}{dt_1}\frac{d\lambda^2}{d\theta} A^2\, sn^2\theta\, dn^2\theta \ , \qquad \theta = \lambda(t+\phi)$$

The integral of the last term vanishes over a period, the integrand being an exact differential. The integral of the first term gives:

$$\frac{dk}{dt_1}\frac{d(\lambda^2A^2)}{dk}\int_0^{4K/\lambda} sn^2\theta\, dn^2\theta\, dt =$$

$$= \frac{dk}{dt_1}\frac{d(\lambda^2A^2)}{dk}\frac{4}{\lambda}\int_0^K \left(sn^2\theta - k^2\, sn^4\theta\right) d\theta$$

Performing the integration we obtain:

$$\frac{dk}{dt_1}\frac{d(\lambda^2A^2)}{dk}\left\{\frac{4(K-E)}{\lambda k^2} - \frac{8(1+k^2)(K-E)}{3\lambda k^2} + \frac{4K}{3\lambda}\right\}$$

where $E = E(k^2)$ is the complete elliptic integral of the second kind.

The last integral gives:

$$\lambda^2 A^2 \int_0^{4K/\lambda} \frac{d\theta}{dk} \frac{d\ sn^2\theta\ dn^2\theta}{d\theta}\, dt \quad , \quad \theta = \lambda(t+\phi)$$

$$= \lambda^2 A^2 \int_{\lambda\phi}^{4K+\lambda\phi} \frac{d\lambda}{dk} \frac{\theta}{\lambda^2}\, dsn^2\theta\ dn^2\theta =$$

$$= A^2 \frac{d\lambda}{dk} \left\{ \theta\ sn^2\theta\ dn^2\theta \Big|_{\lambda\phi}^{4K+\lambda\phi} - \int_{\lambda\phi}^{4K+\lambda\phi} sn^2\theta\ dn^2\theta\ d\theta \right\} \text{ by parts.}$$

The integral on the right hand side has been solved above, thus we have for the second term:

$$A^2 \frac{d\lambda}{dk} \left[4K\ sn^2\ \lambda\phi\ dn^2\ \lambda\phi - \left\{ \frac{4(K-E)}{k^2} - \frac{8(1+k^2)(K-E)}{3k^2} + \frac{4K}{3} \right\} \right] .$$

Combining the terms we have for the left hand side of (2.17):

$$\frac{dk}{dt_1} \left[\left\{ \frac{4(K-E)}{\lambda k^2} - \frac{8(1+k^2)(K-E)}{3\lambda k^2} + \frac{4K}{3\lambda} \right\} \left[\frac{d(\lambda^2 A^2)}{dk} - \lambda A^2 \frac{d\lambda}{dk} \right] + \right.$$

$$\left. + 4A^2 \frac{d\lambda}{dk} K\ sn^2(\lambda\phi)\ dn^2\ (\lambda\phi) \right] . \qquad \ldots (2.18)$$

Turning our attention now to the right hand side of (2.17) we have:

$$f \int_0^{\tau} \cos \omega t_0 \frac{dx_0}{dt_0}\, dt_0 - \delta \int_0^{\tau} \left(\frac{dx_0}{dt_0} \right)^2 dt_0 .$$

The damping integral has been solved above, thus we have:

$$-\delta\lambda^2A^2\left\{\frac{4(K-E)}{\lambda k^2}-\frac{8(1+k^2)(K-E)}{3\lambda k^2}+\frac{4K}{3\lambda}\right\}$$

Finally, we consider the forcing integral:

$$f\int_0^{\tau}\text{Cos }\omega t_0\,\frac{dx_0}{dt_0}\,dt_0 = f\int_0^{\tau}\text{Cos }\omega t_0\,dx_0 =$$

$$= f\left[\text{Cos }\omega t\; x_0\,\Big|_0^{\tau}+\omega\int_0^{\tau}\text{Sin }\omega t_0\; x_0\,dt_0\right]$$

The first term of the above gives:

$$Acn(\lambda\phi)\left\{\text{Cos}\left(\frac{4K\omega}{\lambda}\right)-1\right\}$$

To determine the second term, we use the Fourier series for $cn(\lambda(t+\phi))$:

$$cn(\lambda(t+\phi)) = \frac{2\pi}{kK}\sum_{n=0}^{\infty}\frac{q^{n+\frac{1}{2}}}{1+q^{2n+1}}\text{Cos}\left[\frac{(2n+1)\pi}{2K}(\lambda(t+\phi))\right] \qquad \ldots (2.19)$$

where q is the 'nome' function defined by $q = e^{-\pi K'/K}$ where $K(k^2)$ is the complete elliptic integral of the first kind, and $K'(k^2) = K(1-k^2)$ [1].

This gives for the n'th integral:

$$\int_0^{\tau}\text{Cos}\left[\frac{(2n+1)\pi}{2K}(\lambda(t+\phi))\right]\text{Sin }\omega t\,dt\ ,$$

setting $Q_n = \frac{(2n+1)\pi}{2K}$, we write the integral as:

$$\text{Cos}\,(Q_n\,\lambda\phi\,)\int_0^{\tau}\text{Sin}\,\omega t\,\text{Cos}\,(Q_n\,\lambda t\,)\,dt\,-$$

$$-\,\text{Sin}\,(Q_n\,\lambda\phi\,)\int_0^{\tau}\text{Sin}\,\omega t\,\text{Sin}\,(Q_n\,\lambda t\,)\,dt\,.$$

Performing the integrations and assembling terms gives, finally,

$$f\int_0^{\tau}\text{Cos}\,\omega t_0\,\frac{dx}{dt_0}\,dt_0 =$$

$$= fA\left\{\begin{array}{l} cn(\,\lambda\phi\,)\,[\,\text{Cos}\,(\,\frac{4K\omega}{\lambda}\,)-1\,]+ \\ \\ +\,\frac{2\pi\omega}{kK}\,[\,\{\,\text{Cos}\,(\,\frac{4K\omega}{\lambda}\,)-1\,\}\sum_{n=0}^{\infty}\frac{Cn\omega\,\text{Cos}\,(Qn\,\lambda\phi\,)}{(\,Q_n{}^2\,\lambda^2-\omega^2\,)}+ \\ \\ +\,\text{Sin}\,(\,\frac{4K\omega}{\lambda}\,)\sum_{n=0}^{\infty}Cn\,Qn\,\lambda\,\frac{Sin\,(\,Qn\,\lambda\phi\,)}{(\,Qn^2\,\lambda^2-\omega^2\,)}\,]\end{array}\right\}, \qquad \ldots\ (2.20)$$

where $C_n = \dfrac{q^{n+\frac{1}{2}}}{1+q^{2n+1}}$.

Although we have derived an exact expression for the forcing integral, it is apparent that the expression is too complicated to use in the differential equation for k. Terms will oscillate as k varies, and disappear at harmonic resonances with the forcing frequency ω. We therefore adopt a different strategy and perform the integration near primary resonance, the result will be that we derive a simplified expression, at the expense of restricting the validity of the resulting differential equation to a small region around the resonant value of k. The above procedure will also give us a consistent method for obtaining the differential equation for $\phi(t_1)$ as will be seen later.

The condition for resonance is given by:

$\frac{4K}{\lambda} = \frac{2\pi}{\omega}$, this gives $k^2 = 0.7$ at exact resonance.

We now define a small quantity $\bar{\theta}(k)$ as a measure of the nearness of the system to resonance, hence we write:

$$\frac{4K}{\lambda} = \frac{2\pi}{\omega}\left(1+\bar{\theta} \right)$$

$$\bar{\theta} = \left(\frac{2K\omega}{\lambda\pi} - 1 \right)$$

we write

$$\lambda = \frac{2K\omega}{\pi\left(1+\bar{\theta}\right)} \approx \frac{2K\omega}{\pi}\left(1-\bar{\theta}\right) . \quad (\bar{\theta} << 1) \qquad \ldots (2.21)$$

Inserting (2.21) into (2.19) the Fourier series for $cn(\theta)$, we obtain terms of the form:

$$\mathrm{Cos}\left(\left[2n+1 \right] \left(\omega t_0 + \phi \right) \right) ,$$

where $\phi = \omega\phi\left(1-\bar{\theta}\right) - \omega\bar{\theta}t_1$, the product $\bar{\theta}t$ being ordered so as to give the slowly varying quantity $\bar{\theta}t_1$.

The forcing integral then gives:

$$\frac{fA2\pi}{kK}\left[\mathrm{Cos}\ \omega t \sum_{n=0}^{\infty} Cn\ \mathrm{Cos}\left(2n+1 \right)\left(\omega t + \phi \right) \right|_0^{\tau} +$$

$$+ \omega \int_0^{\tau} \mathrm{Sin}\ \omega t \sum_{n=0}^{\infty} Cn\ \mathrm{Cos}\left(2n+1 \right)\left(\omega t + \phi \right) dt \Big] \qquad \ldots (2.22)$$

We now take τ to be the period of the unperturbed orbit over the t_0 timescale i.e. $\tau = \frac{2\pi}{\omega}$, thus all terms vanish except the integral involving $C_0 \cos\left(\omega t_0 + \phi \right)$, this gives:

$$\frac{fA^2\pi}{kK} \left[C_0\omega \int_0^{2\pi/\omega} \sin \omega t \cos\left(\omega t + \phi \right) dt \right]$$

Performing the integration we obtain, finally, the following expression for the forcing integral:

$$- \frac{2\pi^2 A C_0 f}{kK} \sin \phi \ , \quad C_0 = \frac{qj}{\left(1+q \right)} \ .$$

Thus, combining all three terms, we obtain the following equation for $\frac{dk}{dt_1}$:

$$\frac{dk}{dt_1} \left[\left\{ \frac{4\left(K-E\right)}{\lambda k^2} - \frac{8\left(1+k^2\right)\left(K-E\right)}{3\lambda k^2} + \frac{4K}{3\lambda} \right\} \left[\frac{d\left(\lambda^2 A^2 \right)}{dk} - \lambda A^2 \frac{d\lambda}{dk} \right] + \right.$$

$$\left. + 4A^2K \frac{d\lambda}{dk} \mathrm{Sn}^2\left(\lambda\phi \right) \mathrm{dn}^2\left(\lambda\phi \right) \right] = - \frac{2\pi^2 A C_0 f}{kK} \sin \phi -$$

$$- \delta A^2\lambda^2 \left\{ \frac{4\left(K-E\right)}{\lambda k^2} - \frac{8\left(1+k^2\right)\left(K-E\right)}{3\lambda k^2} + \frac{4K}{3\lambda} \right\}$$

... (2.23)

Having obtained the $\frac{dk}{dt_1}$ equation we now proceed to determine the equation for $\frac{d\phi}{dt_1}$.

Following the general theory (Appendix C) we consider the indefinite integrals:

$$\int S\psi \, dt \ , \qquad S = - \frac{2d\psi}{dt_0 \, dt_1} + f \cos \omega t - \delta\psi$$

Neglecting terms in t, we divide by $\phi^2 = \lambda^2 A^2\ sn^2\theta\ dn^2\theta$, then integrate again and take any resulting secular terms to define the equation for $\frac{d\phi}{dt_1}$.

The integrals we have to consider are of the form:

$$\int^{\theta''} \frac{1}{sn^2\theta'\ dn^2\theta'} \int^{\theta'} sn^2\theta\ dn^2\theta\ d\theta\ d\theta'$$

and

$$\int^{t''} \frac{1}{sn^2\theta'\ dn^2\theta'} \int^{t'} \cos \omega t\ \frac{dcn\theta}{dt}\ dt\ dt' \ , \quad \theta = \lambda(\ t+\phi\ )$$

Considering the former, we have

$$\int sn^2\theta\ dn^2\theta\ d\theta = \left(\ \frac{1-k^2}{3k^2}\ \right)\theta + \left(\ \frac{2k^2-1}{3k^2}\ \right) E(\ sn\theta,\ k\ ) -$$

$$- \frac{sn\theta\ cn\theta\ dn\theta}{3} \qquad \ldots (2.24)$$

We neglect the first term in θ, the third term can be integrated exactly:

$$\int \frac{sn\theta\ cn\theta\ dn\theta}{sn^2\theta\ dn^2\theta}\ d\theta = \int \frac{cn\theta\ d\theta}{sn\theta\ dn\theta} = \ln\left(\ \frac{sn\theta}{dn\theta}\ \right) ,$$

giving no secular terms.

Considering the last term, we expand $E(\ sn\theta,\ k\ )$ as

$$E(\ sn\theta,\ k\ ) = \frac{2E}{\pi}\ sn\theta + sn\theta\ cn\theta\ [\ F(\ sn^2\theta\ )\ ] \ ,$$

where $P(\ sn^2\theta\ )$ is a polynomial in $sn^2\theta$. We then have the integral:

$$\int \frac{sn\theta\ cn\theta}{sn^2\theta\ dn^2\theta}\ P(\ sn^2\theta\ )\ d\theta = -\int \frac{P(\ sn^2\theta\ )\ d(\ dn\theta\ )}{(\ 1-dn^2\theta\ )\ dn^2\theta}$$

$$= -\int G(\ dn^2\theta\ )\ d\ (\ dn\theta\ ) \quad \text{using } sn^2\theta = \frac{1\ -\ dn\theta^2}{k^2}\ ,$$

and where $G(\ dn^2\theta\ )$ is some algebraic function of $dn^2\theta$.

Thus, this term does not give secular terms (terms in θ). We are left, finally, with the integral:

$$\int \frac{sn\theta\ d\theta}{sn^2\theta\ dn^2\theta}\ . \qquad \ldots (2.25)$$

At this point we split,

$$\frac{1}{sn^2\theta\ dn^2\theta}$$

as $\quad \frac{1}{sn^2\theta} + \frac{k^2}{dn^2\theta}$

and consider the Fourier expansions of

$$\frac{1}{sn^2\theta}\ ,\ \frac{1}{dn^2\theta}\ ,\ \text{and } am\theta;$$

$$am\theta = \frac{\pi\theta}{2K} + 2\sum_{n=1}^{\infty} An\ Sin\ (\ \frac{n\pi\theta}{K}\ )\ ,\quad An = \frac{1}{n}\ \frac{q^n}{(\ 1+q^{2n}\ )}\ . \qquad \ldots (2.26)$$

$$\frac{1}{sn2_\theta} = \frac{\pi^2}{4K^2}\ Cosec^2\ (\ \frac{\pi\theta}{2K}\ ) + \frac{(K-E)}{K} - \frac{2\pi^2}{K^2}\sum_{n=1}^{\infty} Bn\ Cos\ (\ \frac{n\pi\theta}{K}\ )\ ,$$

$$Bn = \frac{nq^{2n}}{(\ 1-q^{2n}\ )}\ . \qquad \ldots (2.27)$$

$$\frac{1}{dn^2\theta} = \frac{\pi^2}{2k'^2 K^2}\left[1 + 8\sum_{n=1}^{\infty} Dn\ \mathrm{Cos}\left(\frac{n\pi\theta}{K}\right) + 16\sum_{m=1}^{\infty}\sum_{n=1}^{\infty} Dm\ Dn\ \mathrm{Cos}\left(\frac{m\pi\theta}{K}\right)\mathrm{Cos}\left(\frac{n\pi\theta}{K}\right)\right],$$

$$k'^2 = \left(1 - k^2\right),\ Dn = (-1)^n \frac{q^n}{\left(1+q^{2n}\right)}. \qquad \ldots (2.28)$$

We again neglect the θ term in (2.26) and, on considering the resulting integrals, i.e. integrals of the form:

$$I_n = \int \mathrm{Sin}\left(\frac{n\pi\theta}{K}\right) d\theta,\quad I_n = \int \mathrm{Sin}\left(\frac{n\pi\theta}{K}\right)\mathrm{Cosec}^2\left(\frac{\pi\theta}{2K}\right) d\theta.$$

$$I_n = \int \mathrm{Sin}\left(\frac{n\pi\theta}{K}\right)\mathrm{Cos}\left(\frac{n\pi\theta}{K}\right) d\theta,$$

$$I_n = \int \mathrm{Sin}\left(\frac{n\pi\theta}{K}\right)\mathrm{Cos}\left(\frac{m\pi\theta}{K}\right)\mathrm{Cos}\left(\frac{\rho\pi\theta}{K}\right) d\theta$$

(n, m, ρ integers)

it is apparent that no secular terms occur in (2.25). Therefore, the only source of secular terms will be the forcing integral which we now consider.

The left hand side of Equation (2.22) gives terms of the form:

$$C_n\ \mathrm{Cos}\ \omega t\ \mathrm{Cos}\left(2n+1\right)\left(\omega t + \phi\right)\quad n \geq 0,$$

writing $y = \omega t + \phi$, $\omega t = y - \phi$, we obtain

$$C_n\ \mathrm{Cos}\left(y - \phi\right)\mathrm{Cos}\left(\left(2n+1\right)y\right),$$ which we expand as

$$C_n\ \mathrm{Cos}\left[\left(2n+1\right)y\right]\left\{\mathrm{Cos}\ y\ \mathrm{Cos}\ \phi + \mathrm{Sin}\ y\ \mathrm{Sin}\ \phi\right\} \qquad \ldots (2.29)$$

The n'th integral gives:

$$I_n = Cn \int \text{Sin}\left(y - \phi \right) \text{Cos}\left[\left(2n+1 \right) y \right] dy \qquad n > 0$$

$$= \frac{\text{Cos}\ \phi}{2} \left\{ \frac{\text{Cos}\ 2ny}{2n} - \frac{\text{Cos}\left(2n+2 \right) y}{\left(2n+2 \right)} \right\} -$$

$$- \frac{\text{Sin}\ \phi}{2} \left\{ \frac{\text{Sin}\left(2n+2 \right) y}{\left(2n+2 \right)} + \frac{\text{Sin}\ 2ny}{2n} \right\} . \qquad \ldots (2.30)$$

For n = 0 we obtain:

$$I_0 = - \text{Cos}\ \phi \frac{\text{Cos}^2 y}{2} - \text{Sin}\ \phi \left[\frac{y}{2} + \frac{\text{Sin}\ y\ \text{Cos}\ y}{2} \right] . \qquad \ldots (2.31)$$

The term $-\frac{y}{2}\ \text{Sin}\ \phi$ appeared in the coefficient of f in the $\frac{dx}{dt_1}$ equation and is therefore neglected as were the θ terms in (2.24).

We again use the Fourier series for $\frac{1}{sn^2\theta}$, $\frac{1}{dn^2\theta}$, with terms of the form $\frac{v\theta}{2K}$ replaced by $y = \left(\omega t_0 + \phi \right)$.

The resulting integrals of the products of terms from (2.29), (2.30), (2.31), (2.27) and (2.28) are then inspected for secular terms. The terms in the coefficients of Sin ϕ in (2.29) + (2.31), do not yield secular terms, and hence it is only the coefficients of Cos ϕ which contribute to the $\frac{d\phi}{dt_1}$ equation.

The above procedure would, in principle, yield an infinite number of terms for the coefficient of Cos ϕ, however, we consider only terms up to order k^4, which implies we must take the Fourier expansions (2.27) and (2.28) up to order q^2 where q is the nome function defined earlier.

Performing the integrations yields, finally, the following equation for $\frac{d\phi}{dt_1}$:

$$\frac{d\phi}{dt_1} = f \cos\phi \left(\frac{\pi}{\lambda^2 \, Ak \, K} \right) \left\{ \frac{(K-E)}{2K} C_0 + \right.$$

$$+ \frac{\pi^2}{4K^2} \left(- C_0 - 6C_1 - 10C_2 \right) - \frac{\pi^2 \, B_1 \, C_0}{2K^2} +$$

$$+ \frac{k^2 \, \pi^2}{4k'^2 \, K^2} \left(C_0/2 - 2D_1 \, C_1 + 2C_0 D_1 - 4C_0 D_1 - \right.$$

$$\left. \left. - 4C_1 D_1 + 4D_1^2 C_0 \right) \right\}, \qquad \ldots (2.32)$$

where the C_n, B_n, and D_n are defined in Equations (2.20), (2.27) and (2.28).

Equations (2.23) and (2.32) determine the slow time variation of k and ϕ near primary resonance. The final step, to put the equations into useable form, is to expand the terms in each equation as a power series in k^2, to do this we use the standard expressions [1]:

$$K(k^2) = \frac{\pi}{2} \left[1 + \frac{k^2}{2^2} + \frac{1^2 \times 3^2 \, k^4}{2^2 \times 4^2} + \frac{1^2 \times 3^2 \times 5^2 \, k^6}{2^2 \times 4^2 \times 6^2} + \cdots \right],$$

$$E(k^2) = \frac{\pi}{2} \left[1 - \frac{k^2}{2} - \frac{1^2 \times 3 \, k^4}{2^2 \times 4^2} - \frac{1^2 \times 3^2 \times 5 \, k6}{2^2 \times 4^2 \times 6^2} - \cdots \right],$$

$$q(k^2) = \left[\frac{k^2}{16} + 8\left(\frac{k^2}{16} \right)^2 + 84\left(\frac{k^2}{16} \right)^3 + \cdots \right].$$

We also make a change of variable:

$$y = 2k^2 - 1, \quad \frac{dy}{dt} = 4k \frac{dk}{dt},$$

so that we may treat the terms in

$$A^2 = \frac{2\beta k^2}{(2k^2-1)} \quad , \quad \lambda^2 = \frac{\beta}{(2k^2-1)} \, ,$$

and their derivatives, as exact expressions.

Having made this change of variable, and expanded terms up to y^2, we obtain the following equations for $\frac{dy}{dt_1}$ and $\frac{d\phi}{dt_1}$:

$$\frac{dy}{dt_1} \left[A_1 + A_2 y + A_3 y^2 + \left(A_4 + A_5 y + A_6 y^2 \right) \mathrm{Sin}^2 \left(\omega\phi \left(1-\bar{\theta}\right) \right) \right] =$$

$$= A_7 f y^2 \, \mathrm{Sin}\, \Phi + \delta y \left(A_8 + A_9 y \right)$$

$$\frac{d\phi}{dt} = f A_{10} y^{3/2} \, \mathrm{Cos}\, \Phi \, .$$

Where we have taken the first term of $sn^2(\lambda\phi)\, dn^2(\lambda\phi)$ in the $\frac{dk}{dt_1}$ equation for simplicity, and where the A_i values are given in Appendix A.

Making the change of variable $X = \omega\phi \left(1-\bar{\theta}\right)$:

$\frac{dX}{dt} = \omega \frac{d\phi}{dt} + \left(\text{order } \varepsilon^2 \right)$, we obtain, finally,

$$\frac{dy}{dt} \left[A_1 + A_2 y + A_3 y^2 + \left(A_4 + A_5 y + A_6 y^2 \right) \mathrm{Sin}^2 X \right] =$$

$$= A_7 f y^2 \, \mathrm{Sin} \left(X - \omega\bar{\theta} t \right) + \delta y \left(A_8 + A_9 y \right) , \qquad \ldots (2.33)$$

$$\frac{dX}{dt} = f\omega A_{10} y^{3/2} \, \mathrm{Cos} \left(X - \omega\bar{\theta} t \right) . \qquad \ldots (2.34)$$

The phase plane for Equations (2.33) and (2.34) is shown in Figure (4d). Although the equations are complicated, the most important feature of the solutions is that they increase

exponentially with time. The coupling with the phase produces oscillations in the 'amplitude' y, in a similar fashion to that described for the amplitude ρ in the last section, however, the important feature of the equations would seem to be that the sign of the derivative $\frac{dy}{dt}$ is the same as that of the damping term in δ. This is a direct result of the form of the amplitude and frequency expressions:

$$A = \sqrt{\frac{2\beta}{\alpha}} \left(\frac{k}{2k^2-1} \right)^{\frac{1}{2}}, \quad \lambda = \frac{\sqrt{\beta}}{\sqrt{2k^2-1}}$$

which led to the term: $\left[\frac{d(\lambda^2 A^2)}{dk} - \lambda A^2 \frac{d\lambda}{dk} \right]$ in Equation (2.23) being negative.

Although the above equations are only valid near primary resonance ($k^2 = 0.7$, $y = 0.4$), it is clear that the same qualitative behaviour of the amplitude can be expected for all values of y as it is only the forcing integral which will change its form as y varies. Thus, if we consider $y \neq 0$, the forcing term in (2.33) will decrease as y^2, the dampling term decreasing only as y. Further, resonances of the form: $\frac{4Kn}{\lambda} = \frac{2\pi}{\omega}$ will be encountered at which the forcing integral will vanish altogether. Therefore, although the details of the amplitude equation are complicated, the overall exponential growth of y (and hence decay of A) will hold true in general.

Of course, it is impossible to predict how the phase will vary as y increases, we saw in the last section that the phase of the multiple-scales solution was slowly entrained to a constant with the amplitude and frequency, hence giving a limit cycle solution, however, no such solution exists for outside orbits and the best we

can assume is that the phase is approximately constant at this order.

Setting $f = 0$ and considering only linear terms in y, Equations (2.33) and (2.34) become:

$$\frac{dy}{dt} = \left[\frac{\delta A_8}{A_1 + A_4 \sin^2 X} \right] y \,, \quad \frac{dX}{dt} = 0 \,.$$

with solution $y(t) = \bar{K} e^{\alpha t}$ $\qquad \alpha = \dfrac{\delta A_8}{\left(A_1 + A_4 \sin^2 X \right)}$

The Poincaré Map

We now derive a Poincaré map for the amplitude:

$$A^2 = \frac{2\beta}{\alpha} \left(\frac{k^2}{2k^2 - 1} \right) = \frac{\beta}{\alpha} \frac{(y+1)}{y}$$

The time interval τ is defined to be $\tau = \frac{2\pi}{\omega}$ where ω is the driving frequency. Inserting $y(t) = \bar{K} e^{\alpha t}$ into the above gives:

$$A^2(t) = \frac{\beta}{\alpha} \left(1 + K e^{-\alpha t} \right) \qquad K = 1/\bar{K}$$

Defining $A_n^2 = A^2(n\tau)$ we have:

$$A_n^2 = \frac{\beta}{\alpha} \left(1 + K e^{\frac{-2\pi\alpha n}{\omega}} \right) = \frac{\beta}{\alpha} \left(1 + K e^{-\alpha n \tau} \right)$$

$$A_{n+1}^2 = \frac{\beta}{\alpha} \left(1 + K e^{-\alpha n \tau} e^{-\alpha \tau} \right)$$

Inserting the expression for A_n^2 into the above gives the following relationship between A_{n+1} and A_n

$$A_{n+1} = \left[\frac{\beta}{\alpha} \left(1 - e^{-\alpha \tau} \right) + e^{-\alpha \tau} A_n^2 \right]^{\frac{1}{2}} \qquad \ldots (2.35)$$

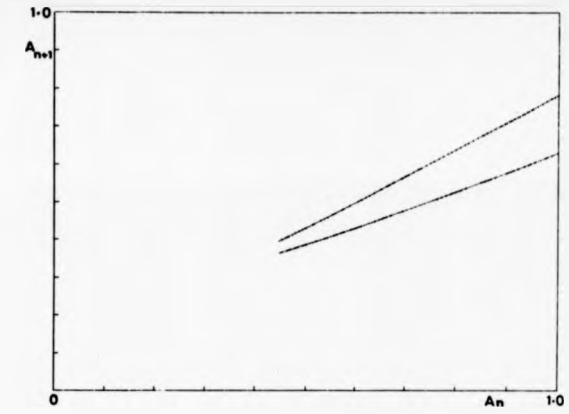

Figure 4e : Poincaré Maps for Outside Orbits

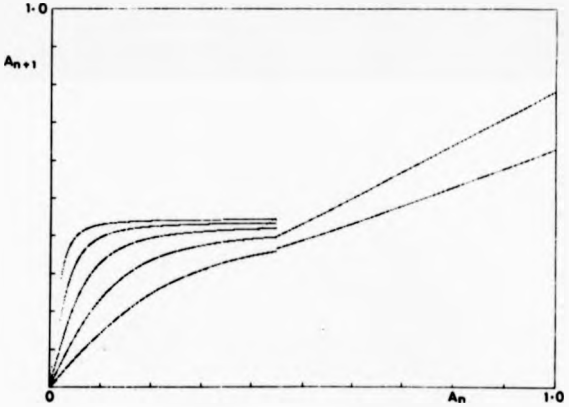

Figure 4f : Inside and Outside Maps Plotted Together

Two plots of the A_n curve are shown in Figure (4a). The factor α is determined by setting $X = 0, \frac{\pi}{2}$, and gives rise to a change of slope, the overall form of the two curves being the same. Each curve lies strictly below the diagonal: $A_{n+1} = A_n$ and iterates of the map bring an initial point into the separatrix region. Thus, although (2.35) is only an approximation to the true map, it possesses the essential feature of modelling the convergence of the outside orbits to the homoclinic orbit. For non-zero f we would expect the curve to be qualitively the same, the coefficients of f in (2.33) and (2.34) being of order y^2 and $y^{3/2}$ respectively, thus although the curve may have a small oscillation, it will still be monotonic and lie strictly below the diagonal, the curves defined by (2.35) are in some sense an average over small oscillations. The mapping outside, then, although difficult to determine, is in some sense trivial, leading to contraction of orbits into the separatrix. The inside map, which we will now determine, should have a fixed point, corresponding to a limit cycle solution, by analogy with the multiple scales analysis of the last section. It is apparent that equations having the form of (2.33) and (2.34) will never pick up a fixed point solution, being non-autonomous, so that different assumptions about the frequency and phase will have to be made when the integral method is applied to orbits lying inside the separatrix.

2.2.2 The Inside Orbits

The unperturbed orbits inside the separatrix have the form:

$$x(t) = A\ dn\ (\ \lambda(t+\phi)\ )$$

$$\dot{x}(t) = -A\lambda k^2 \, sn\left(\lambda(t+\phi)\right) cn\left(\lambda(t+\phi)\right)$$

$$A = \sqrt{\frac{2\beta}{\alpha}} \left(\frac{1}{2-k^2}\right)^{\frac{1}{2}}, \quad \lambda = \left(\frac{\sqrt{\beta}}{2-k^2}\right)^{\frac{1}{2}}$$

We will again use the integral method on the unperturbed solutions to derive a Poincaré map for the amplitude A inside the homoclinic orbit. However, in this case we know from the multiple scales solution that the resulting map will have a fixed point, and that the integral method as applied in the last section will not pick up such an equilibrium. The problem with the outside orbits was that the frequency λ, passed in and out of resonance as the orbit converged inwards, so that an analysis near primary resonance was necessary for f non-zero, although a more global picture could be obtained for f = 0.

It will be recalled that in Section 2.1 the coupling of amplitude and frequency caused small oscillations in ρ, and that as the amplitude converged to a constant, the frequency was entrained to that of the driving term ω, whilst the phase approached a constant value. In this section, therefore, we will assume that, to this order, the frequency is exactly entrained to the driving frequency, and adjust the phase to give limit cycle behaviour for the inside orbits. These assumptions of course, will not give the exact equation for $\frac{dk}{dt}$, however, we will treat the resulting expression for $k(t_1)$ as an average over small oscillations and assume that the Poincaré map will retain the essential dynamics of $k(t_1)$ in much the same way as the Poincaré map of Section 2.1 smoothed over the oscillations in ρ, in essence we are assuming that these oscillations are insignificant over the timescale $\tau = \frac{2\pi}{\omega}$.

We begin by writing the unperturbed solution as:

$$x(t) = A\ dn\ \{\ yt + \phi\ \}$$

where $y(k^2)$ is defined such that:

$$\frac{2K}{y} = \frac{2\pi}{\omega} \quad \text{to this order.}$$

this defines y(k) as:

$$y(k) = \frac{\omega K}{\pi} + \{\ \text{order } \varepsilon^2\ \}$$

The phase ϕ is to be treated as a constant to this order. Performing the integrations, as in the last section, we obtain the following equation for $\frac{dk}{dt_1}$:

$$\frac{dk}{dt_1}\left\{ \frac{2}{k^2}\left\{ \frac{(K-E)}{y} + \frac{K}{3y} - \frac{2(1+k^2)(K-E)}{3k^2y} \right\} x \right.$$

$$\left. x\left[\frac{d(A^2k^4y^2)}{dk} - A^2k^4y\frac{dy}{dk} \right] + 2A^2k^4\frac{dy}{dk} K\ sn^2\phi\ cn^2\phi \right\} =$$

$$= -\frac{2\pi^2 Af}{K} C_1\ Sin\left(\frac{\pi\phi}{K}\right) - 2\delta A^2k^2y\left[(K-E) + \frac{K}{3} - \frac{2(1+k^2)(K-E)}{3k^2} \right]$$

$$C_1 = \frac{q}{(1+q^2)}$$

We now define ϕ to give a limit cycle solution. Setting $\phi = -\frac{K}{2}$, we obtain, after expanding the terms up to k^2

$$\frac{dk^2}{dt_1} = A_1 f - (\ A_2 f + A_3\delta\ )\ k^2 \qquad \ldots (2.36)$$

where the A_I are given in Appendix A.

Setting $y = k^2$ we have:

$$\frac{dy}{dt} = A - By \ , \qquad A = A_1 f \ , \qquad B = A_2 f + A_3 \delta \ .$$

with solution $y(t) = \frac{A}{B} - Ke^{-Bt}$.

Inserting the above into the expression for the amplitude gives:

$$A^2(t) = \frac{2\beta}{\alpha}\left(\frac{1}{2-y}\right) = \frac{2\beta}{\alpha}\frac{1}{(C+Ke^{-Bt})} \ , \quad C = 2 - \frac{A}{B} \ .$$

Discretising time, as before, according to $t \to n\tau$, $\tau = \frac{2\pi}{\omega}$, gives:

$$\frac{\alpha A_n^2}{2\beta} = \frac{1}{(C + Ke^{-Bn\tau})} \ , \quad \frac{\alpha A_{n+1}^2}{2\beta} = \frac{1}{(C + Ke^{-Bn\tau}e^{-B\tau})} \ .$$

Finally, relating A_{n+1} to A_n, we have:

$$A_{n+1} = \frac{A_n}{\left[\frac{\alpha}{2\beta} CA_n^2 \left(1-e^{-B\tau}\right) + e^{-B\tau}\right]^{\frac{1}{2}}} \ . \qquad \ldots (2.37)$$

The curves defined by (2.37) and (2.35) are plotted in Figure (4f). The map has been defined on the interval $\left(0, \sqrt{\frac{2\beta}{\alpha}}\right)$ although the original amplitude is defined on the smaller interval $\left(\sqrt{\frac{\beta}{\alpha}}, \sqrt{\frac{2\beta}{\alpha}}\right)$ we are thus considering (2.37) to be a formal difference map which has been abstracted from the original equations and expresses the dynamics of a quantity related to the amplitude A.

For f = 0 the curves inside and outside (for X = 0) are very close at the homoclinic orbit. As f increases, the inside maps get steeper and the resultant fixed points move closer to the separatrix at $\sqrt{\frac{2\beta}{\alpha}}$. The flattening of these curves with increasing f is due

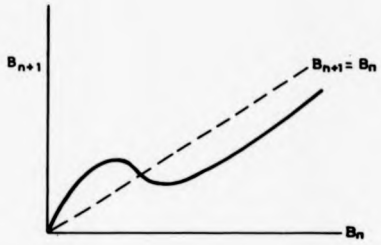

Figure 4g : Suggested Form of Poincaré Map

to the strong contraction to the limit cycle which is always present in the perturbation analysis.

The above figure, then, contains all of the information we are able to derive from a perturbation analysis. The curves, inside and outside, have been derived by using the form of the amplitude in the unperturbed solutions and taking simple exponential solutions for the quantity $k(t_1)$ in each case, the resulting Poincaré map has been assumed to be globally defined from zero to infinity with a discontinuity at the separatrix, this has the effect of abstracting the map from the original amplitude to a quantity, B_n, say defined on $[0, \infty]$.

The global input to the B_n map is to now assume the map to be analytic over the separatrix and to simply join the curves over this region in such a way as to 'break' the fixed point and give chaos. A straight line join would give chaos as the gradient increased with f, but would not give a period doubling cascade. Therefore, the most obvious method is to assume a smooth curve join giving a logistic type map at the separatrix with global attraction to it from either side. The resulting B_n map [Figure (4g)] of the form, say,

$$B_{n+1} = \frac{\alpha B_n + \beta B_n^2 + \gamma B_n^3}{(\eta + \mu B_n^3)} \qquad \left(\lim_{B_n \to \infty} B_{n+1} = \frac{\gamma}{\mu} < 1 \right)$$

where α, β, γ, η, μ are parameterised by f, will give a logistic-type bifurcation sequence, as f increases, leading to chaotic motion in the separatrix region.

3.0 DISCUSSION

The form of the B_n map of Section 2 has been derived by considering the Poincaré map of the amplitudes A_n inside and outside the separatrix region. The existence of a globally attracting limit cycle in the perturbation solutions has led us to consider a one-dimensional map in which the fixed point obtained by the perturbation method can be made to go unstable by considering a smooth curve fit between the 'inside' and 'outside' maps. With regard to the original system, the status of the B_n map, being derived from the amplitudes A_n, is most akin to a 'maximum amplitude' map of an amplitude defined from the origin of the system. In using the A_n's the B_n map takes into account the symmetry breaking by assuming the dynamics left and right of the saddle to be equivalent.

The assumption of constant phase, to give a 1-D map, has not been rigorously justified. However, it would seem a reasonable conjecture that, asymptotically at least, the phase is approximately constant, to this order, with oscillatory terms which, although chaotic, would remain bounded and that the large scale chaotic motion would then reside in the amplitude. The assumption of a 'chaotic' amplitude map rests by analogy with the Lorenz system. The difficulty with the Duffing system is that the chaos resides in a small region around the separatrix so that, although perturbation theory provides information on the converging orbits, the chaos resides precisely at the region where we have to make assumptions about the nature of the map. In the Lorenz case, the chaos is in the amplitude map away from, and up to, the saddle point, so that

perturbation theory is valid in this region and yields an approximation to the Lorenz map (Rowlands [32]).

However, accepting these difficulties, it is apparent that the B_n map suggested in the last section does model the Duffing system inside and at least in some regions outside the homoclinic orbit. The difficulties presented by the outside orbits make it impossible to say how the curve behaves for large amplitudes, however, the qualitative feature of a shallow curve which brings orbits inwards very quickly would seem a reasonable conjecture.

In conclusion then, an analytic one dimensional map has been assumed to exist for the Duffing system. Analysis has indicated that the map will have the form of a logistic map around the homoclinic orbit, with global attraction to it from either side. The map, being one-dimensional, loses the details of the Smale-horseshoe but exhibits the period doubling cascade observed in the physical system.

CHAPTER 5

THE SYMMETRIC MAP

1.0 Introduction

The logistic, Hénon, and Chirikov, maps described in Chapter 3, are all well documented examples of chaotic discrete systems. In fact, they form the archetypal set of such systems, each characterising a different facet of chaotic behaviour. Thus, the logistic map, the 'simplest' of all chaotic systems exhibits a period doubling cascade of stable periodic orbits, ending in a chaotic state which persists over a range of parameter values. Inherent in this bifurcation scenario is a scaling universality, in parameter space, which predicts period doubling to chaos in all 'unimodal' maps.

The Hénon map, although more complex and seemingly intractable than the logistic map, also shows some of the behaviour of the latter, i.e. a period doubling cascade of periodic orbits to chaos. However, the chaotic state is now characterised by a discrete form of strange-attractor. The Hénon system is dissipative with Jacobian $J = -b$, and hence most initial points would be expected to converge onto the strange attractor. This is in contradistinction to the case of the logistic map where the chaotic state is characterised by overall expansion of trajectories (positive Lyapunov exponent).

Finally, the Chirikov, or standard, map provides an example of an 'area preserving' 2-D chaotic system. This system, being abstracted from a Hamiltonian system of equations, is characterised by the gradual break-up of KAM surfaces (invariant tori) under

perturbation. Thus, although there is no attraction to a strange attractor as such, the existence of homoclinic and heteroclinic points, and the infinite sequences of resonant islands, leads to behaviour which we may term chaotic and indeed, may be represented as a diffusion-like process [25].

The salient features of the above short resumé of chaotic discrete maps is that quite different types of behaviour can be expected to occur for systems according to the value of the appropriate Jackobian (or derivative in 1-D) of the map.

The Hénon and Chirikov maps both have constant Jacobian (-b, and +1 respectively) leading to either strange attractor or resonant island behaviour accordingly. The logistic map is characterised by its Lyapunov exponent which is negative for periodic behaviour and positive for chaotic behaviour.

It would seem to be of some interest then to ask what might be expected of a discrete map whose Jacobian could take on a range of values from negative to positive, including the area preserving case J = 1, and singular case J = 0.

In this chapter, such a map is investigated. The fact that the Lyapunov exponent for the logistic map takes on both negative and positive values according to the value of the parameter, leads us to consider two logistic maps coupled through their parameters. The resulting 2-D map is then investigated, particularly with reference to the 1-D logistic map and its parameter space, to try to ascertain whether features of the 1-D case carry over to 2-D. The effect of parameterising the system is then considered and finally a

perturbation method is applied to the map to attempt to generate the structure of the strange attractor of the system.

This latter is found to be of only limited success due to the complicated nature of the governing equations, thus although a recursive set of equations is not found, the equations obtained do exhibit the same complex behaviour as the original equations, suggesting a universal characteristic of coupled non-linear discrete maps.

1.1 The Map

In order to construct a chaotic map whose Jackobian takes on both positive and negative values, we combine 2 logistic maps, (one in the variable x_n, the other in y_n say), in such a way as to retain the form of the 1-D map in each variable.

This precludes simply adding a term proportional to the 'opposite' variable in each case (see, however, [17] and below). Thus, we are led to couple the maps through their parameters and we do this in a symmetric way to give a map which shall be denoted the 'symmetric map' for convenience:

$$x_{n+1} = 1 - (1 + y_n)\, x_n^2 \quad , \qquad x_n, y_n \in [\, -1.0, 1.0\,]$$

$$y_{n+1} = 1 - (1 + x_n)\, y_n^2 \quad . \qquad \ldots (1.1)$$

Inspection of Equations 1.1 reveals that each variable is governed by a logistic map whose parameter is 1 plus the opposite variable. The variables range between -1.0 and $+1.0$ and thus the addition of one to each variable allows the effective parameters to vary between 0 and 2. That is, in each equation the variable is

governed by a logistic map whose parameter can vary from the periodic through to the chaotic regime.

Evaluation of the Jacobian of the map gives:

$$J = \begin{vmatrix} \frac{df}{dx_n} & \frac{df}{dy_n} \\ \frac{dg}{dx_n} & \frac{dg}{dy_n} \end{vmatrix} = 4\,(1 + x_n)\,(1 + y_n)\,x_n y_n - x_n^2 y_n^2 \quad , \qquad \ldots (1.2)$$

where: $f = f(x_n, y_n) = 1 - (1 + y_n)\,x_n^2$,
$g = g(x_n, y_n) = 1 - (1 + x_n)\,y_n^2$.

Although the expression for the Jacobian is relatively complicated, regions of different 'J' values are easily obtained numerically in the 'state space': $x_n \in [-1,1]$, $y_n \in [-1,1]$. In particular, the equation J = 0 can be solved to give the solutions:

$$x_n y_n = 0 \quad , \qquad \ldots (1.3)$$

and $y_n = \dfrac{-4\,(1 + x_n)}{(4 + 3x_n)}$

We thus have a 2-D map whose Jacobian can take values from the negative to the positive, through zero.

Although Equations (1.1) are quite complicated, a couple of qualitative features of the system are apparent. Firstly, there are a pair of period 2 fixed points at $(x_n, y_n) = (0, +1)$, $(x_n, y_n) = (+1, 0)$, a pair at $(x_n, y_n) = (-1, -1)$, $(x_n, y_n) = (+1, +1)$, and two period one fixed points at $(x_n, y_n) = (-1, +1)$, $(x_n, y_n) = (+1, -1)$, none of which are attracting. Secondly, it is apparent that the diagonal line, $x_n = y_n$, is an invariant under the map, i.e. any point started on the diagonal will remain there for all time. Given these remarks we

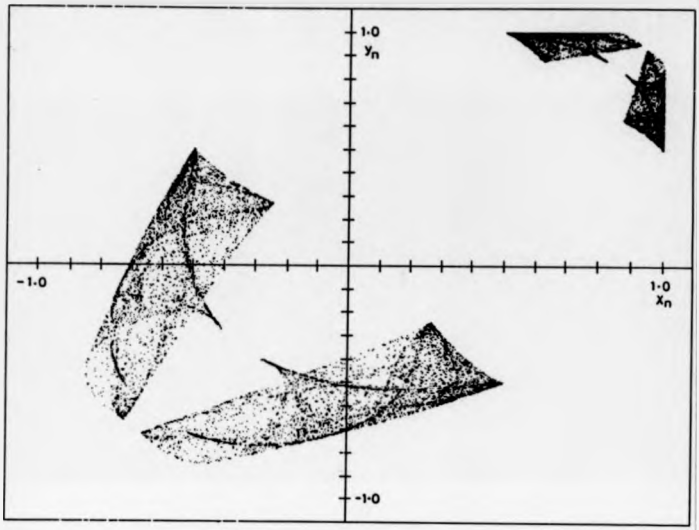

Figure 5a : Symmetric Map Attractor

must now turn to numerical iteration of the map to view the overall asymptotic behaviour of 'typical' initial conditions.

1.2 Strange Attractor

In Figure (5a), the result of applying the map 50,000 times to the initial point $(x_0, y_0) = (0.7, 0.3)$ is shown. The first few iterates of the point are ignored to allow transients to die away. The contraction to the 'strange attractor' is extremely rapid and so only a few (= 50) 'settling down' interations are necessary.

The most obvious features apparent in Figure (5a) are the four regions of attraction in the state space. Colour coding of trajectories reveals that these regions are each visited in a certain order, indicating a basic period 4 process. Also of interest is the similarity in form of the two large attracting regions and the two small ones. Closer inspection of the attracting regions reveals a complex network of lines criss-crossing the attractor. In fact, the large cusps which branch out from each region 'point' to two of a set of four period 4 fixed points which lie on the diagonal and attract almost all points initiated on the diagonal. The other two members are 'indicated' by smaller cusps branching from near the top of each region.

The basic features of the symmetric map described above, have been observed to hold for many initial conditions and many (= 500,000) iterations of the map. It would therefore appear justified to refer to the attracting regions as the 'period 4 strange attractor'.

In the next section an attempt will be made to explain the qualitative features of this attractor.

1.3 Investigation of the Symmetric Map

1.3.1 The Diagonal Map

The existence of a stable period four orbit on the invariant diagonal is easily understood by considering Equations 1.1 with the condition $x_n = y_n$. In this situation we have 2 uncoupled equations of the form:

$$x_{n+1} = 1 - x_n^2 - x_n^3 \quad , \quad x_n \in [-1,1] \quad ,$$

which possesses a stable period 4 orbit. Thus, all points initiated on the diagonal are constrained to remain there for all time, and further, almost all of these points will be attracted to the stable period 4 orbit (the points $(-1,-1)$, $(+1,+1)$ are examples of initial conditions which do not converge to the stable period 4 orbit).

1.3.2 Period 4 Attractor-Enslaving

Considering now the 'fourfold' nature of the attractor, the symmetry across the diagonal can be seen to arise from the symmetry of the map. Thus, an attracting region centred on a point (x_1,y_1) say, will be mirrored by one centred on (y_1,x_1), furthermore, both regions will have the same shape and structure.

The second plane of symmetry, i.e. that between the two small and two large attractors, is much more difficult to understand, and is not at all obvious from the form of Equation (1.1).

The symmetry can be understood qualitatively by considering the 1-D parameterised logistic map. It will be recalled that each variable in Equation 1.1 is 'driven' by a logistic map in which the parameter takes on values between zero and 2. There is thus a

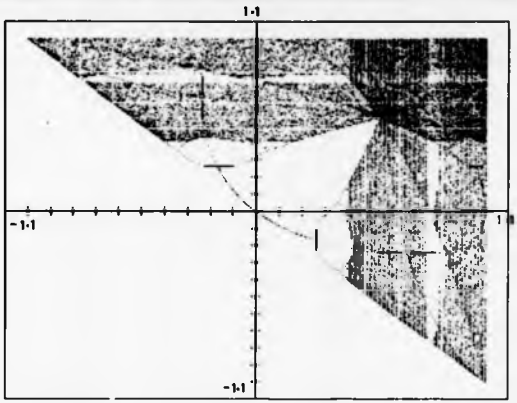

Figure 5b : Cross-Plots of Bifurcation Diagrams

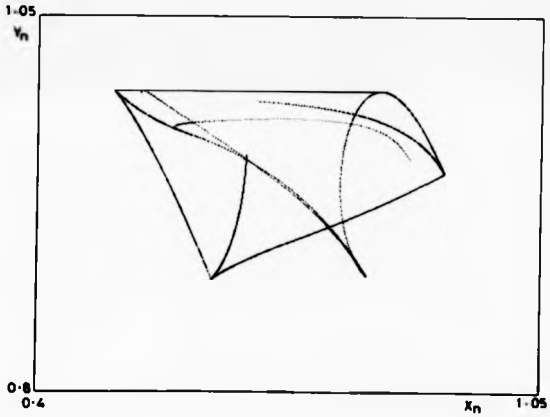

Figure 5c : Iterates of J = 0 Line

direct correspondence between the state-space for the system: $[-1,1] \times [-1,1]$, and the parameter space for (two) logistic maps: $[0,2] \times [0,2]$.

Therefore, an initial condition (x_o, y_o) will define a point in state space and also 2 logistic map parameters, namely: $\lambda_1 = 1 + y_o$. and $\lambda_2 = 1 + x_o$, which will determine whether the next iterate of the map: $x_1 = 1 - \lambda_1 x_o^2$, $y_1 = 1 - \lambda_2 y_o^2$, is determined by a chaotic map: $\lambda_1, \lambda_2 > \lambda_\infty$, or a periodic map: $\lambda_1, \lambda_2 < \lambda_\infty$, or both: $\lambda_1(\lambda_2) < \lambda_\infty$, $\lambda_2(\lambda_1) > \lambda_\infty$.

This situation is made clearer by comparing a cross-plot of the bifurcation diagrams for x_n, and y_n, Figure (5b), with the regions occupied by the strange attractor.

Upon comparison it is found that the small attractor lies within the chaotic region of parameter space, whilst the large one lies wholly in the periodic region. What would appear to be happening, then, is that the dynamical system possesses an attractor (symmetric about $x_n = y_n$) in the chaotic parameter region. One iterate of this attractor under the mapping takes it outside the chaotic parameter region into the periodic region. Here, since the logistic map has only slight curvature over much of this region, the attractor will be mapped back to the chaotic region with only slight distortion in shape. The system is therefore enslaved to the chaotic region.

Having said all this, it should be pointed out that there does not appear to be an exact correspondence between the extent of the attractor in state space and the chaotic region in parameter space.

Thus the attractor sits within the region where both x_n, and y_n, are chaotic, but does not occupy the whole of the region.

Therefore, the attempt to link the dynamics of the symmetric map to those of the 1-D logistic map are limited quantitatively, although the broad aspects of its behaviour can be understood qualitatively from this point of view.

Also, because of the nature of the logistic map curves, a region in state space where $y_n > x_n$ will be mapped to a region $x_n > y_n$, when x_n and y_n lie in the chaotic parameter region, and to a region $y_n > x_n$ when x_n and y_n lie in the periodic parameter region, and similarly for the region $x_n > y_n$. This crossing of the diagonal every other iterate, together with the enslaving, leads to the basic period 4 behaviour observed.

1.3.3 Lyapunov Exponents and Boundary Behaviour

The last three sections have attempted to give a qualitative explanation of the overall dynamical behaviour of the symmetric map. In this section we will concentrate on the fine details of the dynamics within the attractor, and begin by calculating the Lyapunov exponents, for the map, numerically.

Following Lichtenberg and Liebermann [21] we take the Lyapunov exponents to be:

$$\sigma_i = \lim_{n \to \infty} \frac{1}{n} \ln [v_i] \quad , \quad i = 1,2 \qquad \ldots (1.4)$$

where v_i = eigenvalues of matrix

$$J_n(x_0) = [\, J(x_n)\, J(x_{n-1}) \ldots J(x_0) \,]$$

where J is the Jacobian matrix, Equation (1.2), and x_0 is an initial condition.

The above expression was evaluated for n = 1000, and various initial conditions. To reduce numerical errors, each matrix J_i in the product was divided by $\det(J_i)$ so that the matrices each had unit Jacobian.

After 1000 iterates, the exponents had converged to:

$\sigma_1 = 0.117$, $\sigma_2 = 0.076$

The most noteworthy point is that both the exponents converge to positive values. This is contrary to what we would expect for a dissipative system (see Chapter 3) where the sum of the exponents would need to be negative to provide global contraction.

The key to understanding this result is to think by analogy with the logistic map. In that situation we have a system which, when in the chaotic regime, has a positive Lyapunov exponent. That is, we have overall expansion on average, of initial conditions, however, the orbits remain bounded because of the shape of the logistic curve, or more accurately, because of singularities in the distribution of the map which form boundaries between different regions of chaos.

As mentioned in Chapter 3, these singularities are caused by iterates of the maximum of the map, a point of infinite contraction.

It would therefore seem plausible that a similar situation pertained to the 2-D symmetric map. In this case, the points of infinite contraction would correspond to the lines J = 0 as defined earlier (Equations 1.3). We might then expect iterates of these

lines to map out the boundaries of our chaotic regions in state space.

In accordance with the above, the lines: $y_n = \frac{-4(1 + x_n)}{(4 + 3x_n)}$, and $x_n = 0$, were iterated under the map. To prevent stretching of the lines between the periodic points at (0,1), (1,0) etc., only those segments of the lines lying within the strange attractors were iterated (larger segments of line would eventually 'fold in' to the attracting region).

Upon iteration, the line $y_n = \frac{-4(1 + x_n)}{(4 + 3x_n)}$, was observed to become increasingly convoluted and, although the line stayed within each succeeding attracting region eventually filling them, no obvious boundary demarkation was apparent.

When the $x_n = 0$ line was iterated, however, the line very clearly marked out a boundary curve of each successive region until it too became very convoluted after about the 7th iteration.

In order to see this boundary demarkation more clearly, we exploit the symmetry of the map to confine attention to one given region of the attractor.

We first consider the period 2 map given by:

$$x_{n+2} = 1 - (2 - (1 + x_n)\, y_n^2)\, (1 - (1 + y_n) x_n^2)^2,$$

$$y_{n+2} = 1 - (2 - (1 + y_n)\, x_n^2)\, (1 - (1 + x_n) y_n^2)^2. \qquad \ldots (1.5)$$

Recognising that the above would give us a period 2 chaotic attractor symmetric about $x_n = y_n$, we simply swap the expressions for x_{n+2} and y_{n+2} which gives us four attracting regions which are

independent, instead of one period 4 region. The same result could have been obtained by considering the period 4 mapping, although the form of the equations would have been much more complicated.

The equations now become:

$$x_{n+1} = 1 - (2 - (1 + y_n)\, x_n^2)\, (1 - (1 + x_n)\, y_n^2)^2 \quad , \qquad \ldots (1.6)$$
$$y_{n+1} = 1 - (2 - (1 + x_n)\, y_n^2)\, (1 - (1 + y_n)\, x_n^2)^2 \quad ,$$

and the first four iterates of the line $y_n = 1$, $x_n \in [0.5, 0.85]$, under this map gives Figure (5c), which clearly shows the boundary demarkation of the attractor by the J = 0 line.

Particularly noticeable in the above figure is the inner cusp-like structures formed from the convoluted J = 0 line. These features are apparent in the strange attractor where they show up as lines of increased density. We can now understand the fine scale dynamical behaviour of the symmetric map in terms of the successive wrapping of the J = 0 lines.

Regions on one side of a line J = 0 will be folded over to the other side, thus the boundary lines of the strange attractor will fold in points exterior to it. These points are then trapped within the attractor and undergo chaotic motion as a result of the successive foldings due to the presence of the convoluted J = 0 lines.

1.3.4 Conclusion

In this section the main features of the symmetric map have been described and, to some extent, explained. It has been found that there is no direct link with the dynamics of the 1-D logistic

map, although confinement of orbits due to singularities in the map is common to both the ons, and two dimensional maps.

The fact that both Lyapunov exponents appear to be positive, and the phenomenon of enslaving of orbits to the chaotic regions appear to be new features which are not present in the standard 2-D maps mentioned in the first section.

One restricting feature of the symmetric map is that it does not contain a parameter. In the next section the system will be parameterised in a seemingly 'natural' way and the resulting system studied.

Finally, a form of perturbation theory is brought to bear on the system, the results of which show behaviour very like the original.

2.0 Parameterised Map

We parameterise the system in the following way:

$$x_{n+1} = 1 - [a + (2 - a)\, y_n]\, x_n^2 \quad ,$$
$$y_{n+1} = 1 - [a + (2 - a)\, x_n]\, y_n^2 \quad , \qquad \ldots (2.1)$$

where 'a' is the parameter.

It is then apparent that the parameter value a = 2 corresponds to the two maps being uncoupled, whilst a = 1 gives the symmetric map previously studied.

Equations (2.1) represent, then, a smooth parameterisation of the symmetric map, taking it from a coupled to an uncoupled system as 'a' ranges between 1 and 2, with as yet unknown behaviour between

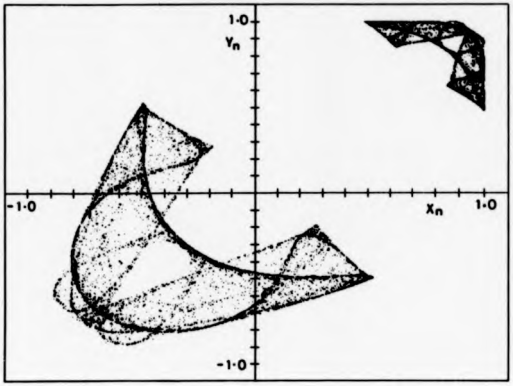

Figure 5d : Attractor for a = 1.02

these limits. A typical numerical iteration of Equation (2.1) is shown in Figure (5d) for the parameter value: a = 1.02. Although a fourfold attractor similar to that considered in the last section would appear to be present in Figure (5d), the points actually move randomly around the state-space, showing none of the fourfold periodicity previously uncovered by colour coding of orbits. In fact this would seem to be true for all 'a' values strictly greater than 1. As 'a' is decreased from two (at which value, initial conditions randomly fill the whole state space) the area of attraction gradually diminishes in size , and becomes more akin in shape to the symmetric map attractor. Points tend to move around the attracting region in a completely random fashion until, at the parameter value a = 1, a kind of symmetry breaking occurs in which four attracting regions separate out to form the period 4 attractor.

This, then, is the situation pertaining to the parameter regime $1 < a < 2$, and apart from the symmetry breaking at a = 1 it is apparent that there is little of interest in the dynamics of the system in this regime.

A totally different situation exists, however, if we allow the parameter to take on values less than one.

At the value a = 0.8907 a stable period 4 orbit exists, whose members lie at positions symmetrical with respect to the diagonal and the second plane of symmetry between 'small' and 'large' attractors described in the last section. It should be noted, however, that the basin of attraction of this orbit does not extend over all state space and consequently, some initial conditions

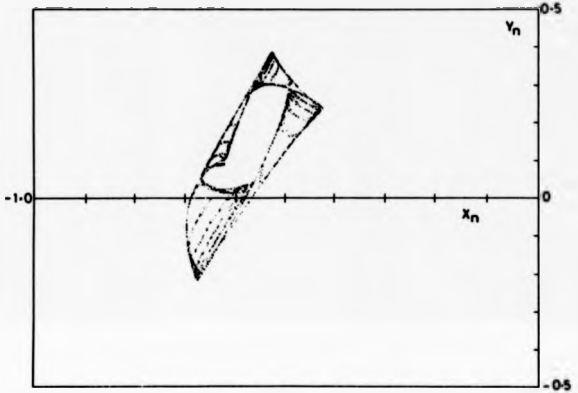

(iii)

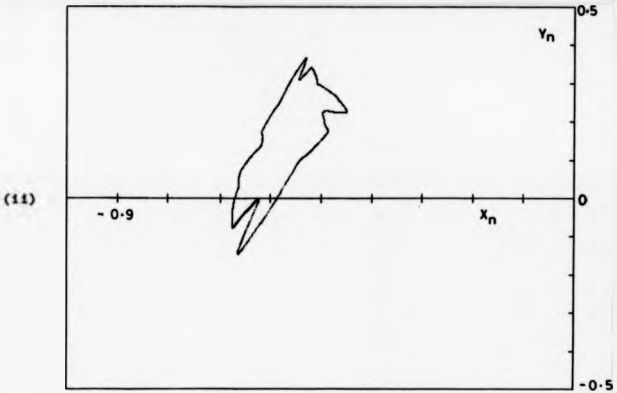

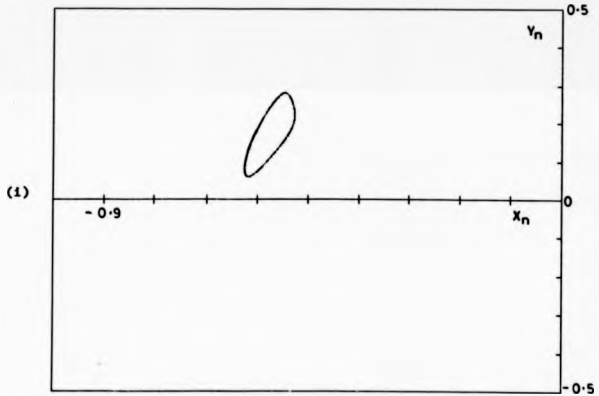

Figure 5a : Attractors for Various Values of a
(i) a = 0.9 (ii) a = 0.93 (iii) a = 0.94

escape to infinity. Also, at parameter values below the above value, 'almost all' initial conditions blow up in this way.

As 'a' is increased to 1, each point of the stable orbit undergoes a Hopf bifurcation to give four periodic islands, these islands contort into more complex shapes as the parameter is increased. Thus, we see the situation in Figures (5a) for various values of 'a'. For some parameter values extremely complicated attractors exist (only one of the four attractors is shown in each figure), whilst at other values, these attractors collapse into quasiperiodic or periodic orbits. The appearance of periodic attractors amongst the (supposedly) chaotic attractors seems to be random with respect to the parameter space. There is a striking similarity here between the type of behaviour described above, and that found for a two parameter system of the form:

$$x_{n+1} = \alpha y_n + \beta x_n + 2x_n^2$$
$$y_{n+1} = \alpha x_n + \beta y_n + 2y_n^2 \qquad \ldots (2.2)$$

as described by Fröyland [11], and similar systems studied by Hogg and Hubermann [17], and Jeffries [20]. In particular, the former considers the case of 'frequency locking' (periodicity) and subsequent 'frequency slippage' (quasiperiodicity) as described above, to be generic features of coupled oscillators, whilst Jefferies considers systems of the above form as models of chaotic behaviour in resonantly driven p-n junctions in silicon. The similarity between the numerical and experimentally observed strange attractors in this case suggests that although the features of coupled parameterised maps as described above, are extremely complex, there is, nevertheless, evidence that physical structures can, and do, support such behaviour.

2.1 Analytical Results

It was mentioned earlier in this section that at a = 0.8907, a period four orbit exists, consisting of four fixed points which subsequently undergo a Hopf bifurcation to give quasiperiodic islands. This situation suggests that the parameterised system is amenable to a perturbation analysis around each stable fixed point. The incentive here is provided by a paper by Rowlands and Bridges [3], in which a perturbation analysis of the Hénon map, around a fixed point, led to an iterative scheme which reproduced the Hénon attractor to a high degree of accuracy.

Although the attractor in the present case is much more complicated in structure than the Hénon case, it might be hoped that some features of the parameterised system might be evident in the perturbative solution for some range in parameter and state-space.

We begin then by 'collapsing' the period four attractor to a period one attractor, for the parameterised system, by the method of the last section. Thus, we have:

$$x_{n+1} = 1 - \left(2 - b(a + by_n)x_n^2 \right) \left(1 - (a + bx_n)y_n^2 \right)^2,$$

$$y_{n+1} = 1 - \left(2 - b(a + bx_n)y_n^2 \right) \left(1 - (a + by_n)x_n^2 \right)^2. \qquad \ldots (2.3)$$

where $b = (2 - a)$.

For some parameter value $a = \bar{a}$ we have four stable fixed points of Equation (2.3) one of which is at $(x,y) = (\bar{x},\bar{y})$.

We now wish to expand Equation 2.3 around $(\bar{a},\bar{x},\bar{y})$, writing:

$$x_n = \bar{x} + \delta x_n, \quad y_n = \bar{y} + \delta y_n, \quad a = \bar{a} + \delta a;$$

In accordance with standard multiple scales methodology we order the variables δx, δy, δa, thus:

$$\delta x_n = \varepsilon \overset{1}{x_n} + \varepsilon^2 x_n^2 + \ldots \text{ etc.}$$

$$\delta y_n = \varepsilon \overset{1}{y_n} + \varepsilon^2 y_n^2 + \ldots \text{ etc.}$$

$$\delta a = \varepsilon^2$$

Then expanding Equations 2.3 according to the above, we obtain for first order (order ε):

$$\begin{aligned} \overset{1}{x}_{n+1} &= A\overset{1}{x}_n + B\overset{1}{y}_n \ , \\ \overset{1}{y}_{n+1} &= C\overset{1}{x}_n + D\overset{1}{y}_n \ , \end{aligned} \qquad \ldots (2.4)$$

where $A = A(\bar{a},\bar{x},\bar{y})$ etc., are functions of $\bar{a},\bar{x},\bar{y}$, given in Appendix B. We now reduce Equations 2.4 to one second order equation thus,

$$\begin{aligned} \overset{1}{x}_{n+2} &= (A + D)\ \overset{1}{x}_{n+1} + (BC - AD)\ \overset{1}{x}_n \ , \\ \overset{1}{x}_{n+2} &= \bar{\phi}\overset{1}{x}_{n+1} - \bar{\psi}\overset{1}{x}_n \ , \end{aligned} \qquad \ldots (2.5)$$

or, $\hat{L}\ \overset{1}{x}_n = 0$,

$$\bar{\phi} = A + D, \quad \bar{\psi} = AD - BC$$

To solve Equation 2.5 we write:

$$\overset{1}{x}_n = e^{\lambda n} \ ,$$

which gives a condition on e^{λ}:

$$e^{\lambda} = \sqrt{\bar{\psi}}\ \left\{\frac{\bar{\phi}}{2\sqrt{\bar{\psi}}} \pm i\ \left[1 - \left(\frac{\bar{\phi}}{2\sqrt{\bar{\psi}}}\right)\right]^{\frac{1}{2}}\right\} \ . \text{ (taking } 4\bar{\psi} > \bar{\phi}^2\text{)}$$

The critical point (Hopf bifurcation) is given by:

$$\lambda = i\omega \quad ,$$

which implies $\overline{\psi} = 1$, $\cos\omega = \frac{\overline{\phi}}{2\sqrt{\psi}}$

we can now write:

$x_n^1 = \phi e^{i\omega n} + \psi e^{-i\omega n}$, where ϕ and ψ, are constants to this order. The solution for y_n^1 is obtained from Equations 2.4 thus,

$$x_{n+1}^1 = Ax_n^1 + By_n^1 \Rightarrow$$

$$\Rightarrow y_n^1 = \xi e^{i\omega n} + \eta e^{i\omega n}, \text{ where } \xi = \frac{1}{B}\left(\phi e^{i\omega} - A\phi\right],\ \eta = \frac{1}{B}\left[\ \psi e^{-i\omega} - A\psi\ \right]$$

Combining the above results gives the first order solutions:

$$\begin{aligned} x_n^1 &= \phi e^{i\omega n} + \psi e^{-i\omega n}, \\ y_n^1 &= \xi e^{i\omega n} + \eta e^{i\omega n}, \end{aligned} \qquad \ldots (2.6)$$

with ϕ, ψ, ξ, η, constants to this order.

Proceeding in similar fashion to the second order we obtain the following equation for $x^2{}_n$:

$$\hat{L}x_n^2 = A'\left(x_n^1\right)^2 + B'\left(y_n^1\right)^2 + C'\,x_n^1\,y_n^1 + E'\left(x_{n+1}^1\right)^2 + F'\left(y_{n+1}^1\right) + G'\left(x_{n+1}^1\,y_{n+1}^1\right) + D'\,\delta s \ , \qquad \ldots (2.7)$$

where the A', B', etc., are listed in Appendix B.

Inserting the expressions for x_n^1 and y_n^1 in Equation 2.7 gives:

$$\hat{L}x_n^2 = \bar{\bar{A}}e^{2i\omega n} + \bar{\bar{B}}e^{-2i\omega n} + \bar{\bar{C}} \quad , \qquad \ldots (2.8)$$

with solution:

$$x_n^2 = \bar{A}e^{2i\omega n} + \bar{B}e^{-2i\omega n} + \bar{C} \quad , \qquad \ldots (2.9)$$

where $\bar{A} = \dfrac{\bar{\bar{A}}}{(e^{4i\omega} - \bar{\phi}e^{2i\omega} + \bar{\psi})}$, $B = \dfrac{\bar{\bar{B}}}{(e^{-4i\omega} - \bar{\phi}e^{-2i\omega} + \bar{\psi})}$, and

$\bar{C} = \dfrac{\bar{\bar{C}}}{(1 - \bar{\phi} + \bar{\psi})}$, with $\bar{\bar{A}}$, $\bar{\bar{B}}$, $\bar{\bar{C}}$ given in Appendix B.

Substituting for y_n^2 gives:

$$y_n^2 = \bar{\bar{D}}e^{2i\omega n} + \bar{\bar{E}}e^{-2i\omega n} + \bar{\bar{F}} \quad , \qquad \ldots (2.10)$$

with $\bar{D}$, $\bar{E}$, and $\bar{F}$ given in Appendix B.

The third order equations are derived in a similar manner, the main steps being sketched in Appendix B. However, at this stage we are interested only in the secular terms i.e. terms in $e^{i\omega n}$, and $e^{-i\omega n}$.

Referring to Equation B.4 in the appendix, we have the third order equation:

$$\hat{L}x_n^3 = BT_n - DS_n + S_{n+1} \quad . \qquad \ldots (2.11)$$

We rewrite the solution for x_n^1 (Equation 2.6) as:

$$x_n^1 = \phi e^{i\omega n} + \phi^* e^{-i\omega n} = \phi e^{i\omega n} + c.c. \qquad \ldots (2.12)$$

where $\phi^* = \bar{\phi}$ = complex conjugate of ϕ.

We now take ϕ (and ϕ^*) to be slowly varying functions of n, in the sense that $(\phi_{n+1} - \phi_n) \sim O(\epsilon)$. thus, retaining terms in $e^{i\omega n}$ ($e^{-i\omega n}$), the right hand side of Equation 2.11 takes the form:

$$S_1\ \phi_n{}^2\ \phi_n{}^* + S_2\ \phi_n + S_3\ \phi^2{}_{n+1}\ \phi^*{}_{n+1} + S_4\ \phi_{n+1} + c.c. \qquad \ldots (2.13)$$

where the S_i are functions of $\bar{x}$, $\bar{y}$, $\bar{a}$.

In Equations 2.5 we wrote:

$\hat{L}x_n^1 = 0$ to the first order.

Now, at third order, we substitute $\phi \to \phi_n$ etc., into the above to give the 'multiple timescale' terms analogous to the derivative terms in the continuous case. The terms so obtained will then be set equal to the expression in Equation 2.13 to form the required consistency condition for the vanishing of secular terms.

Expanding Equation 2.5 we have:

$$\hat{L}x_n^1 = \phi_{n+2} e^{i\omega n} e^{2i\omega} - \bar{\phi}\ \phi_{n+1} e^{i\omega n} + \phi_n e^{i\omega n} \qquad \ldots (2.14)$$

Splitting ϕ_{n+1} as $\phi_n + (\phi_{n+1} - \phi_n)$ etc., we obtain:

$$\hat{L}x^1 = \phi_n \left[e^{2i\omega} - \bar{\phi} e^{i\omega} + 1 \right] + \left(\phi_{n+2} - \phi_n \right) e^{2i\omega} - \left(\phi_{n+1} - \phi_n \right) \bar{\phi} e^{i\omega} = \left(\phi_{n+2} - \phi_n \right) e^{2i\omega} - \left(\phi_{n+1} - \phi_n \right) \bar{\phi} e^{i\omega} \qquad \ldots (2.15)$$

the coefficient of ϕ_n above vanishing by virtue of the definition of ϕ. Equation 2.15 can be further simplified to:

$$Lx^1 = (\phi_{n+2} - \phi_{n+1})\, e^{2i\omega} - (\phi_{n+1} - \phi_n) \qquad \ldots (2.16)$$

We thus obtain, finally, the following consistency condition in the ϕ_n:

$$\phi_{n+2} = (A + iB)\ \phi_n^2\ \phi_n^* - (C + iD + \delta a\ (E + iF))\ \phi_n + \\ + (G + iH)\ \phi^2_{n+1}\ \phi^*_{n+1} + (J + iK + \delta a\ (L + iM))\ \phi_{n+1} \qquad \ldots (2.17)$$

with the coefficients A to M given in Appendix B. This is the equation which we will now study.

2.2 Numerical Results

The difference equation given by Equation 2.17 being of the second order with complex coefficients, is quite complicated. However, an indication of the type of solutions to be expected can be obtained by numerically iterating the equation for various values of the parameter δa.

We begin by writing:

$$\phi_n = \psi_n + i\sigma_n, \quad \phi^*_n = \psi_n - i\sigma_n \text{ etc.}$$

This then gives two coupled nonlinear equations in the real and imaginary parts of the function ϕ_n:

$$\psi_{n+2} = (A\psi_n - B\sigma_n)\ (\psi_n^2 + \sigma_n^2) - (C + \delta aE)\ \psi_n + (D + \delta aF)\ \sigma_n + \\ + (G\psi_{n+1} - H\sigma_{n+1})\ (\psi_{n+1}^2 + \sigma_{n+1}^2) + (J + L\delta a)\ \psi_{n+1} - \\ - (K + M\delta a)\ \sigma_{n+1}\ ,$$

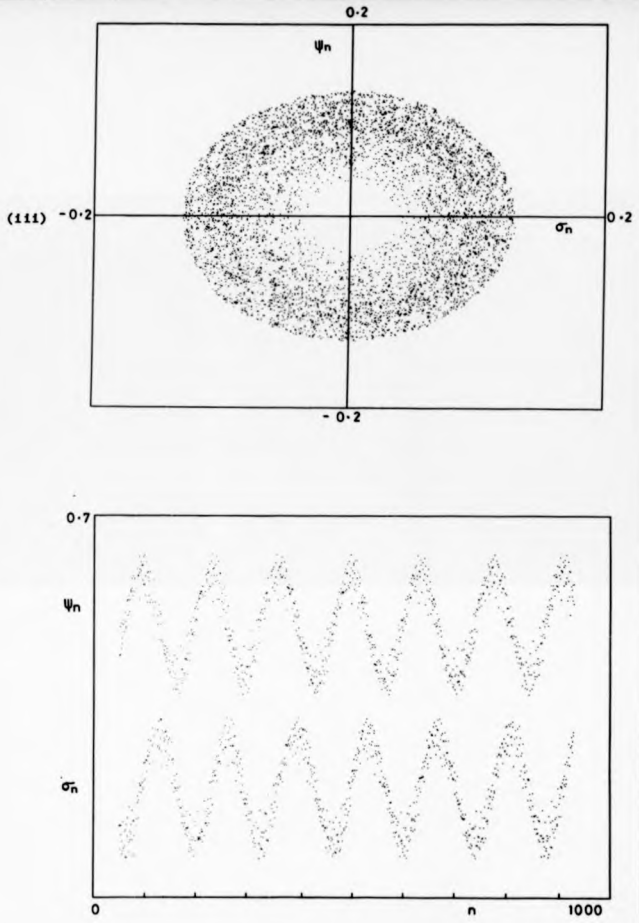

Figure 5g : Amplitudes for $\delta a = 0.165$

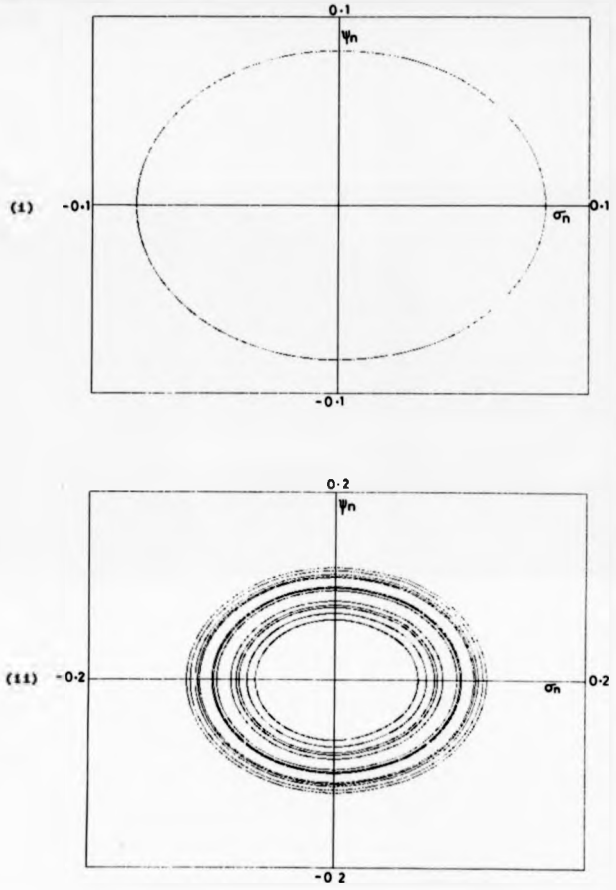

Figure 5f : Perturbation Solutions for Various Values of δa
(i) $\delta a = 0.1$ (ii) $\delta a = 0.15$ (iii) $\delta a = 0.165$

$$\sigma_{n+2} = (A\sigma_n + B\psi_n)(\psi_n^2 + \sigma_n^2) - (C + \delta aE)\sigma_n - (D + \delta aF)\psi_n + \\ + (G\sigma_{n+1} + H\psi_{n+1})(\psi_{n+1}^2 + \sigma_{n+1}^2) + (J + L\delta a)\sigma_{n+1} + \\ + (K + M\delta a)\psi_{n+1}$$

... (2.18)

Upon inserting the numerically determined values:

$\overline{a} = 0.8907,$

$\overline{x} = -0.5733,$

$\overline{y} = 0.1842,$

$\overline{b} = 1.1093,$

and suitable initial conditions for ψ_n, ψ_{n+1}, σ_n, σ_{n+1}, Equations (2.18) were iterated a large number of times, the results being shown in Figure (5f) as plots of ψ_n against σ_n for various δa values.

For δa in the range $0 < \delta a < 0.12$, sinusoidal behaviour of the ψ_n, σ_n was observed. This was manifest as a circle in ψ_n, σ_n space whose radius increased from zero (at $\delta a = 0$), to a maximum at $\delta a = 0.12$. With reference to the original solution of the equations given in Equation 2.12 above, it is apparent that this behaviour corresponds to the growth of the limit cycle created in the Hopf bifurcation of the original system. For δa in the range $0.12 < \delta a < 0.17$, however, the periodic cycle is observed to bifurcate to an apparently chaotic state. For $\delta a > 0.17$ all initial conditions investigated were observed to 'blow up' with no apparent attracting set present.

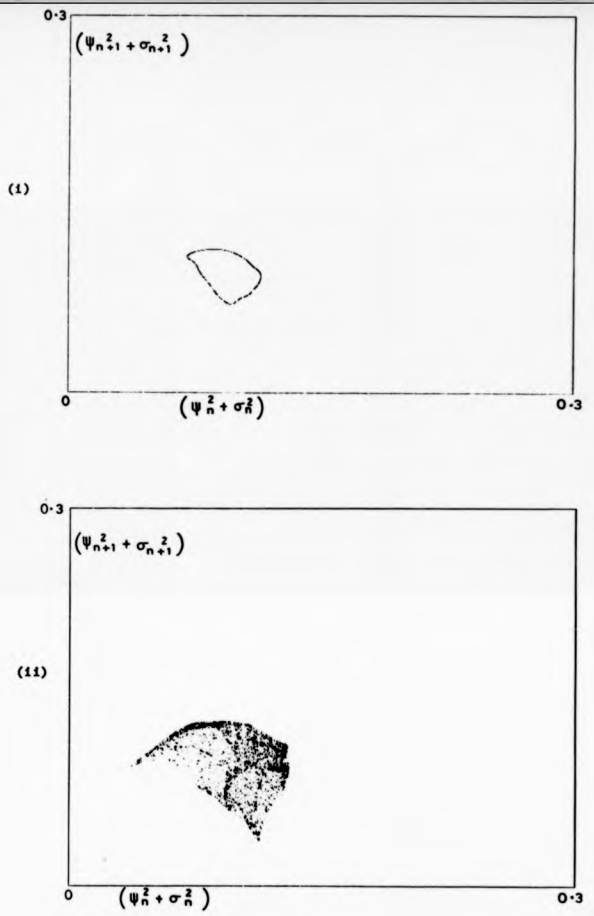

Figure 5h : Amplitude Maps for Two Values of $\delta\alpha$
(i) $\delta\alpha = 0.14$ (ii) $\delta\alpha = 0.165$

Finally, in Figure (5g) both ψ_n and σ_n are plotted as functions of n for $\delta a = 0.165$. It is apparent that there is a (slow) sinusoidal amplitude variation of each function, on top of which is imposed a (fast) chaotic response.

In order to investigate the bifurcation to chaos further, a numerical plot of $(\psi_n^2 + \sigma_n^2)$ against $(\psi_{n+1}^2 + \sigma_{n+1}^2)$ was made for δa values in the interval (0.12, 0.17). This corresponds to considering only the amplitude variation of ϕ_n, neglecting the phase variation, and is thus a projection of the full 4-dimensional system.

Some results are shown in Figure (5h), and show a striking similarity to the behaviour of the original system.

As δa is increased a fixed point is observed to undergo a Hopf bifurcation to a limit cycle which then grows in amplitude and contorts in shape. A region of periodic motion is then encountered interspersed with regions of chaotic motion. A typical strange attractor is shown in Figure (5h(ii)). The attractor possesses characteristics similar to the strange attractor of the original system, in particular the cusp-like structures, and 'folding' within the attractor.

The question is now, is the behaviour exhibited by the consistency equations related to the behaviour of the original system?

An affirmative answer would imply that the chaos had been 'captured' by the discrete multiple-time expansion in contrast to the continuous case where the consistency conditions cannot themselves exhibit chaotic behaviour.

Upon reflection it would seem that the answer to the above question must be negative. Firstly, the parameter range for which chaotic motion is present in Equations 2.18 lies outside the range of the original system parameter i.e. δa varies between 0 and 0.17 instead of 0 and about 0.11, and whilst this difference could be accounted for by numerical errors it casts doubt on the relationships between the chaos in the two systems.

Secondly, we have implicitly assumed ϕ_n to be slowly varying in the perturbation analysis, whilst periodic and chaotic motion are inherently fast. It would therefore appear that our assumptions have already broken down by the time the chaotic regime is encountered.

Having said this, however, it is apparent from Figure (5g) that the amplitude of ϕ_n is indeed a slowly varying quantity, in some sense, with a fast chaotic component superimposed.

Thus, although it is difficult to resolve the above question, it would appear that a perturbation analysis, such as the one described, can capture the limit cycle behaviour of the original system. The subsequent complicated bifurcation and chaotic behaviour would then seem to be typical, generic, behaviour for this type of system.

CHAPTER 6

CONCLUSION

The work in this thesis falls into two parts. The aim of the first part was to derive a Poincaré map for the Duffing equations using approximate analytical solutions of the system. The justification for this type of approach has not yet been made rigorous, although successful attempts have been made in the past to derive Poncaré maps for the 'Lorenz' and 'Forced Brusselator' equations [32], [4]. In both these cases, additional 'global' information had to be input to the derived difference map in order for the maps to become chaotic. The nature of this additional information depends on the particular system in hand and it is therefore difficult to justify the method as a whole.

The 'multiple scales' method used in the above papers and this thesis cannot be expected to give chaotic solutions, as the method was developed to study bounded periodic behaviour. However, if we postulate that 'non-expandable' terms i.e. terms of the form $e^{-1/t}$, for example, which are 'missed' by the perturbation expansion, are important features of the chaotic solutions, then the past success of the method appears more understandable. In such a situation, although the error in the approximate solution grows continuously in time, the error introduced into the discrete return map is only of order $e^{-1/\tau}$ per iteration, where τ is the period of the return.

The fact that these errors are only additive may explain why the difference scheme gives a good representation of the chaotic behaviour of the above systems.

In applying the above methodology to the Duffing equations, it was found necessary to develop a slightly different perturbation method based on exact solutions of a Hamiltonian system.

Because of the complexity of the resulting expressions, it was necessary to assume the solutions to be at resonance with the driving frequency of the system. With such an assumption, it was possible to derive a 1-D Poincaré map both inside and outside the homoclinic orbit. The mapping is somewhat abstracted from the original system and its relevance is therefore open to question. Further, the 'global input' is to join the curves precisely at the point where chaos occurs i.e. the homoclinic orbit. This, combined with the flattening of the 'inside' curve due to the strongly attracting, fixed point, means that 'critical' values of the forcing 'f' for the onset of period doubling and chaos cannot be derived from the map for comparison with experiment.

It would appear, therefore, that the chaotic dynamics of the Duffing system can only be reduced to a two dimensional system, and that efforts to derive this 2-D Poincaré map from perturbation theory would need to 'break' the stability of the attracting limit cycles in the perturbation solution.

The second part of the thesis considered the behaviour of a symmetrically coupled 2-D discrete map.

The characteristic behaviour of typical chaotic orbits was explained by reference to the 1-D logistic map and its parameter space. Singularities in the distribution function of the map were shown to bound the chaotic motion in state-space, and hence explain the existence of two positive Lyapunov exponents for the map.

A parameterisation of the map was given, and the extremely complicated bifurcation behaviour of the system was described.

Finally, a perturbation method was applied to the system. The perturbation solutions were found to exhibit a Hopf bifurcation followed by period doubling to a chaotic state. The existence of chaos in the perturbation solutions of the discrete system is in sharp contrast to the continuous case, where solutions obtained by perturbation theory must always be periodic or quasi-periodic.

The relavance of the appearance of chaos in the perturbation solutions to the chaotic behaviour of the original system is unclear. The perturbation theory assumes slowly varying quantities whilst the chaotic motion implies a rapidly varying quantity. Given this, it is apparent from numerical studies that the solutions are indeed slowly varying quantities with a superimposed chaotic component.

The extremely complicated bifurcation behaviour of both the original parameterised system and the perturbation solutions appears to be the generic behaviour to be expected of this type of system.

APPENDIX A

The following definitions refer to Equations given in Chapter 4.

Equation (2.13)

$A_1 = 9D^2 + B^2$, $A_2 = D^4 - 2ABC + B^2 D^2$, $A_3 = 6D$, $A_4 = 2D^2$

$A_5 = -2C$, $A_6 = 6D$, $A_7 = 6D^3 + 2B^2 D$, $A_8 = -6DC$, $A_9 = 2D^2$,

$B_1 = -2C$, $B_2 = -(2CD^2 + B^2C)$, $B_3 = A^2C - 2ABD^2$, $B_4 = -A^2$,

$B_5 = -2A^2D$, $B_6 = -A^2D^2$, $B_7 = -2AB$, $B_8 = -4ABD$.

Equation (2.14)

$$\overline{A}_1 = -(A_1 \rho_0^2 + A_9 \rho_0^2 + B_1 - B_4 \rho_0^6 - B_7 \rho_0^4)$$

$$\overline{A}_2 = -(6A_2 \rho_0^2 + B_2 - 15B_3 \rho_0^4 - 28B_6 \rho_0^6)$$

$$\overline{A}_3 = -A_3 \rho_0^2$$

$$\overline{A}_4 = -(3A_4 \rho_0^2 + A_5)$$

$$\overline{A}_5 = -(2A_4 \rho_0^3 + 2A_5 \rho_0)$$

$$\overline{A}_6 = -(A_7 \rho_0^3 + A_8 \rho_0 - B_5 \rho_0^7 - B_8 \rho_0^5)$$

$$\overline{A}_7 = -(3A_7 \rho_0^2 + A_8 - 7B_5 \rho_0^6 - 5B_8 \rho_0^4)$$

Equations (2.33), (2.34)

$A_1 = 1.206$

$A_2 = 0.042$

$A_3 = -0.168$

$A_4 = 1.172$

$A_5 = 1.404$

$A_6 = 0.304$

$A_7 = 0.927$

$A_8 = 0.804$

$A_9 = 0.564$

$A_{10} = -0.539$

Equation (2.36)

$$A_1 = \frac{2}{\omega}\sqrt{\frac{\alpha}{\beta}}$$

$$A_2 = \frac{7}{4\omega}\sqrt{\frac{\alpha}{\beta}}$$

$$A_3 = \frac{1}{2}$$

APPENDIX B

The following definitions refer to equations given in Chapter 5.

Equation 2.4

$$A = 2\overline{ab}\,\overline{x} + 4\overline{b}\overline{y}^2 + 2\overline{b}^2\overline{yx} - 4\overline{a}^2\overline{bxy}^2 - 4\overline{ab}\overline{y}^4 - 6\overline{ab}^2\overline{x}^2\overline{y}^2 -$$
$$- 4\overline{ab}^2\overline{xy}^3 - 4\overline{b}^2\overline{xy}^4 - 6\overline{b}^3\overline{x}^2\overline{y}^3 + 2\overline{a}^3\overline{by}^4\overline{x} + 6\overline{a}^2\overline{b}^2\overline{x}^2\overline{y}^4 +$$
$$+ 2\overline{a}^2\overline{b}^2\overline{xy}^5 + 4\overline{ab}^3\overline{x}^3\overline{y}^4 + 6\overline{ab}^3\overline{x}^2\overline{y}^5 + 4\overline{b}^4\overline{x}^3\overline{y}^5$$

$$B = 8\overline{ay} + 8\overline{bxy} + \overline{b}^2\overline{x}^2 - 8\overline{a}^2\overline{y}^3 - 4\overline{a}^2\overline{bx}^2\overline{y} - 16\overline{abxy}^3 -$$
$$- 4\overline{ab}^2\overline{x}^3\overline{y} - 6\overline{ab}^2\overline{y}^2\overline{x}^2 - 8\overline{b}^2\overline{x}^2\overline{y}^3 - 6\overline{b}^3\overline{x}^3\overline{y}^2 + 4\overline{a}^3\overline{bx}^2\overline{y}^3 +$$
$$+ 8\overline{a}^2\overline{b}^2\overline{x}^3\overline{y}^3 + 5\overline{a}^2\overline{b}^2\overline{x}^2\overline{y}^4 + 4\overline{ab}^3\overline{x}^4\overline{y}^3 + 10\overline{ab}^3\overline{x}^3\overline{y}^4 + 5\overline{b}^4\overline{x}^4\overline{y}^4$$

where $\overline{b} = 2 - \overline{a}$.

C is given by exchanging $\overline{x}$ and $\overline{y}$ in the expression for A, i.e. $C(\overline{x},\overline{y}) = A(\overline{y},\overline{x})$.

D is given by exchanging $\overline{x}$ and $\overline{y}$ in the expression for B, i.e. $D(\overline{x},\overline{y}) = B(\overline{y},\overline{x})$.

Equation 2.7

Define:

$$E = \overline{ab} + \overline{b}\,\overline{y} - 2\overline{a}^2\overline{by}^2 - 6\overline{ab}^2\overline{xy}^2 - 2\overline{ab}^2\overline{y}^3 - 2\overline{b}^2\overline{y}^4 - 6\overline{b}^3\overline{xy}^3 +$$
$$+ \overline{a}^3\overline{by}^4 + 6\overline{a}^2\overline{b}^2\overline{xy}^4 + \overline{a}^2\overline{b}^2\overline{y}^5 + 6\overline{ab}^3\overline{x}^2\overline{y}^4 + 6\overline{ab}^3\overline{xy}^5 + 6\overline{b}^4\overline{x}^2\overline{y}^5$$

$$F = 4\overline{a} + 4\overline{bx} - 12\overline{a^2y^2} - 2\overline{a^2bx^2} - 24\overline{abxy^2} - 2\overline{ab^2x^3} -$$

$$- 6\overline{ab^2yx^2} - 12\overline{b^2x^2y^2} - 6\overline{b^3x^3y} + 6\overline{a^3bx^2y^2} + 12\overline{a^2b^2x^3y^2} +$$

$$+ 10\overline{a^2b^2x^2y^3} + 6\overline{ab^3x^4y^2} + 20\overline{ab^3x^3y^3} + 10\overline{b^4x^4y^3}$$

$$G = 8\overline{by} + 2\overline{b^2x} - 8\overline{a^2bxy} - 16\overline{aby^3} - 12\overline{ab^2x^2y} - 12\overline{ab^2y^2x} -$$

$$- 16\overline{b^2xy^3} - 18\overline{b^3x^2y^2} + 8\overline{a^3bxy^3} + 24\overline{a^2b^2x^2y^3} + 10\overline{a^2b^2xy^4} +$$

$$+ 16\overline{ab^3x^3y^3} + 30\overline{ab^3x^2y^4} + 20\overline{b^4x^3y^4}$$

$$L = 4\overline{y^2} + (\overline{b-a})\overline{x^2} - 4\overline{xy^2} - 2\overline{byx^2} - 4\overline{ay^4} - 2(2\overline{ab-a^2})\overline{x^2y^2} -$$

$$- 4(\overline{b-a})\overline{xy^4} - 2(\overline{b^2-2ba})\overline{x^3y^2} - 2(\overline{b^2-2ba})\overline{y^3x^2} + 4\overline{bx^2y^4} +$$

$$+ 6\overline{b^2x^3y^3} + (3\overline{a^2b-a^3})\overline{x^2y^4} + 2(2\overline{ab^2-2ba^2})\overline{x^3y^4} +$$

$$+ (2\overline{ab^2-2ba^2})\overline{x^2y^5} + (\overline{b^3-3ab^2})\overline{x^4y^4} + 2(\overline{b^3-3ab^2})\overline{x^3y^5} -$$

$$- 4\overline{b^3x^4y^5}$$

and $H(\overline{x},\overline{y}) = E(\overline{y},\overline{x})$,

$J(\overline{x},\overline{y}) = F(\overline{y},\overline{x})$,

$K(\overline{x},\overline{y}) = G(\overline{y},\overline{x})$,

$M(\overline{x},\overline{y}) = L(\overline{y},\overline{x})$,

Then:

A' = BH-ED

B' = BJ-FD

C' = BK-GD

D' = BM+L - LD

E' = E

F' = F

G' = G

Equation 2.8

Define: $T = 2\,\phi\psi$, $S = 2\,\xi\,\eta$, $W = \phi\eta + \chi\,\xi$. Then:

$$\bar{A} = A'\phi^2 + B'\xi^2 + C'\phi\xi + E'e^{2i\omega}\phi^2 + F'e^{2i\omega}\xi^2 + G'e^{2i\omega}\phi\xi \quad .$$

$$\bar{B} = A'\psi^2 + B'\eta^2 + C'\psi\eta + E'e^{-2i\omega}\psi^2 + F'e^{-2i\omega}\eta^2 + G'e^{-2i\omega}\psi\eta \quad .$$

$$\bar{C} = A'T + B'S + C'W + D'\delta a + E'T + F'S + G'W \quad .$$

$$\bar{D} = \frac{1}{B}\left\{ \bar{A}e^{2i\omega} - A\bar{A} - E\phi^2 - F\xi^2 - G\phi\xi \right\}$$

$$\bar{E} = \frac{1}{B}\left\{ \bar{B}e^{-2i\omega} - A\bar{B} - E\psi^2 - F\eta^2 - G\psi\eta \right\}$$

$$\bar{F} = \frac{1}{B}\left\{ \bar{C} - A\bar{C} - ET - FS - GW - L\delta a \right\}$$

Equations Leading To Equation 2.11

Define:

$$\rho_1 = -2\bar{a}\bar{b}^2y^2 - 2\bar{b}^3y^3 + 2\bar{a}^2\bar{b}^2y^4 + 4\bar{a}\bar{b}^3xy^4 + 2\bar{a}\bar{b}^3y^5 + \\ + 4\bar{b}^4xy^5$$

$$\rho_2 = -8\bar{a}^2y - 16\bar{a}\bar{b}xy - 2\bar{a}\bar{b}^2x^2 - 8\bar{b}^2x^2y^2 + 4\bar{a}\bar{b}^2x^4y + \\ + 20\bar{a}\bar{b}^3x^3y^2 + 10\bar{b}^4x^4y^2$$

$$\rho_3 = 2\overline{ab} + 2\overline{b^2y} - 4\overline{a^2by^2} - 12\overline{ab^2xy^2} - 4\overline{ab^2y^3} - 4\overline{b^2y^3} -$$

$$- 12\overline{b^3xy^3} + 2\overline{a^3by^4} + 12\overline{a^2b^2xy^4} + 2\overline{a^2b^2y^5} + 12\overline{ab^3x^2y^4} +$$

$$+ 12\overline{ab^3xy^5} + 12\overline{b^4x^2y^5}$$

$$\rho_4 = 8\overline{a} + 8\overline{bx} - 24\overline{a^2y^2} - 4\overline{a^2bx^2} - 48\overline{abxy^2} - 4\overline{ab^2x^3} -$$

$$- 12\overline{ab^2yx^2} - 24\overline{b^2y^2x^2} - 12\overline{b^3x^3y} + 12\overline{a^3bx^2y^2} + 24\overline{a^2b^2x^3y^2} +$$

$$+ 20\overline{a^2b^2x^2y^3} + 12\overline{ab^3x^4y^2} + 40\overline{ab^3x^3y^3} + 20\overline{b^4x^4y^3}$$

$$\rho_5 = 8\overline{by} - 8\overline{a^2bxy} - 16\overline{aby^3} - 12\overline{ab^2x^2y} + 2\overline{b^2x} -$$

$$- 12\overline{ab^2y^2x} - 16\overline{b^2xy^3} - 18\overline{b^3x^2y^2} + 8\overline{a^3bxy^3} + 24\overline{a^2b^2x^2y^3} +$$

$$+ 10\overline{a^2b^2xy^4} + 16\overline{ab^3x^3y^3} + 30\overline{ab^3x^2y^4} + 20\overline{b^4x^3y^4}$$

$$\rho_6 = 8\overline{by} + 2\overline{b^2x} - 8\overline{a^2bxy} - 16\overline{aby^3} - 12\overline{ab^2x^2y} - 12\overline{ab^2y^2x} -$$

$$- 16\overline{b^2xy^3} - 18\overline{b^3x^2y^2} + 8\overline{a^3bxy^3} + 24\overline{a^2b^2x^2y^3} + 10\overline{a^2b^2xy^4} +$$

$$+ 16\overline{ab^3x^3y^3} + 30\overline{ab^3x^2y^4} + 20\overline{b^4x^3y^4}$$

$$\rho_7 = 4\overline{b} - 4\overline{a^2bx} - 24\overline{aby^2} - 6\overline{ab^2x^2} - 12\overline{ab^2yx} - 24\overline{b^2xy^2} -$$

$$- 18\overline{b^3x^2y} + 12\overline{a^3bxy^2} + 36\overline{a^2b^2x^2y^2} + 20\overline{a^2b^2xy^3} +$$

$$+ 24\overline{ab^3x^3y^2} + 60\overline{ab^3x^2y^3} + 40\overline{b^4x^3y^3}$$

$$\rho 8 = \overline{b}^2 - 4\overline{a^2by} - 12\overline{ab^2xy} - 6\overline{ab^2y^2} - 8\overline{b^2y^3} - 18\overline{b^3xy^2} +$$

$$+ 4\overline{a^3by^3} + 24\overline{a^2b^2xy^3} + 5\overline{a^2b^2y^4} + 24\overline{ab^3x^2y^3}$$

$$+ 30\overline{ab^3xy^4} + 30\overline{b^4x^2y^4}$$

$$\rho 9 = \delta a\{(\overline{b-a})2\overline{x} - 4\overline{y^2} - 4\overline{byx} - 4(2\overline{ab-a^2})\overline{xy^4} - 4(\overline{b-a})\overline{y^4} -$$

$$- 6(\overline{b^2-2ba})\overline{x^2y^2} - 4(\overline{b^2-2ba})\overline{y^3x} + 8\overline{bxy^4} + 18\overline{b^2x^2y^3} +$$

$$+ 2\overline{xy^4}(3\overline{a^2b-a^3}) + 12\overline{x^2y^4}(\overline{ab^2-ba^2}) + 4\overline{xy^5}(\overline{ab^2-2ba^2}) +$$

$$+ 4\overline{x^3y^4}(\overline{b^3-3ab^2}) + 6\overline{x^2y^5}(\overline{b^3-3ab^2}) - 16\overline{b^3x^3y^5}\}$$

$$\rho 10 = \delta a\ (8\overline{y}-8\overline{xy} - 2\overline{bx^2} - 16\overline{ay^3} - 4\overline{x^2y}\ (2\overline{ab-a^2}) -$$

$$- 16(\overline{b-a})\overline{xy^3} - 4(\overline{b^2-2ba})\overline{x^3y} - 6(\overline{b^2-2ba})\overline{y^2x^2} + 16\overline{bx^2y^3} +$$

$$+ 16\overline{b^2x^3y^2} + 4\overline{x^2y^3}(3\overline{a^2b-a^3}) + 16\overline{x^3y^3}(\overline{ab^2-ba^2}) +$$

$$+ 10(\overline{ab^2-ba^2})\overline{x^2y^4} + 4\overline{x^4y^3}(\overline{b^3-3ab^2}) + 10\overline{x^3y^4}(\overline{b^3-3ab^2}) -$$

$$- 20\overline{b^3x^3y^4}$$

and $\sigma_i(\overline{x},\overline{y}) = \rho_i(\overline{y},\overline{x})$, $i = 1, \ldots, 10$, then we obtain the third-order equation:

$$x_{n+1}{}^3 = Ax_n^3 + By_n^3 + \rho_1(x_n{}^1)^3 + \rho_2(y_n{}^1)^3 + \rho_3(x_n{}^1x_n{}^2) +$$

$$+ \rho_4(y_n{}^1y_n{}^2) + \rho_5(x_n{}^1y_n{}^2) + \rho_6(y_n{}^1x_{n2}) +$$

$$+ \rho_7(x_n{}^1(y_n{}^1)^2) + \rho_8(y_n{}^1(x_n{}^1)^2) + \rho_9\ x_n{}^1 + \rho_{10}\ y_n{}^1$$

$$y_{n+1}{}^3 = Cx_n{}^3 + Dy_n{}^3 + \sigma_1(x_n{}^1)^3 + \sigma_2(y_n{}^1)^3 + \sigma_3(x_n{}^1x_n{}^2) +$$
$$+ \sigma_4(y_n{}^1y_n{}^2) + \sigma_5(x_n{}^1y_n{}^2) + \sigma_6(y_n{}^1x_n{}^2) +$$
$$+ \sigma_7(x_n{}^1(y_n{}^1)^2) + \sigma_8(y_n{}^1(x_n{}^1)^2) + \sigma_9\, x_n{}^1 + \sigma_{10}\, y_n{}^1$$

... (B.1)

We rewrite these as:

$$x_{n+1}{}^3 = Ax_n{}^3 + By_n{}^3 + \hat{S}_n$$

... (B.2)

$$y_{n+1}{}^3 = Cx_n{}^3 + Dy_n{}^3 + \hat{T}_n$$

Which gives:

$$x_{n+2}{}^3 = (A+D)x_{n+1}{}^3 - (AD-BC)x_n{}^3 - D\hat{S}_n + B\hat{T}_n + \hat{S}_{n+1}$$

... (B.3)

And finally,

$$\hat{L}x_n{}^3 = B\hat{T}_n - D\hat{S}_n + \hat{S}_{n+1}$$

... (B.4)

Equation 2.17

Inserting expressions for $x_n{}^1$, etc., into Equation B.4, together with parameter values: $\bar{a} = 0.8907$, $\bar{x} = -0.5733$, $\bar{y} = 0.1842$, we obtain Equation 2.17 with:

A = -114.3595

B = -23.0654

C = -0.9614

D = 0.2751

J = 0.0386

K = 0.2751

L = 2.1191

M = -4.2293

APPENDIX C

C1 THE METHOD OF MULTIPLE SCALES

The method of multiple scales, to be described below, is one of a host of perturbation methods which have great power in deriving periodic solutions of weakly nonlinear systems [27],[28]. In essence, all such methods rely on perturbing the response of a corresponding linear system. In so doing, due account must be taken of the coupling of amplitude and frequency in the response of a non-linear system. It is the way in which this coupling is accounted for which broadly distinguishes the various perturbation methods.

Before describing the multiple scales method, some incentive for its use will be provided by considering the limitations of a straightfoward expansion method.

C2 STRAIGHT FORWARD EXPANSION

Consider the system:

$$\ddot{x} + f(x) = 0 \qquad \ldots (C.1)$$

We take the system to have a centre at $x = 0$, i.e. $f(0) = 0$, $f'(0) > 0$, and assume that f can be expanded in x. Thus (C.1) becomes:

$$\ddot{x} + \sum_{n=1}^{N} \alpha_n x^n = 0$$

$$\alpha_n = \frac{1}{n!} f^{(n)}(0) \qquad \ldots (C.2)$$

We assume that the solution of (C.2) can be expanded as follows:

$$x(t,\varepsilon) = \varepsilon x_1(t) + \varepsilon^2 x_2(t) + \varepsilon^3 x_3(t) + \ldots \qquad \ldots (C.3)$$

Substituting (C.3) into (C.2) and equating like powers of ε gives the following:

$$\begin{aligned} &\text{Order } \varepsilon \quad && \ddot{x}_1 + \omega_o^2 x_1 = 0 \\ &\text{Order } \varepsilon^2 \quad && \ddot{x}_2 + \omega_o^2 x_2 = -\alpha_2 x_1^2 \\ &\text{Order } \varepsilon^3 \quad && \ddot{x}_3 + \omega_o^2 x_3 = -2\alpha_2 x_1 x_2 - \alpha_3 x_1^3 \end{aligned} \qquad \ldots (C.4)$$

where $\omega_o = \sqrt{\alpha_1}$.

The general solution for $x_1(t)$ can be written:

$$x_1(t) = a \cos (\omega_o t + \beta) \qquad \ldots (C.5)$$

Substituting this into the equation for x_2 gives:

$$\ddot{x}_2 + \omega_o^2 x_2 = -\frac{1}{2} \alpha_2 a^2 [1 + \cos (2\omega_o t + 2\beta)] \qquad \ldots (C.6)$$

with general solution:

$$x_2(t) = \frac{\alpha_2 a^2}{6 \omega_o^2} [\cos (2\omega_o t + 2\beta) - 3] \qquad \ldots (C.7)$$

The homogeneous solution of (C.6) (and all subsequent equations) can be neglected in the above, as the imposition of initial conditions at the last step of the expansion renders them unecessary[28].

The equation for $x_3(t)$, using the above results is:

$$\ddot{x}_3 + \omega_o^2 x_3 = \left(\frac{5a_2^2}{6\omega_o^2} - \frac{3a_3}{4} \right) a^3 \cos\left(\omega_o t + \beta \right) - \left(\frac{a_3}{4} + \frac{a_2^2}{6\omega_o^2} \right) \cos\left(3\omega_o t + 3\beta \right) \quad \ldots (C.8)$$

Any particular solution of (C.8) will contain the term:

$$\left(\frac{10a_2^2 - 9a_3 \omega_o^2}{24\ \omega_o^3} \right) at \sin\left(\omega_o t + \beta \right) \quad \ldots (C.9)$$

and subsequent orders will give rise to terms in $t^n \cos\left(\omega_o t + \beta \right)$, $t^n \sin\left(\omega_o t + \beta \right)$. These 'secular terms' imply that the solution obtained by this method is not valid for all time. The problem is that the frequency-amplitude coupling has not been provided for in the method.

The method of multiple scale accounts for amplitude-frequency coupling by considering the solution of (C.1) to be a function of multiple independent timescales. With this method, secular terms can be elliminated through the solutions dependence on the various timescales. The criteria for the allimination of secular terms leads directly to the required amplitude-frequency dependance.

C3 MULTIPLE SCALES METHOD

We assume the solution of (C.1) to be of the form:

$$x(t,\varepsilon) = \varepsilon x_1 (T_0, T_1, T_2 \ldots) + \varepsilon^2 x_2 (T_0, T_1, T_2 \ldots) + \ldots \quad \ldots (C.10)$$

where the new independent variables, or 'timescales', are:

$$T_n = \varepsilon^n t \quad , \quad n = 0, 1, 2 \ldots$$

Derivatives are therefore transformed to:

$$\frac{d}{dt} = \frac{dT_0}{dt}\frac{\delta}{\delta T_0} + \frac{dT_1}{dt}\frac{\delta}{\delta T_1} + \ldots \quad = D_0 + \varepsilon D_1 + \ldots$$

$$\frac{d^2}{dt^2} = D_0^2 + 2\varepsilon D_0 D_1 + \varepsilon^2 (D_1^2 + 2D_0 D_2) + \ldots \quad \ldots (C.11)$$

The number of timescales needed depends on the order to which the expansion is carried out.

Substituting (C.10), (C.11), into (C.1), and equating like powers of ε gives:

$$D_0^2 x_1 + \omega_0^2 x_1 = 0$$

$$D_0^2 x_2 + \omega_0^2 x_2 = - 2D_0 D_1 x_1 - \alpha_2 x_1^2$$

$$D_0^2 x_3 + \omega_0^2 x_3 = - 2D_0 D_1 x_2 - D_1^2 x_1 - 2D_0 D_2 x_1 - 2\alpha_2 x_1 x_2 - \alpha_3 x_1^3 \quad \ldots (C.12)$$

We write the solution for x_1 as:

$$x_1 = A(T_1, T_2)\exp(i\omega_o T_o) + \bar{A}(T_1, T_2)\exp(-i\omega_o T_o) \quad \ldots (C.13)$$

where $\bar{A}$ = complex conjugate of A.

The equation for x_2 is then:

$$D_o^2 x_2 + \omega_o^2 x_2 = -2i\omega D_1 A \exp(i\omega_o T_o) - \alpha_2 [A^2 \exp(2i\omega_o T_o) + A\bar{A}] + c.c. \quad \ldots (C.14)$$

where c.c. = complex conjugate.

The solution will contain a secular term: $T_o \exp(i\omega_o T_o)$, unless $D_1 A = 0$, i.e. A is independent of the timescale T_1. Using this condition, the solution for x_2 is given by:

$$x_2 = \frac{\alpha_2 A^2}{3\omega_o^2}\exp(2i\omega_o T_o) - \frac{\alpha_2}{\omega_o^2} A\bar{A} + c.c. \quad \ldots (C.15)$$

where the homogeneous solution is again not needed.

The governing equation for x_3 is given by:

$$D_o^2 x_3 + \omega_o^2 x_3 = -\left[2i\omega_o D_2 A - \frac{10\alpha_2^2 - 9\alpha_3\omega_o^2}{3\omega_o^2} A^2\bar{A} \right] x$$

$$x \exp(i\omega_o T_o) - \frac{3\alpha_3\omega_o^2 + 2\alpha_2^2}{3\omega_o^2} x$$

$$x A^3 \exp(3i\omega_o T_o) + c.c. \quad \ldots (C.16)$$

The condition for the elimination of secular terms is that:

$$2i\omega_o D_2 A + \frac{9\alpha_3 \omega_o^2 - 10\alpha_2^2}{3\omega_o^2} A^2 \bar{A} = 0 \qquad \text{... (C.17)}$$

Equation (C.17) is solved by writing A in polar form:

$$A = \frac{a}{2} \exp(i\beta),$$

where a and β are real functions of T_2. This gives:

$$\omega a' = 0 \quad , \quad \omega_o a \beta' + \frac{10\alpha_2^2 - 9\alpha_3 \omega_o^2}{24\omega_o^2} a^3 = 0 \quad , \qquad \text{... (C.18)}$$

where $a' = \frac{\delta a}{\delta T_2}$, $\beta' = \frac{\delta \beta}{\delta T_2}$

The solution of (C.18) gives the following expression for A(t):

$$A(t) = \frac{1}{2} a \exp\left[i \frac{9\alpha_3 \omega_o^2 - 10\alpha_2^2}{24\omega_o^3} \varepsilon^2 a^2 t + i \beta_o \right], \qquad \text{... (C.19)}$$

where we have used the definition: $T_2 = \varepsilon^2 t$.

Substituting the above results into (C.10) gives the following second-order expression for x(t):

$$x(t) = \varepsilon a \cos(\omega t + \beta_o) - \frac{\varepsilon^2 a^2 \alpha_2}{2\alpha_1} \left(1 - \frac{1}{3} \cos(2\omega t + 2\beta_o) \right) + O(\varepsilon^3),$$

where

$$\omega = \sqrt{\alpha_1} \left[1 + \frac{9\alpha_3 \alpha_1 - 10\alpha_2^2}{24\alpha_1^2} \varepsilon^2 a^2 \right] + O(\varepsilon^3), \qquad \text{... (C.20)}$$

expressing the second-order amplitude-frequency dependence.

The applicability of the multiple scales method is not restricted to systems of the form (C.1). In particular, the method can successfully treat damped, and forced, systems of the form:

$$\ddot{x} + \omega_0^2 x = \varepsilon f(x, \dot{x}) + E(t) \qquad \ldots (C.21)$$

where E(t) is oscillatory: E(t) = a Cos (Ωt) for example.

In dealing with such systems, care must be taken to order the terms correctly so that resonances due to the periodic forcing do not cause infinite amplitude oscillations. In practice this means bringing the forcing, damping, and non-linearities in at the same order of the expansion.

C4 THE INTEGRAL METHOD

The method to be described utilises a multiple time-scales expansion of systems of equations, as described in the last section. In this case, however, the perturbation analysis is performed around the solutions of a non-linear first order equation. The criterion for the elimination of secular terms is, now, that a certain integral should vanish over one period of the first order solution.

The above method gives an expression for the slow time variation of the amplitude of the solution. However, the terms involving the slow-time (εt) derivative of the phase vanish identically over one period. Therefore, a further method is applied to the equations in order to obtain an expression for the slow phase variation.

C4.1 Amplitude Equation

Consider an equation of the form:

$$\ddot{x} + g(x) = \epsilon S_1 \qquad \ldots (C.22)$$

where $g(x) = \alpha_1 x + \alpha_2 x^2 + \ldots$, is a polynomial expression in x, and S_1 is a source term due to damping and/or forcing.

Here, ϵ is the expansion parameter, the source term being taken as order ϵ. Both x and its derivatives are expanded as in the last section:

$$x = x_o + \epsilon x_1 + \epsilon^2 x_2 + \ldots ,$$

$$\frac{d}{dt} = \frac{d}{dt_o} + \epsilon \frac{d}{dt_1} + \ldots , \quad \text{etc.}$$

The first order equation is then:

$$\frac{d^2 x_o}{dt_o^2} + g(x_o) = 0 \ , \qquad \ldots (C.23)$$

with solution: $x = x_o (t_o, t_1, \ldots)$

The second order equation can be written:

$$\frac{d^2 x_1}{dt_o^2} + g'(x_o)\, x_1 = -2 \frac{d^2 x_o}{dt_o\, dt_1} + S_1 = S \ , \qquad \ldots (C.24)$$

or $\hat{L} x_1 = S$,

where $g'(x_o) = \left.\frac{dg}{dx}\right|_{x_o}$, and S is a new source term.

A solution of $\frac{d^2 x}{dt_o^2} + g'(x_o)x = 0$, is:

$$x(t_o) = \psi(t_o) = \frac{dx_o}{dt_o} \qquad \text{... (C.25)}$$

We multiply both sides of (C.24) by $\psi(t)$ and integrate the resulting expression over one period of $x_o(t_o)$. Then, the criterion for x_1 to be a periodic function of t_o is that [30]:

$$\int_o^T \psi \, Lx_1 \, dt_o = \int_o^T x_1 \, L \, \psi \, dt_o = 0 \quad \text{(by virtue of (C.25))} \qquad \text{... (C.26)}$$

This periodicity condition can be understood by integrating by parts and observing that x_1 and $\frac{dx_1}{dt_o}$ must be periodic for certain terms to vanish and leave the above equality.

Equality (C.26) implies:

$$\int_o^T S \, \psi \, dt_o = 0 \qquad \text{... (C.27)}$$

This integral provides the required consistency condition for the t_1 variation of the amplitude.

C4.2 Phase Equation

As mentioned above, the terms involving the time t_1 derivative of the phase of x_o (t_o, t_1, ...), vanish identically over a period. In order to derive an equation for the phase we assume x_1 to be of the form:

$$x_1 (t_o, t_1, \ldots) = \eta (t_o, t_1, \ldots) \frac{dx_o}{dt_o} =$$

$$= \eta (t_o, t_1, \ldots) \psi (t_o, t_1, \ldots) \qquad \text{... (C.28)}$$

Substituting (C.28) into (C.24) gives:

$$\frac{1}{\psi}\frac{d}{dt_o}\left(\psi^2 n'\right) = S \quad , \quad n' = \frac{\delta n}{\delta t_o} \quad , \qquad \ldots (C.29)$$

or,

$$x_1 = \psi \int \frac{dt'}{\psi^2} \int^{t'} S\,\psi\, dt'' + \psi \int \frac{\beta_1 dt}{\psi^2} + \beta_2\,\psi \quad ,$$

where β_1, β_2 are integration constants. Setting $\beta_1 = \beta_2 = 0$, we obtain:

$$x_1 = \psi \int \frac{dt'}{\psi^2} \int^{t'} S\,\psi\, dt'' \qquad \ldots (C.30)$$

The consistency condition for x_1 is now that no secular terms in t, t^2, etc., should appear on the right hand side of (C.30).

The inner integral in (C.30) is the one considered for the amplitude equation. Therefore, all terms in t' resulting from this integral can be neglected, as they have already been accounted for in the derivation of the amplitude equation. After performing the outer integration, the sum of secular terms is set to zero to give the required differential equation for the phase.

REFERENCES

1. Abramowitz, M. and Stegun, I.A., Handbook of Mathematical Functions, Dover, New York (1972).

2. Arnold, V.I., Ordinary Differential Equations, M.I.T. Press (1973).

3. Bridges, R. and Rowlands, G.,. "On the Analytic Form of Some Strange Attractors", Phys. Lett. 63A, pp 189-90 (1977).

4. Broomhead, D., McCreadie, G., and Rowlands, G., "On the Analytic Derivation of Poincaré Maps - The Forced Brusselator Problem", Phys. Lett. 84A, p 229 (1981).

5. Broomhead, D., and Rowlands, G., "On the Use of Perturbation Theory in the Calculation of the Fractal Dimension of Strange Attractors", Physica 10D, pp 340-52 (1984).

6. Broomhead, D. and Rowlands, G., "On the Analytic Treatment of Non-Integrable Difference Equations", J. Phys. 16A, pp 9-24 (1983).

7. Broomhead, D., and Rowlands, G., "A Simple Derivation of The Mel'Nikov Condition for the Appearance of Homoclinic Points", Preprint.

8. Chirikov, B.V., "A Universal Instability of Many-Dimensional Oscillator Systems", Phys. Rep. 52, pp 263-379 (1979).

9. Chow, S.N., "An Example of Bifurcation to Homoclinic Orbits", J. Diff. Eq. 37, pp 351-73 (1980).

10. Collet, P., and Eckmann, J.P., "Iterated Maps on the Interval as Dynamical Systems", Birkhauser, Boston (1980).

11. Froyland, J., "Some Symmetric, Two-Dimensional, Dissipative Maps", Physica 8D, pp 423-34 (1983).

12. Goldstein, H., Classical Mechanics, Addison-Wesley (1964).

13. Gradshteyn, I.S., and Ryzhik, I.M., Table of Integrals, Series, and Products, Academic Press, London (1980).

14. Gu, Y., et al, "Crises and Hysteresis in Coupled Logistic Maps", Phys. Rev. Lett. 52, pp 701-04 (1984).

15. Guckenheimer, J., and Holmes, P., Nonlinear Oscillations, Dynamical Systems, and Bifurcations of Vector Fields, Springer, New York (1983).

16. Henon, M., "A Two-Dimensional Mapping with Strange Attractor", Comm. Math. Phys. 50, pp 69-77 (1976).

17. Hogg, T., and Huberman, B.A., "Generic Behaviour of Coupled Oscillators", Phys. Rev. 29A, pp 275-81 (1984).

18. Holmes, P. (Ed.), New Approaches to Nonlinear Problems in Dynamics, SIAM, Philadelphia (1980).

19. Holmes, P., "A Nonlinear Oscillator with a Strange Attractor", Phil. Trans. R. Soc. A292, pp 419-48 (1979).

20. Jeffries, C.D., "Chaotic Dynamics of Instabilities in Solids", Physica Scripta T9, pp 11-26 (1985).

21. Lichtenberg, A.J., and Lieberman, M.A., Regular and Stochastic Motion, Springer-Verlag, New York (1983).

22. Lorenz, E.N., "Deterministic Nonperiodic Flow", J. Atmospheric. Sci. 20, pp 130-41 (1963).

23. Mandelbrot, B.B., The Fractal Geometry of Nature, W.H. Freeman, San Francisco (1982).

24. May, R.M., "Simple Mathematical Models with Very Complicated Dynamics", Nature 261, pp 459-67 (1976).

25. McCreadie, J., Thesis (1983).

26. Moon, F.C., "Fractal Boundary for Chaos in a Two-State Mechanical Oscillator", Phys. Rev. Lett. 53, pp 962-64 (1984).

27. Nayfeh, A.H., Perturbation Methods, Wiley, New York (1973).

28. Nayfeh, A.H., and Mook, D.T., Nonlinear Oscillations, Wiley, New York (1979).

29. Rogers, D.T., "Remarks on Multiparameter Mappings: Controlled-Parameter and Threshold Maps", Math. Biosciences 63, pp 57-69 (1983).

30. Romeiras, F.J., and Rowlands, G., "Stability of Strong Electromagnetic Waves in Overdense Plasmas Against Long-Wavelength Perturbations", J. Plasma Phys. 33, pp 285-301 (1985).

31. Rowlands, G., "On the Stability of Solutions of the Non-linear Schrodinger Equation", J. Inst. Maths. Applic. 13, pp 367-77 (1974).

32. Rowlands, G., "An Approximate Analytic Solution of the Lorenz Equations", J. Phys. 16A, pp 585-90 (1983).

33. Shaw, R., "Strange Attractors, Chaotic Behaviour, and Information Flow", Z. Nat. 36A, pp 80-112 (1981).

34. Smale, S., "Differentiable Dynamical Systems", Bull. Am, Math. Soc. 73, 747-817 (1967).

35. Sparrow, C., The Lorenz Equations: Bifurcations, Chaos, and Strange Attractors, Springer, New York (1982).

36. Steeb, W.H., and Erig, W., "Chaotic Behaviour and Limit Cycle Behaviour of Anharmonic Systems with Periodic External Perturbations", Phys. Lett. 93A, pp 267-70 (1983).

37. Young, L.S., "Dimension, Entropy, and Lyapunov Exponents in Differentiable Dynamical Systems", Physica 124A, pp 639-45 (1984).

TITLE CHAOTIC DYNAMICS IN FLOWS AND DISCRETE MAPS

AUTHOR ANTHONY CURRIE

INSTITUTION and DATE University of Warwick 1984